Seasonality and Discharge as Key Drivers of Headwater Stream Carbon Dioxide Emissions in the Landscape Carbon Budget

Hannah D. Conroy

A dissertation

submitted in partial fulfillment of the

requirements for the degree of

Doctor of Philosophy

University of Washington

2025

Reading Committee:

David Butman, Chair

Erin Hotchkiss

Erkan Istanbulluoglu

Becca Neumann

Program Authorized to Offer Degree:

Civil and Environmental Engineering

University of Washington

Abstract

Seasonality and Discharge as Key Drivers of Headwater Stream Carbon Dioxide Emissions in the Landscape Carbon Budget

Hannah D. Conroy

Chair of the Supervisory Committee:
David Butman
Civil and Environmental Engineering

Quantifying carbon losses from inland waters has emerged as an uncertainty in our understanding of the global carbon cycle. Streams and rivers are of particular interest because of their potential to emit carbon dioxide (CO_2) to the atmosphere with some estimates predicting riverine carbon emissions will alter the calculation of terrestrial net ecosystem exchange (NEE), the balance between how much carbon land ecosystems absorb and how much they release. Headwater streams, small tributaries of rivers at the highest end of a watershed, are especially important when quantifying these CO_2 emissions and carbon losses because of their tight coupling to the terrestrial environment and high turbulence. Heterogeneity within headwater stream networks, both spatially and temporally, makes measuring and upscaling these emissions challenging because measurements of carbon dioxide in streams are often limited to a few monitoring points.

In this dissertation, we sought to fill knowledge gaps regarding spatial and temporal variability in CO_2 emissions across a range of biomes. In Chapter 2, we demonstrated how under high flow conditions, a stream network in the Pacific Northwest, can have much greater total carbon emissions than during low flow conditions (1.22 Mg C day^{-1} vs. 0.034 Mg C day^{-1}). Increased

stream network area, higher gas exchange, and greater terrestrial connectivity all contributed to these increased emissions in our stream network model. We found these carbon emissions during high flow in November accounted for a much larger percentage of NEE than during base flow in August (54% vs. 0.62%), emphasizing the need to better quantify carbon emission during flow events.

In Chapter 3, we expanded this analysis by modeling carbon emissions from five headwater stream networks in different biomes, incorporating stream network extent to account for dynamic flow and a stream network model to account for spatial and temporal variations in CO_2 emissions on an annual scale. We found that while accounting for the extent of the stream network due to drying does not change modeled annual emissions substantially (0.06-4.3%), it does change the timing and spatial distribution of emissions and CO_2 concentrations. We found discharge was the main driver of emissions at all sites, with 50% of carbon emissions occurring in the top 3-29% of discharge conditions. Spatially, our analysis highlighted that first-order streams consistently produced higher areal emissions compared to higher-order streams, attributed to steeper slopes and connectivity to the source of pCO_2, terrestrial soils and groundwater.

Finally, in Chapter 4, we estimated CO_2 emissions from a stream in an agricultural catchment, an understudied biome in regards to carbon dynamics. We found that in this low-lying catchment with high nutrient and organic matter inputs, the expected coupling between discharge and CO_2 emissions was dampened because of a weaker relationship between slope and gas exchange velocity. Instead, we found the hydrologic regime regulated the magnitude of emissions by regulating the source, namely the higher in-stream metabolism contribution (46%) to emissions at a site with high nutrient and organic matter inputs. Across the three chapters, we demonstrate how the hydrologic regime of a stream network governs the timing, source, and magnitude of CO_2 emissions. We also show that carbon dynamics in headwater streams vary across networks, influenced by differences in biome, topography, land use, and geology, highlighting the complexity of accurately quantifying carbon losses from these systems.

Table of Contents

List of Figures iii
List of Tables vii
Acknowledgments viii
Chapter 1 Introduction 1
Chapter 2 Seasonality Drives Carbon Emissions along a Stream Network 5
Abstract 7
Plain Language Summary 7
Introduction 9
Material and Methods 12
Results 26
Discussion 33
Conclusions and Next Steps 40
Acknowledgements 41
Open Research 42
Supplementary Information 43
Chapter 3 Hydrologic regimes shape stream network CO_2 dynamics and emissions 50
Abstract 52
Introduction 53
Methods 56
Results 72
Discussion 85
Conclusions 96
Acknowledgments 97
Supplementary Information 99
Chapter 4 Dynamic contribution by aquatic metabolism to carbon dioxide emissions from a low-land agricultural catchment 114
Abstract 115
Introduction 115
Methods 118

Results 120
Discussion 128
Conclusions 135
Supplementary Information 136
Chapter 5 Conclusions 151
References 156

List of Figures

Figure 2.1 The Martha Creek Watershed location in Stabler, WA, USA[39, 40]. The location of the water quality sensors maintained by NEON are shown[41]. The gage is located at the most downstream sensor. .13

Figure 2.2 Discharge at Martha Creek at the basin mouth in 202147. The sampling periods are highlighted in green. January 2021 included an large flood (>6 m3 s-1) that resulted in sensor washouts and data gaps at the site. 15

Figure 2.3 Observed pCO2 concentrations in August and November 2021 along the length of Martha Creek. Stream lines were derived from the USGS NHDPlus dataset and adjusted based on field observations. 27

Figure 2.4 Initial Non-Adjusted Model results for August and November. 30

Figure 2.5 Observed (measured) vs. predicted (modeled) pCO2 concentrations for August (left) and November (right) using the non-adjusted modeling approach (Figure 2.4) Line is 1:1. 31

Figure 2.6 Adjusted model results pCO2 for August and November.....32

Figure 2.7 Carbon emissions at each point along the stream in August and November. 32

Figure 3.1 Study stream networks located at five National Ecological Observatory Network stream monitoring sites throughout the United States. Plots show the average daily discharge (Q; mean from 2018-2023) for each site over a water year in black with the minimum and maximum discharge from the six-year time period highlighted in grey. Average daily water temperature for the water year shown in blue. 58

Figure 3.2 Proportion of emission that occur at varying network sizes. The majority of emissions occur when the stream networks are at full network size. The right plot shows the total emissions that occur at each stream network size. The left plot shows the proportion of emissions that occur at each network size, where the majority of emissions for each stream network when the network is at 75-100% of its maximum size. King's Creek has the smallest proportion of emissions that occur at 75-100% of network size because it is only at full network size 1% of the time. Caribou Creek, on the other hand, is at full

network size 100% of the time. Emissions when the network size is 0-25% are less than 0.4% at all sites. 73

Figure 3.3 Modeled-static predicted pCO_2 at the network outlet versus modeled-dynamic predicted pCO2 at the network outlet for stream networks with modeled-dynamic scenario runs. Including periods of stream intermittence within the network results in higher pCO_2 at the network outlet for stream networks with modeled-dynamic scenario runs. 74

Figure 3.4 Percent of flux from each modeled point in the stream network during the 2018-2023 model time period. To create the figure, total annual emissions from each point were divided by the total annual emissions for the entire network. For Martha Creek, King's Creek, Walker Branch, and Como Creek, the modeled-dynamic scenarios are shown; for Caribou Creek, the measured-static scenario is shown. The scale bars denote the differing watershed sizes. The outlet of each network is the NEON downstream stream monitoring site used to validate modeled CO_2 and generate other parameter estimates for the network CO_2 model. 76

Figure 3.5 Carbon emissions percentage by stream order. The majority of emissions occur for all stream networks in first order stream segments. Martha Creek and Walker Branch are the only fourth order network. Como Creek is a 2nd order stream. 77

Figure 3.6 Modeled comparisons to the CO_2 sensor at Martha Creek. We ran the model by multiplying k_{600} and C_{gw} by a constant to optimize the mean absolute error. We show that both adjustments provided a better fit for the sensor pCO_2, however the groundwater adjustment resulted in a much larger increase in total annual emissions at the stream network. 80

Figure 3.7 Lorenz curves of cumulative emissions with the x-axis ordinated by increasing discharge. Emissions of CO_2 are unequal, with the majority of emissions under the 1:1 line delivered at the highest discharge from all networks. Caribou Creek and Como Creek are denoted with a dashed line to note emissions were only modeled from May–September and May–October to avoid periods when the stream was frozen. 82

Figure 3.8 Monthly carbon exports by stream network colored by flux type: stream network CO_2 emissions, dissolved inorganic carbon (DIC) export, and dissolved organic carbon (DOC) export). Discharge is plotted on the secondary y-axis as a dashed line. Caribou Creek and Como Creek were only modeled from May–September and May–October to avoid periods when the stream was frozen. 83
Figure 4.1 Site map of the Hågaån stream catchment. The catchment is composed of 21% arable land; most of the stream network drains directly through areas of arable land. 119
Figure 4.2 Mean daily data of measured water temperature, oxygen, turbidity, CO_2 concentration, and discharge at Hågaån, together with modeled metabolism (ER and GPP) and CO_2 emissions. The black line shows 2020 data when CO_2 measurements were included. The red dashed line shows the mean daily average from 2020-2023. 123
Figure 4.3 The metabolism contribution to total stream CO_2 emissions in 2020. The percent metabolism contribution is shown in blue. The total emissions colored by contributions (metabolism and other) are shown in grey and orange. The median contribution for available days of data in 2020 was 46%. 125
Figure 4.4 C-Q and P-Q plots for selected variables with significant breakpoints. Breakpoints were determined using Davies tests. All values are log-transformed and points are colored by water temperature. 127
Figure 4.5 Conceptual framework for carbon cycling and CO_2 emissions low-gradient agricultural streams. During high flow, ER will increase with increased inputs of organic matter and nutrients while GPP will decrease with increased turbidity and less light. The gas transfer velocity (k_{600}) will only increase slightly in low sloped networks ultimately limiting CO_2 emissions. During low flow typically occurring in the summer, the CO_2 source into the network can remain high with high ER driven by non-limiting nutrients and high temperatures. While the groundwater and soil inputs of CO_2 remain unresolved, increased respiration in both soil and the stream during the summer months could support high observed CO_2 concentrations (and therefore decrease the metabolism contribution to total emissions), which in turn cause slightly higher CO_2 emissions in the summer. 133

Figure 5.1 Discharge versus percent total carbon losses of NEE. The relationship is mainly driven by a tight relationship between discharge and carbon losses. 153

List of Tables

Table 2.1 Surface Water and Groundwater Field Sampling Results 17

Table 2.2 Variables used in the Stream Network Model 21

Table 2.3 Comparison of Regression Relationships to NEON Gas Exchange Experiments at the NEON reach 29

Table 2.4 Total Carbon Emissions and Emission Comparison 33

Table 3.1 Stream Network Comparisons 60

Table 3.2 Description of combined stream network model scenarios 67

Table 3.3 Daily average range of model inputs for each stream network 69

Table 3.4 WEPP modeled-dynamic and modeled-static scenario results 72

Table 3.5 Stream network model fit to measurements values and measurement impacts on emissions estimates 79

Table 3.6 Total carbon losses per watershed area and proportion of total carbon losses[1] 84

Table 5.1 Total carbon losses per watershed area and proportion of total carbon losses[1] 152

Acknowledgments

There are many people I would like to thank for their support throughout my PhD journey the last five years. First, to my advisor David Butman who I feel very lucky to have had guiding me through this process, challenging me and allowing me space to grow as a scientist, and recognizing that there is more to life than grad school. I was not sure if I would continue on with the PhD, but knowing I had David in my corner made it much easier to make the decision. I am so grateful for his support and mentorship over these long five years. To Erin Hotchkiss for her kindness and support in becoming a better researcher. Thank you to the other members of my committee Erkan Istanbulluoglu, Becca Neumann, and Abby Swann for their expertise, guidance, and helpful feedback on this work.

Funding from this work came from the National Science Foundations and the Valle Program. Thank you to the CO_2 Macrosheds group for their collaboration, interesting science discussions, data help, and engaging meetings. To the Ecosystem Biogeochemistry group (and the Supergroup), both current and former members, for feedback throughout my five years, commiseration when doing hard things, writing sessions, and field and laboratory support (shout-out to Anthony Stewart for trekking with me through Martha Creek in the worst weather ever). Thank you to Marcus Wallin, who advised me while spending 9 months living in Uppsala, Sweden. Your kindness while introducing me to a new country, including to my new favorite sport (cross-country skiing!), made living abroad easier, and I know it is an experience I will remember forever. Thanks also to those I met at SLU for the many fikas and welcoming me to their university.

Thank you to my friends in Seattle for creating a community that feels like a family when living far from home and to my friends afar who have only been a phone call away when I need them. To Steph, for showing me the way to getting a PhD and laughing a lot while doing it. To my dog, Lucy, who I adopted at the beginning of this program and whose cuddles and reluctant walks I have needed every day. To my brothers and extended family for their support. And, to my partner Sam – whose love, support (even from thousands of miles away), distractions, laughter, and encouragement was vital to my survival in the last few years of this program.

Finally to the most important supporters in my life, my parents. Dad, I would not have pursued this journey without your influence and career of 30 years at the Environmental Protection Agency. You taught me how a love for the outdoors can go hand-and-hand with science. Now more than ever, it is clear how important public service is for protecting the environment, and I am so thankful to you for showing me the way. Mom, you have always been my biggest cheerleader and confidant. The number of phone calls we have had during this five years is definitely longer than the number of pages in this dissertation – I am so grateful for your advice, your listening ear, and of course, coming all the way to Kansas to spend five days wading around in a stream.

Chapter 1 Introduction

Carbon is a fundamental element that plays a critical role in regulating the Earth's climate. Humans have significantly altered the global carbon cycle through the burning of fossil fuels and contributed to the warming of the global climate that will affect the environment, ecosystems, and human health. Forest ecosystems have been recognized as the largest terrestrial sink on the planet, and managing these terrestrial carbon stocks can be an effective strategy for reducing carbon emissions[1, 2]. However, continental landscapes are made up of a mosaic of ecosystems, with some areas storing CO_2 and others releasing it. In the last twenty years, inland waters, including streams, rivers, lakes, and reservoirs have been highlighted as a missing component of our understanding of the global carbon cycle [3-5]. Inland waters transfer carbon to oceans, store carbon in lakes and reservoirs, transform organic and inorganic carbon, and emit CO_2 to the atmosphere[4]. In 2013, inland waters were included for the first time in the Intergovernmental Panel on Climate Change (IPCC) as a net source of CO_2 to the atmosphere.

Streams and rivers are of particular interest because they are often supersaturated with CO_2 relative to the atmosphere, making them a net source of atmospheric carbon[4, 6, 7]. A number of studies have attempted to better constrain CO_2 emissions from rivers and streams[3, 6, 8, 9]; for example, in North America emissions from stream and rivers are estimated to be 125 Tg C yr^{-1} compared to a net forest sink of 157 Tg C yr^{-1} [10, 11]. Despite increasing interest, these riverine carbon emissions still have substantial uncertainty with global estimates ranging from 0.7 to 2.0 Pg C yr^{-1} [3, 5, 12]. Some estimates predict riverine carbon emissions will alter the calculation of

terrestrial net ecosystem exchange (NEE), the balance between how much carbon land ecosystems absorb and how much they release[3, 13-15].

Headwater streams, small tributaries of rivers at the highest end of a watershed, have emerged as especially important sources of CO_2 emissions[9, 15]. Despite their small size, headwater streams make up 89% of the total stream and river length[16]. Their tight hydrological connection to the terrestrial environment including groundwater and soils, coupled with high turbulence, create ideal conditions for elevated CO_2 concentrations and high rate of CO_2 exchange with the atmosphere[15, 17]. Quantifying CO_2 emissions from headwater streams is therefore essential for improving our understanding of the global carbon cycle, and also informing strategies to manage terrestrial carbon stocks at watershed and regional scales.

Our current estimates of carbon emissions from headwater streams have large uncertainties, and are sometimes even excluded from global estimates[15], because the processes controlling CO_2 concentrations and emissions vary in space, time, and between biomes. CO_2 concentrations within headwater streams are shaped by multiple sources and sinks including inputs of CO_2-rich groundwater, production or breakdown of organic carbon from in-stream metabolism, removal of CO_2 from mineral weathering, or transformation of CO_2 from carbonate buffering[17-19]. These sources and sinks fluctuate across a stream network and will vary between ecosystems, making it challenging to measure and scale up emissions from sparse sampling points.

CO_2 concentrations and emissions will also vary temporally with changes in temperature, flow, light, and stream size. The flow regime of a stream network emerges as an important influence in stream CO_2 emissions, with global estimates predicting CO_2 emissions from streams and rivers vary between 112 and 209 Tg of carbon per month[12]. High flow and storm events will increase

turbulence and therefore gas exchange with the atmosphere, especially in high sloped headwater networks[20, 21]. Discharge events may also influence CO_2 concentrations due to the dilution of gas concentrations, increased supply of gases from groundwater, and changes in-stream metabolism[21-23]. Furthermore, headwater networks are not static; stream lengths expand and contract with precipitation and evapotranspiration, altering the surface area available for emissions and connection to the terrestrial environment[24, 25]. Many of these dynamic streams are unaccounted for in conventional maps or incorrectly classified as perennial or ephemeral, leading to uncertainty in emissions estimates[12, 26, 27]. All of these processes in space and time will vary between ecosystems with different flow regimes, productivity, geology, and topography.

In this dissertation, I sought to better constrain CO_2 emissions estimates from headwater streams by examining spatial and temporal variability across a range of biomes. I focused on methods that provide more spatial and temporal resolution for measuring CO_2 concentrations, including longitudinal sampling campaigns to sample entire stream networks and continuous CO_2 sensors to measure CO_2 at high-resolution frequencies at the sensor location. In addition to field observations, I developed and applied models to estimate CO_2 emissions and processes in both space and time. Over the next three chapters, I explore which key uncertainties most influence our ability to scale up CO_2 emissions across larger spatial scales and compare to fluxes from the surrounding terrestrial landscapes.

In Chapter 2, I focused on spatial variability in headwater CO_2 emissions within a Pacific Northwest forested watershed during low and high flow. We modified a stream network model to reflect real measurements made during base flow and high flow to examine how CO_2 emissions change during two extreme flow regimes incorporating spatial variability in both CO_2

concentrations and the stream network area. In Chapter 3, I expanded this analysis temporally and across biomes by examining how CO_2 emissions change on an annual scale across five U.S. watersheds representing different climates and biomes. We incorporated estimates of stream permanence using a hydrologic model to examine the effect of flow regime on carbon emissions estimates. In Chapter 4, I examine CO_2 emissions from agricultural landscapes, an ecosystem type that covers nearly half of the Earth's land surface but remains underrepresented in stream carbon studies. Here, we used continuous oxygen and CO_2 sensor data to assess the impact of in-stream metabolism and its contribution to CO_2 emissions on these human-impacted systems. We explored how discharge and seasonality shape both respiration and emissions and discuss the trade-offs between high carbon supply and low gas exchange in low-gradient agricultural streams. Finally in Chapter 5, I summarize the findings of this dissertation, highlight key uncertainties in estimating carbon emissions from streams, and provide context for our carbon emissions estimates by quantifying surrounding terrestrial watershed fluxes.

Chapter 2 Seasonality Drives Carbon Emissions along a Stream Network

Seasonality Drives Carbon Emissions along a Stream Network

Hannah Conroy[1], Erin R. Hotchkiss[2], Kaelin M Cawley[3], Keli Goodman[3], Robert O. Hall Jr. [4], Jeremy B. Jones[5], Wilfred M. Wollheim[6], David Butman[1]

[1]University of Washington

[2]Virginia Tech

[3]National Ecological Observatory Network

[4]Flathead Lake Biological Station, University of Montana

[5]University of Alaska Fairbanks

[6]Department of Natural Resources and the Environment, University of New Hampshire

Key Points:

- Seasonality can drive variation in carbon emissions from headwater stream area with changes in flow and stream network area.
- Stream networks can emit a large percentage of the terrestrial net ecosystem exchange (NEE), especially under high flow conditions.

This chapter has been previously published as:

Conroy, H. D., Hotchkiss, E. R., Cawley, K. M., Goodman, K., Hall, R. O., Jr., Jones, J. B., et al. (2023). Seasonality drives carbon emissions along a stream network. Journal of Geophysical Research: Biogeosciences, 128, e2023JG007439. https://doi.org/10.1029/2023JG007439.

Abstract

Headwater stream networks contribute significantly to the global carbon dioxide terrestrial flux because of high turbulence and coupling with terrestrial environments. Heterogeneity within headwater stream networks, both spatially and temporally, makes measuring and upscaling these emissions challenging because measurements of carbon dioxide in streams are often limited to a few monitoring points. We modified a stream network model to reflect real measurements made under base flow and high flow conditions at Martha Creek in Stabler, WA in the US Pacific Northwest. We found that under high flow conditions, the stream network had much greater total carbon emissions than during low flow conditions (1.22 Mg C day^{-1} vs. 0.034 Mg C day^{-1}). We attribute this increase to a larger overall stream network area (0.04 km^2 vs 0.01 km^2) and discharge (1.9 m^3/s vs. 0.005 m^3/s) in November versus August. Our results demonstrate the need to understand the nonperennial stream reaches when calculating carbon emissions. We compared the stream network emissions with the terrestrial net ecosystem exchange (NEE) estimated by local eddy covariance measurements per area of the watershed (-5.5 Mg C day^{-1} in August and -2.2 Mg C day^{-1} in November). Daily stream emissions in November accounted for a much larger percentage of NEE in August (54% vs. 0.62%). We concluded that the stream network can emit a large percentage of the forest NEE in the winter months, and annual estimates of stream network emissions must consider the flow regime throughout the year.

Plain Language Summary

Streams contribute to the global carbon cycle because they can release carbon dioxide to the atmosphere. It can be difficult to measure these emissions because the concentration of carbon dioxide will change along a stream length and from season to season. We modeled carbon

dioxide emissions from a stream during August in base flow and during November in high flow. We found that emissions increased during November with an increased stream network size and stream discharge and that this emission can be a large fraction of whole watershed net carbon emission. We determined that seasonality is an important indicator of carbon emissions in headwater streams.

Introduction

Accurate accounting of carbon storage and flux in terrestrial ecosystems is essential for understanding the global carbon cycle. Aquatic carbon emissions are not fully accounted for and can alter the calculation of terrestrial net ecosystem exchange (NEE)[3, 13-15]. Headwater streams in particular account for a large portion of net terrestrial carbon dioxide (CO_2) emissions (an estimated 0.93 Pg C year) relative to their size because of their high turbulence and coupling with terrestrial environments[15, 17]. An estimated 36-64% of total CO_2 emissions from rivers and streams are released by headwater streams[15].

Headwater streams are typically supersaturated with respect to the atmosphere and act as a net source of atmospheric CO_2 [4, 6, 7]. Dissolved CO_2 (pCO_2) concentrations are influenced by multiple sources and sinks that can vary along a stream network including: (1) inputs of carbon via groundwater from direct soil CO_2 in runoff and oxidation of soil-derived DOC or leaf inputs,[17, 28] (2) production or breakdown of organic carbon from in-stream metabolism,[17, 18, 29] (3) removal of CO_2 from mineral weathering, and (4) alkalinity-dependent transformation of CO_2 due to carbonate buffering[19] .

To estimate total CO_2 emission from headwater streams, we must understand how pCO_2 changes throughout a stream network. Physical and chemical heterogeneity within headwater streams makes measuring and upscaling CO_2 concentrations and fluxes challenging because measurements of pCO_2 in streams are often limited to one or two sample or monitoring points. In reality, pCO_2 will vary between points within stream networks because streams are heterogeneous in groundwater inputs and surface water turbulence[17, 30]. Few studies have

considered the spatial variability of carbon emissions from an entire stream network, with estimates of flux often based on averages of pCO_2 for different stream orders[31].

In reality, the inputs and outputs of carbon will change spatially along a stream network. Subsurface flow into a stream will fluctuate in both space and time due to variability in underlying geology and storm events[32]. These variations in underlying geology and soils include the presence of macropores, large size pores that drain water by gravity[33]. Connected macropores can form cracks and soil pipes that support large fluxes of water and solutes into streams via advective transport[17, 33]. Flow intensity and surface water turbulence also change along streams due to variable slope and morphology, such as pools, riffles, and small waterfalls. These variations in turbulence throughout a stream network will result in different rates of gas exchange of carbon with the atmosphere. As a result, studies have observed inputs of high pCO_2 groundwater into stream networks followed by rapid decay within the first 20-100 m of the seepage area[7, 17], leading to considerable variability in stream pCO2.

Assessing ecosystem carbon biogeochemistry from a single sampling location will provide a limited view of larger-scale dynamics because pCO_2 concentrations in headwater stream networks vary temporally with changes in flow, production, and temperature[13, 14]. Stream discharge is an especially important variable in the determination of CO_2 emissions. CO_2 emissions from headwater streams increase during high discharge events, including snowmelt and rainstorms[21, 34, 35]. Stream discharge and gas exchange rates often have a positive relationship, although the relationship can vary spatiotemporally within a stream and between ecosystems[34, 36, 37]. In particular, streams and reaches with steeper slopes show a positive relationship between discharge and gas exchange[20, 21, 37]. Discharge events may also influence

pCO_2 due to the dilution of gas concentrations or increased supply of gases from groundwater[21, 22].

The climate, hydrologic, and productivity regime of the watershed will influence stream discharge and carbon inputs. The rate of carbon transport from terrestrial ecosystems within a catchment will vary seasonally based on the variations in water table depth and discharge[27]. Many headwater stream networks expand and contract seasonally in response to runoff and evapotranspiration, which can also affect carbon inputs and carbon emissions[24]. Seasonal variations in temperature and day length will influence the productivity of the stream network as well as the surrounding terrestrial environment[27]. Streams are likely to have different carbon emissions relative to the terrestrial environment in regions with rainy seasons compared to those with more consistent precipitation throughout the year. The Pacific Northwest is a potential hotspot for stream carbon emissions due to the prevalence of forested areas, steep slopes, and above average seasonal precipitation. The highly variable climate provides an informative case study in seasonal changes to carbon emissions because of extreme changes in precipitation across seasons.

The objective of this study was to develop new estimates for the emissions of CO_2 along an entire stream network. We used a stream network model developed in headwaters of the Rockies[38], and then modified the model to reflect real measurements made under base flow and high flow conditions at Martha Creek in Stabler, WA in the Pacific Northwest. To achieve this objective we:

1. Collected dissolved gas samples every 100 m at Martha Creek over two flow conditions in August and November.

2. Modeled gas evasion from the stream by comparing predictive regression equations and empirical gas evasion experiments.
3. Incorporated in situ estimates of stream metabolism into the stream network model.
4. Placed the estimated stream emissions in the context of the surrounding terrestrial landscape.

This study provided an opportunity to examine the relative contribution of the stream to the carbon balance of the watershed on a seasonal basis.

Material and Methods

Study Site

The study was conducted at Martha Creek, a wadeable stream located in Stabler, WA in the Wind River Experimental Forest (WREF) (Figure 2.1). Martha Creek is part of the National Ecological Observatory Network (NEON), a continental-scale observation facility that collects comprehensive standardized aquatic and terrestrial data across a range of ecosystems in the United States. NEON began monitoring the site in 2017.

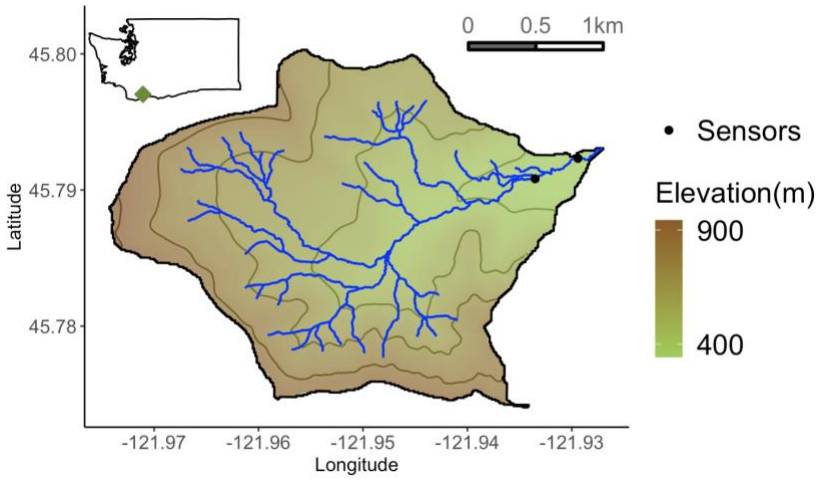

Figure 2.1 The Martha Creek Watershed location in Stabler, WA, USA[39, 40]. The location of the water quality sensors maintained by NEON are shown[41]. The gage is located at the most downstream sensor.

The Martha Creek watershed is 6.2 km^2 and ranges in elevation from 340 m to 940 m with a mean slope of 0.25 (m/m) (Figure 2.1). The watershed consists of 1st to 4th order Strahler order streams. The stream is surrounded by old and new growth mixed deciduous and coniferous forest with areas of dense understory shrubs[41, 42]. The underlying geology is primarily volcanic in origin with basalt bedrock and some colluvial and glacial till[43]. Precipitation occurs as both rain and snow with an average annual accumulation of 2187 mm[41, 44]. In the winter, alternating periods of snow accumulation and snow melt are common with an average snow fall of 1834 mm[41, 44]. The area experiences warm and dry conditions in the summer and cool and wet conditions in the fall and winter (-11.8-39.0 ºC, median: 8.0 ºC)[45]. Streamflow typically peaks in response to snowmelt and rainfall events in the winter and spring and decreases to annual lows in August and September[41].

NEON maintains Martha Creek and the surrounding terrestrial site, the Wind River Experimental Forest, as aquatic and terrestrial field sites, respectively. At Martha Creek, NEON collects continuous measurements at two sensor sites (Figure 2.1) that includes water quality

measurements, elevation of surface water, and temperature of surface water[46]. Martha Creek is surrounded by six groundwater wells (depth: 2.5 – 2.8 meters) near the stream sensor sites equipped with sensors that measure specific conductivity, water temperature, and the elevation of groundwater (Supplementary Figure 2.1). At the terrestrial site, NEON maintains a flux tower used to measure eddy-covariance turbulent exchange of CO_2.

Sampling Methods

We sampled Martha Creek longitudinally over two 5-day sampling periods in August 2021 and November 2021. Samples were taken every ~100 m longitudinally along the stream beginning at the upstream NEON stream sensor (Figure 2.1). In August, samples (n = 55) were taken upstream until the points of spring emergence of each tributary. In November, sampling access (n = 45) was more limited based on terrain and conditions. Samples in August were taken during an annual low flow for the stream at the basin mouth at the downstream NEON sensor (average discharge 5.0×10^{-3} m^3 s^{-1}). Samples in November were taken during a rain precipitation event at a time of high flow for the stream (average discharge 1.9 m^3 s^{-1}) (Figure 2.2). The median annual flow for the stream is 0.17 m^3 s^{-1}.

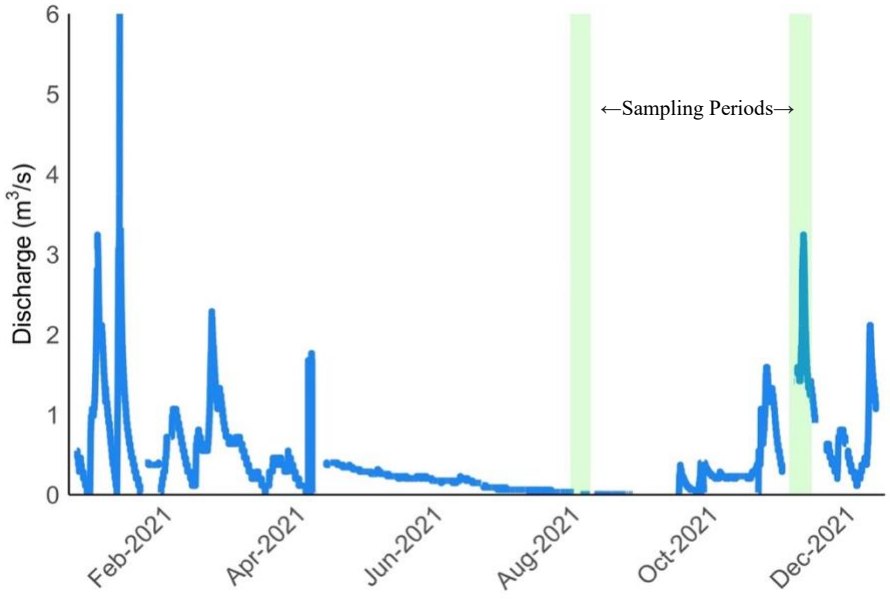

Figure 2.2 Discharge at Martha Creek at the basin mouth in 202147. The sampling periods are highlighted in green. January 2021 included an large flood (>6 m^3 s^{-1}) that resulted in sensor washouts and data gaps at the site.

At each point along the stream, we took pCO_2 measurements using a headspace equilibrium method by equilibrating three gas-tight syringes with 30 mL of stream water with 30 mL of nitrogen gas in the field[48, 49]. The syringes were shaken for 3 minutes before injection of the equilibrated headspace into a pre-evacuated exetainer. Samples were analyzed using a Shimadzu GC-2014 Gas Chromatograph equipped with a methanizer and a flame ionization detector set to 100°C. Dissolved pCO_2 in the original water sample was calculated from a mass balance of the headspace equilibrium system using standards of known concentration, temperature measured in the field, local pressure, and the volume of water and the headspace[48, 49]. The molar quantity of carbon dioxide in the headspace is calculated as:

$$n_{headspace} = \frac{[CO_2] \times V_{headspace}}{0.08206 \times T} \quad \textbf{(2-1)}$$

where $[CO_2]$ is the concentration of CO_2 calculated from standards of known concentration, $V_{headspace}$ is the volume of the headspace in the vial, and T is the temperature (K). The molar quantity of carbon dioxide in the sample water is calculated as:

$$n_{water} = \frac{\alpha \times [CO_2] \times V_{water}}{0.08206 \times T} \quad \textbf{(2-2)}$$

where α is the solubility coefficient calculated based on the temperature[50, 51]. The molar quantity of carbon dioxide in the headspace and water are then added together to find the total concentration.

To examine patterns along the stream reach, we took additional samples that were filtered with 0.22-µm filters at each sample point for DIC, DOC, total alkalinity (TA). DIC samples were injected into exetainers containing 50 µL H_3PO_4 for preservation; DIC analysis was performed using a Shimadzu GC-2014 Gas Chromatograph equipped with a flame ionization detector set to 100°C. DOC was analyzed using a Shimadzu TOC5000A analyzer using NPOC mode. TA was determined by the inflection point titration method and calculated using the USGS Alkalinity Calculator[52, 53]. A YSI EXO2 Multiparameter Water Quality Sonde was used to take additional measurements including pH, conductivity, dissolved oxygen, and temperature. Mean discharge from the sampling period was taken from the continuous discharge data product provided by the gages managed by NEON[47].

To relate to terrestrial inputs, we collected well samples during the two sampling periods. NEON maintains six shallow groundwater wells instrumented with water level, conductivity and temperature sensors (Supplementary Figure 2.1). At the time of both sampling periods, only two wells had sufficient water to sample (Wells 3 and 6, Table 2.1). Samples were taken using a

peristaltic pump after the well was flushed the length of the tubing. The same samples were collected (pCO_2, DOC, DIC, TA, and water isotopes). Temperature and pH were measured in the wells using a YSI EcoSense pH100A probe. Results of the sampling campaign are shown in Table 2.1.

Table 2.1 Surface Water and Groundwater Field Sampling Results

		pH	Water temperature (°C)	Alkalinity (meq L^{-1})	DOC (mg C L^{-1})	DIC (mg C L^{-1})	pCO_2 (µmol L^{-1})	Mean discharge at gage (m^3 s^{-1})
August 2021 Surface Water (n = 55)	Range	6.4–7.5	6.8–18.6	0.2-0.8	0.01-1.1	8.0-43.8	13.3-282	5.0×10^{-3}
	Median	7.0	15.4	0.5	0.19	22.5	61.4	
August 2021 Wells (n = 2)	Range	5.6-6.0	9.8-14.9[a]	0.55	3.5-4.5	50.4-58.8	451-696	NA
November Surface Water 2021 (n = 45)	Range	5.7-7.5	6.7-9.9	0.13-0.45	1.7-6.5	12.5-37.7	14.2 - 230	1.9
	Median	7.2	7.4	0.35	3.0	18.5	37.3	
November 2021 Wells (n = 2)	Range	6.1-6.2	9.8-11.1[a]	0.13-0.24	3.7-7.0	37.1- 84.5	392-817	NA

a. Temperature ranges taken from NEON continuous temperature of groundwater dataset over sample dates[54].

Stream Network Model

We updated the stream network model developed by Saccardi and Winnick (2021)[38] to predict pCO_2 for the Martha Creek network. The stream network model allows us to address the issue of heterogeneity by accounting for variability in hydrology throughout the stream. We updated the model by including measured groundwater concentrations and a stream metabolism model instead of optimization. We were also able to compare the gas exchange coefficient used with

experimental data from the site. The model was used to predict pCO_2 concentrations based on the advection-reaction equation for solute transport:

$$\frac{\partial C}{\partial t} = -v\frac{\partial C}{\partial x} + \frac{1}{A}\frac{\partial Q}{\partial x}\left(C_{gw} - C_i\right) - k_{CO_2}(C - C_{atm}) + \frac{-NEP}{h} \quad \textbf{(2-3)}$$

Similar to Saccardi and Winnick (2021), we solved the equation assuming steady state conditions and using a backwards-difference finite approximation scheme at points along the stream located ~20 m apart:

$$0 = -v\frac{C_i - C_{i-1}}{\Delta x} + \frac{1}{A}\left(\frac{\Delta Q}{\Delta x}\right)\left(C_{gw} - C_i\right) - k_{CO_2}(C_i - C_{atm}) + \frac{-NEP}{h} \quad \textbf{(2-4)}$$

where the concentration of CO_2 at each point (C_i; µmol L^{-1}) is a function of the concentration upstream (C_{i-1}; µmol L^{-1}), atmospheric CO_2 assumed to be constant at 400 ppm, (C_{atm}; µmol/ L^{-1}) groundwater CO_2 (C_{gw}; µmol L^{-1}), and net internal stream production represented as net ecosystem production (NEP; µmol L m^{-2}). The model also requires inputs of the distance between points (Δx; m), the cross-sectional area of the stream (A; m^2), gas transfer velocity (k_{CO2}; m day^{-1}), and the depth of the stream (h; m).

NEP is the difference between gross primary production (GPP) and ecosystem respiration (ER) and is typically negative in streams because ER exceeds GPP when supported by external organic carbon subsidies[55]. It is thus represented by -NEP to impose a positive CO_2 flux when negative:

$$NEP = GPP - |ER| \quad \textbf{(2-5)}$$

We measured groundwater pCO_2 (C_{gw}; µmol L^{-1}) from NEON groundwater wells at the site during the sampling period.

Flow at each point (Q; $m^3\ s^{-1}$) was calculated based on conservation of mass within the drainage basin using the gage at the NEON sensor location (Equation 2-6). We calculated the flow at each point (Q) as a function of the drainage area upstream of the point (A_i), the upstream drainage area of the gage (A_g), and the average flow at the gage during the sampling period (Q_g) from the NEON continuous discharge dataset[47, 56, 57]. The constant, c is the scaling power dependency and commonly set to 1 in hydrology to assume discharge scales linearly with drainage area[56, 57]:

$$Q = Q_g \frac{{A_i}^c}{{A_g}^c}$$

(2-6)

We estimated the stream cross-sectional area (A, width × depth; m^2) at each point using scaling relationships with width (w) and depth (h)[9, 38]. Velocity was also estimated using these scaling relationships[9]:

$$w = 7.104\ Q^{0.447}$$

(2-7)

$$h = 0.298\ Q^{0.222}$$

(2-8)

$$v = 0.668\ Q^{0.365}$$

(2-9)

We confirmed the discharge-width relationship in November using the width measured in the field (Supplementary Figure 2.2). In August, this discharge-width relationship (Equation 2-7) broke down due to low flow in the stream. The relationships were originally developed for discharges between 0.02-2.26 $m^3\ s^{-1}$ [9]. We developed a linear scaling relationship between the calculated widths from Equation 2-7 and width for August based on our field measurements:

$$w_{August} = 6.568w - 0.7614$$

(2-10)

The stream lines were derived from the NHDPlus data set[39] and modified based on observations in the field (Figure 2.3). In August, we were able to make observations along the entire stream. In November, we were unable to access areas higher up in the reach due to terrain and conditions. We therefore identified the stream lines as having an additional order, which we will denote "zero order", based on observations where we were able to sample. The network was broken into points ~20 m apart (n = 433 in August and n = 1005 in November). Slope was calculated from a digital elevation model of the area[40]. Table 2.2 includes a description of each variable.

Table 2.2 Variables used in the Stream Network Model

Variable	Description	August Range (Median)	November Range (Median)	Data source/calculation
$\boldsymbol{Q}$	Discharge at each point (m^3 s^{-1})	5.9×10^{-6} – 5.4×10^{-3} (5.2×10^{-4})	7.2×10^{-4} – 2.0 (0.060)	Calculated from conservation of mass (Equation 2-6)
$\boldsymbol{C_{gw}}$	Groundwater CO_2 (μmol L^{-1})	610	690	Well sampling. C_{i-1} set equal to C_{gw} from well concentrations at the stream origins. Assumed constant at the origins.
$\boldsymbol{\Delta x}$	Distance between measurement points (m)	0.27 – 28.6 (20.9)	0.19 – 28.7 (21.1)	Points set every ~20 m.
w	Stream channel wetted width (m)	8.4×10^{-3} – 4.2 (1.2)	0.27 – 6.6 (1.6)	Based on scaling relationships and adjusted from field data (Equation 2-7)
h	Mean stream channel depth (m)	0.022 – 0.093 (0.06)	0.063 – 0.34 (0.16)	Based on scaling relationships (Equation 2-8)
$\boldsymbol{k_{600}}$	Normalized air–water gas exchange velocity (m day^{-1})	3.28 – 49.0 (4.68)	19.8 – 336 (17.9)	Calculated from slope and velocity (Equation 2-10)
$\boldsymbol{k_{CO_2}}$	Gas transfer velocity of CO_2 (m day^{-1})	2.8 – 43.9 (4.10)	14.4 – 235 (12.8)	Calculated from k_{600} and the Schmidt number (Equation 2-11)
$\boldsymbol{NEP}$	Net Ecosystem Respiration (g CO_2 m^{-2} day^{-1})	0.41	1.10	Estimates of whole-stream metabolism from diel dissolved O_2 sensor data in one lower stream reach using *streamMetabolizer*. Assumed constant across the stream.
$\boldsymbol{s}$	Stream slope (m/m)	0.017-0.53 (0.16)	0.017-0.78 (0.22)	Digital elevation model
$\boldsymbol{T}$	Temperature (ºC)	13.5 – 15.7 (14.7)	7.1 – 8.6 (8.1)	Set based on stream order and sample data (Supplementary Figure 2.3)

To predict pCO_2 at each point in the Martha Creek watershed, we solved equation 2-3 sequentially along the stream network starting with first order streams for August and zero order streams for November[38]. The initial condition for C_i was set to the groundwater pCO_2 at the

headwater measured from the NEON wells and the discharge-weighted input of pCO_2 from each reach at the stream junctions. The model was implemented in R by using a for loop to solve for the concentration of CO_2 at each point (C_i; μmol L^{-1}) where i represents each point ~20m apart. We calculated the (F_{CO2}; kg day^{-1}) emissions for each reach from the modeled concentration at each point:

$$F_{CO_2=} k_{CO_2}(C_{atm} - C_i)$$

(2-11)

After running the model for both months with the inputs described above, we ran the model again for both months by including our measured pCO_2 values. We set the C_i of the points in the model that were located at our sampling locations (n = 55 for August and n = 45 for November) equal to that of our sampled concentrations. The model was then allowed to run sequentially with these known concentrations as inputs. We compared this adjusted model to the preliminary model runs.

To compare the carbon emissions from the stream network with other landscape carbon fluxes, we estimated the baseline terrestrial carbon net ecosystem exchange (*NEE*; g C m^{-2} day^{-1}). *NEE* was measured from the NEON eddy flux tower located in the Wind River Experimental Forest. We used the monthly data created by the NCAR-NEON project that was gap-filled with the R package ReddyProc[58, 59]. We averaged half-hourly measurements of NEE over our 5-day sampling periods to estimate the terrestrial *NEE*. We used the resulting *NEE* to estimate the carbon emissions from the Martha Creek watershed by multiplying the *NEE* by the area of the watershed. We then used this value to compare the flux from the watershed to the carbon emissions from the stream. We defined negative values for NEE to denote the loss of carbon from the atmosphere by convention.

The flux tower is located outside of the Martha Creek watershed (3.6 km away); although its footprint does have similar vegetation, land use, and geology as the watershed[41]. We confirmed the spatial representativeness of the tower footprint by comparing the normalized difference vegetation index (NDVI) of the weighted footprint of the flux tower and the watershed. The NDVI was collected by NEON's Airborne Observation Platform (AOP) in 2021 [60]. We compared the distribution of the NDVI of the footprint to that of the watershed during the flyover period and found them similar (mean 0.89 vs. 0.86, Supplementary 2.4).

Net Ecosystem Production

We estimated NEP from the two downstream NEON locations using *streamMetabolizer* in R, a state-space Bayesian stream metabolism model that gives the best fit of GPP, ER, and air-water gas exchange of oxygen to match modeled and measured dissolved oxygen[61]. We used the NEON measurements of discharge, dissolved oxygen, PAR, and temperature as inputs for the 2020-2021 time frame at the two sensor locations. Average stream channel depth was calculated using the scaling relationships with discharge by averaging the depth we calculated across the entire stream (Equation 2-6 and 2-8). Change in depth at each time step was found by relating the depth to discharge (Equations 2-6). We grouped discharge into 6 bins to associate with binned air–water gas exchange rate ($K_{600;}$ d^{-1}) estimates in the hierarchical modeling framework to decrease the likelihood of equifinality of metabolism parameter estimates and to constrain the air-water gas exchange as a function of discharge[62]. We estimated K_{600} from discharge using the relationship developed from gas exchange experiments run by NEON at the site between the two sensors. We ran the model with 400 warm-up steps after inspecting the traceplots with the rstan package[63, 64] to select when the model began to converge. Stream metabolism was run using the

Bayesian implementation in *streamMetabolizer* by accounting for both observation and processing errors with 2000 saved steps.

After running *streamMetabolizer*, we quality-checked model estimates before assigning NEP values to the stream network model. First, we removed days with biologically-impossible parameter estimates of negative GPP or positive ER. We inspected the Gelman-Rubin convergence statistic ($\hat{R}$) values to assess model convergence and removed days when $\hat{R} > 1.1$ [62, 65]. We plotted the K_{600} vs. ER and K_{600} vs. GPP to check for equifinality; the downstream sensor (sensor 2) displayed equifinality with a relationship between these variables ($R^2 = 0.69$) so we used the results from the upstream (sensor 1) for our estimate ($R^2 = 0.16$). After removing days with incomplete data or data that did not pass our model quality checks, we were left with 367 days of metabolism estimates over the two-year time frame.

We calculated NEP as the difference of the modeled output of gross primary production (GPP) and ecosystem respiration (ER) (Equation 2-5). We estimated NEP across the sampling periods by averaging values from 10 days surrounding the sample week depending on the dates that passed the quality checks described above (July 25-August 22, October 31 – November 23). We then divided NEP by depth across the stream at each point to use in the network model. We assumed that NEP was spatially constant throughout the stream network. We assumed a respiratory quotient of 1 mol C to 1 mol O to convert these oxygen-based estimates to carbon equivalents.

Gas Exchange

The model requires a gas exchange input (k_{600}; m day^{-1}) throughout the stream network. Both the gas exchange experiments conducted by NEON and *streamMetabolizer* provide an estimate for the gas exchange rate. The air–water gas exchange velocity will generally scale with velocity, discharge, and slope and will therefore vary throughout the stream network[34]. To predict this heterogeneity in the air-water gas exchange, we ran the stream network model with nine different regression equations from the literature[20, 51].We confirmed that the values predicted for k_{600} for the regression equations were on the same magnitude as those predicted by *streamMetabolizer* and the NEON gas exchange experiments. We found using the lower limit of the confidence interval of the models produced a better fit and used these equations for the comparison. We selected the equation[51] that provided the best fit (R^2) for August and November for measured pCO_2 compared to the modeled pCO_2 where v is velocity and s is slope:

$$k_{600} = 970 \times v^{0.90} s^{0.80} \quad \textbf{(2-12)}$$

We also selected this equation because it provided the closet values for both August and November to the k_{600} derived from gas exchange experiments performed by NEON at Martha Creek. NEON performed gas exchange experiments with an inert gas (SF_6) at Martha Creek between the two sensor locations from 2018-2021[66]. The experiments were performed during a range of discharge (0.0062 m^3 s^{-1} - 1.30 m^3 s^{-1}), and the relationship between discharge and k_{600} was estimated using a multilevel Bayesian model of exponential decline in SF6 with distance as the downstream model[63, 64]. We compared the k_{600} derived from these gas exchange experiments to the k_{600} predicted by the Raymond model above for the locations between the sensor locations.

We also checked that the k_{600} estimates from *streamMetabolizer* were similar in magnitude to the values we used in the stream network model.

The gas transfer velocity (k_{CO2}; m day^{-1}) was then calculated from k_{600} using a temperature-corrected Schmidt number for CO_2 (sc_t) and a scaling factor of 0.5 [67]:

$$k_{CO_2} = \frac{k_{600}}{(600/sc_t)^{-0.5}}$$

(2-13)

The Schmidt number for CO_2 was calculated from the stream temperature (T; K) measured in the field as follows[50]:

$$sc_t = 1911 - 118.11T + 3.453T^2 - 0.0413T^3$$

(2-14)

Results

Observations

Measured pCO_2 concentrations varied throughout the network in August (13.3 – 282 µmol L^{-1}) and November (14.2 – 230 µmol L^{-1}) with consistently higher concentrations in August (August mean: 61.4 µmol L^{-1}; November mean: 37.3 µmol L^{-1}) (Figure 2.3).

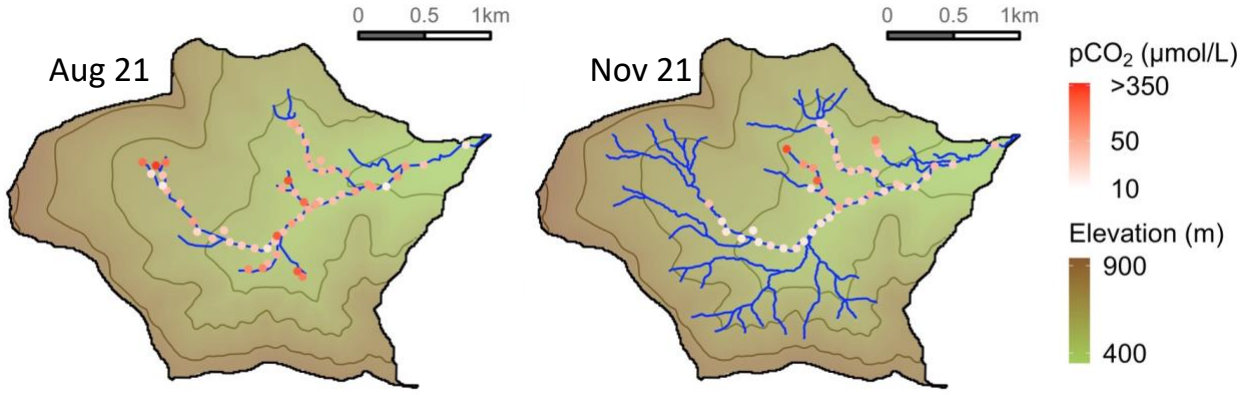

Figure 2.3 Observed pCO2 concentrations in August and November 2021 along the length of Martha Creek. Stream lines were derived from the USGS NHDPlus dataset and adjusted based on field observations.

Over both time periods, higher pCO_2 was more typical in the lower order headwater streams in the network. We define the stream network as a third order stream with the outermost tributaries as first order streams. In November, we noted flow in additional sections of the stream, which we denote "zero order" streams. In August average concentrations for first order streams, second order streams, and third order streams were 109 µmol L^{-1}, 47.2 µmol L^{-1}, and 43.8 µmol L^{-1} respectively. In November, average concentrations for zero order streams, first order streams, second order streams, and third order streams were 87.1 µmol L^{-1}, 48.9 µmol L^{-1}, 22.3 µmol L^{-1}, and 24.9 µmol L^{-1}, respectively.

Other sampling variables changed between the two sampling periods. Median DIC concentration was higher in August (22.5 mg C L^{-1}) compared to November (18.5 mg C L^{-1}). Median total alkalinity was also higher in August (0.50 meq L^{-1}) compared to November (0.35 meq L^{-1}). This increase corresponds with the higher pCO_2 observed in August. Higher pCO2 could be due to deeper flow paths with high pCO_2 and DIC concentrations dominating under low flow conditions as well as dilution of higher concentrations during high flow conditions in November[7, 14, 68].

Median DOC concentration in August (0.19 mg C L^{-1}) was lower compared to November (3.0 mg C L^{-1}). DOC has been observed to dominate when shallow flow pathways dominate and under increased flow[69, 70].

November had a much higher discharge compared to August (1.9 vs. 0.005 m^3 s^{-1}). Cumulative stream length was longer (19.2 km vs. 7.9 km) in November due to flowing intermittent/ephemeral channels (Figure 2.3). The stream area represented a small amount of the total area of the watershed over both sampling periods (0.01 km^2, 0.9% in August and 0.04 km^2, 1.23% in November). The November sampling period occurred during a storm based on the hydrograph for Martha Creek, while the August sampling period represented an annual low for the stream (Figure 2.2).

Gas transfer velocity (k_{600}) as a Model Input

The gas transfer velocity (k_{600}) varied with the method selected and proved to be an important input into the model. Depending on the regression selected, the total emissions from the stream network ranged from 0.031-0.051 Mg C day^{-1} in August and 1.10-1.42 Mg C day^{-1} in November. (Raymond et al. (2012)[51] Equation 2 predicted the lowest emissions and the Ulseth et al. (2019)[20] equation predicted the highest emissions, Table 2.3). The choice of model also affected the range of k_{600}, especially the maximum values. In August the maximum k_{600} value ranged from 50.8 – 109.1 m day^{-1}, and in November the maximum k_{600} value ranged from 355-983 m day^{-1} depending on the model selected (Supplementary Figure 2.5). The fit of the modeled pCO_2 compared to the measured pCO_2 (R^2) ranged from 0.13-0.27 for August and 0.58-0.61 for November depending on our selection of k_{600} (Supplementary Table 2.1).

We also compared the resulting k_{600} for the preliminary model created from gas exchange experiments at Martha Creek for the reach between the NEON sensor locations. The sensors were located near the outlet of the stream network in an area with a lower slope, greater width, and greater discharge than much of the stream. For example, the average slope between the sensors is 0.04 compared to 0.25 over the entire stream length. The gas-exchange values predicted by the gas exchange experiments are specific to the sensor locations and cannot be directly compared to the gas-exchange derived from regression relationships over the entire stream length. We compared the results of the gas exchange experiments to the results of the regression relationships between the sensor locations (Table 2.3). We selected the Raymond et al. (2012) Equation 3 (Equation 2-11 in this paper) for the stream network model because it provided the closet fit for both August and November to the k_{600} derived from gas exchange experiments performed by NEON at Martha Creek, in addition to having the best fit of the modeled pCO_2 compared to the measured pCO_2 (R^2).

Table 2.3 Comparison of Regression Relationships to NEON Gas Exchange Experiments at the NEON reach.

Model	k_{600} Mean (m day^{-1}) between Sensor Locations	
	August	November
Raymond et al. (2012) Equation 1	7.54	110
Raymond et al. (2012) Equation 2	10.1	NA
Raymond et al. (2012) Equation 3	8.21	62.2
Raymond et al. (2012) Equation 4	10.3	55.0
Raymond et al. (2012) Equation 5	12.9	95.0
Raymond et al. (2012) Equation 6	9.23	56.4
Raymond et al. (2012) Equation 7	12.9	96.2
Ulseth et al. (2019)	14.3	176
NEON Gas Exchange Experiments	0.30	1.43
Stream Metabolizer	0.84	51.2

The regression relationships consistently predict higher gas transfer velocities than calculated from the NEON gas exchange experiments at the sensor locations or estimated using the stream metabolizer model.

Stream network CO_2 flux

Modeled pCO_2 concentrations ranged from 13.3-610.2 µmol L^{-1} in August and 14.2-689.7 µmol L^{-1} in November (Figure 2.4). In both months, concentrations were highest at the uppermost network sites we sampled; we set the concentrations of these sites equal to the groundwater concentration observed in the wells in the model (August: 610.2 µmol L^{-1}, November: 689.7 µmol L^{-1}). After the initial groundwater input, concentrations quickly leveled off throughout the rest of the stream network. We compared the modeled concentrations to the measured concentrations; the model fit in August was poor (R^2 = 0.23) and slightly better in November (R^2 = 0.61) (Figure 2.5). The preliminary model underestimated emissions in August and overestimated emissions in November.

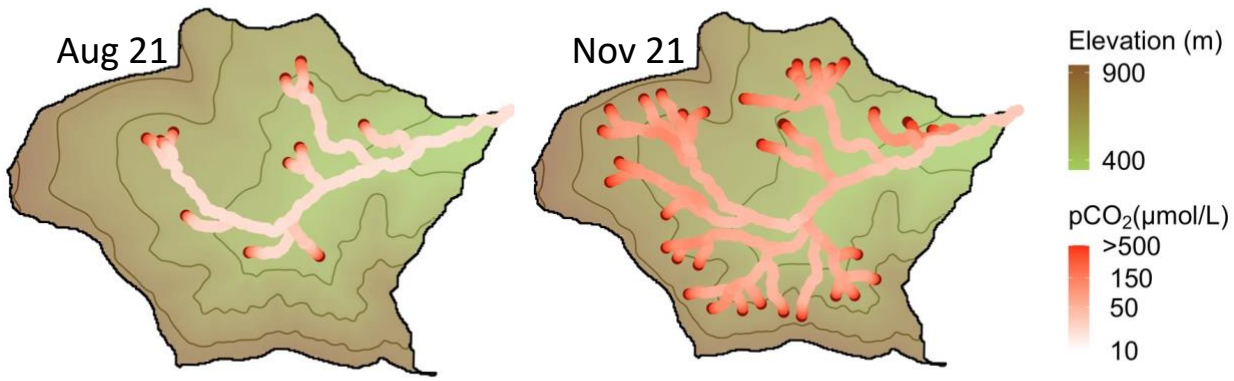

Figure 2.4 Initial Non-Adjusted Model results for August and November.

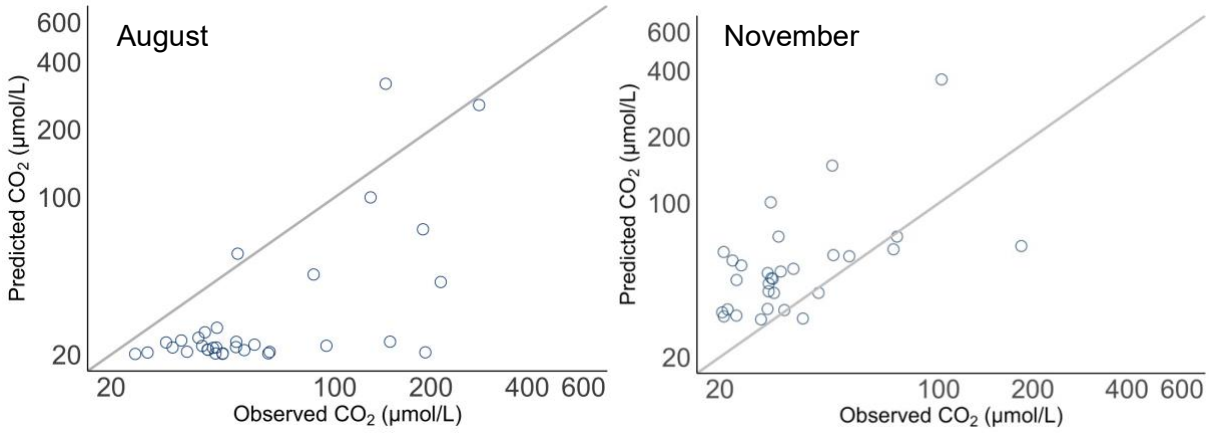

Figure 2.5 Observed (measured) vs. predicted (modeled) pCO2 concentrations for August (left) and November (right) using the non-adjusted modeling approach (Figure 2.4) Line is 1:1.

A model with measured concentrations as inputs provided better predictions than the ones ran without the measured data. We set model points with a matching sample point equal to the measured pCO_2 values and ran the model for both time periods (Figure 2.6). The adjusted stream network model with these additional inputs was used to predict the total carbon emissions from Martha Creek during both sampling periods (Figure 2.6) as well as an areal flux from each network point (Figure 2.7). We compared the total carbon emissions from the preliminary model runs to the adjusted model with the measured concentrations (Supplementary Table 2.2). The adjusted model predicted an increase in total carbon emissions from the preliminary model for August (415% increase) and a decrease for November (12.2% decrease).

Carbon emissions varied with stream order. Zero order streams had a mean flux of 62.7 g C m^{-2} day^{-1} in November, and first order streams had a mean flux of 3.7 g C m^{-2} day^{-1} in August. This compares to a mean flux of 42.8 g C m^{-2} day^{-1} in November and 2.9 g C m^{-2} day^{-1} in August across the entire stream length.

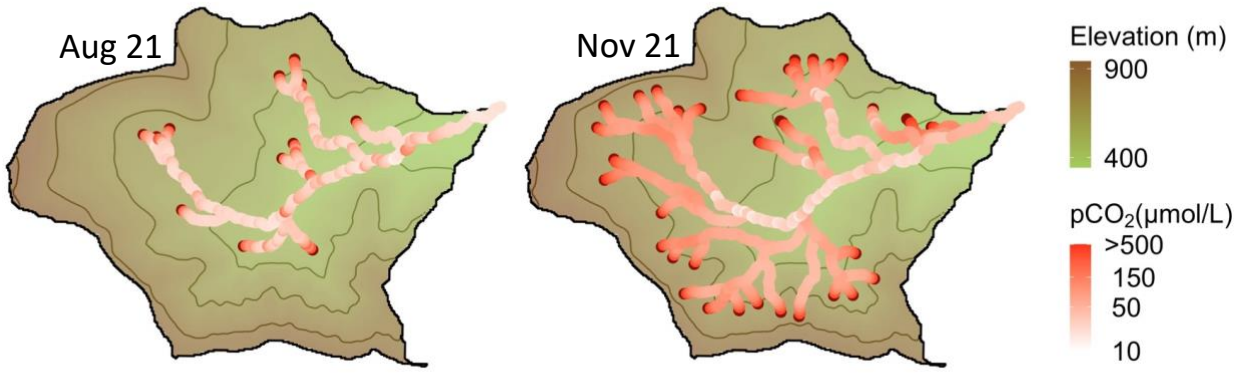

Figure 2.6 Adjusted model results pCO2 for August and November.

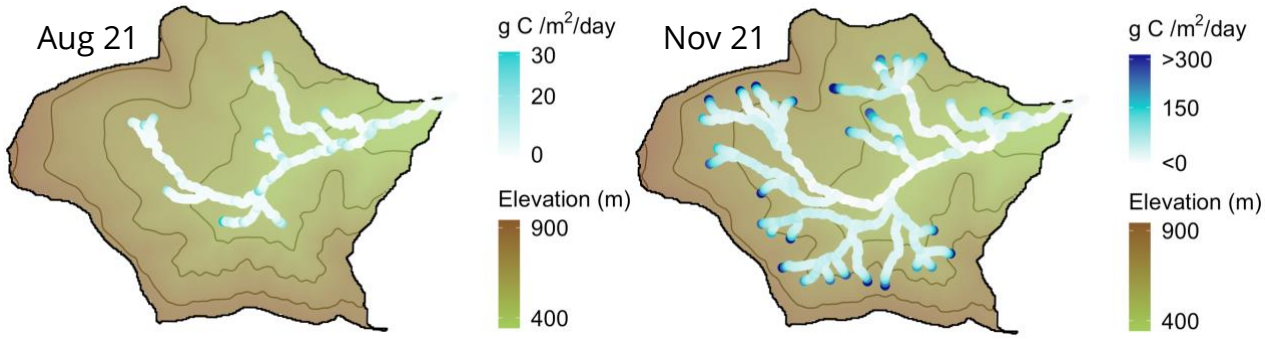

Figure 2.7 Carbon emissions at each point along the stream in August and November.

The modeled rate of in-stream metabolism in Martha Creek represented a small portion of the total carbon emissions from the stream (0.41-1.1 g CO_2 m^{-2} day^{-1}). The in-stream metabolism represented 0-10% and 0-3% of the total pCO_2 predicted by the stream network model in August and November, respectively.

CO_2 emissions from the stream network were a large fraction (54%) of watershed NEE in November and a small fraction in August (Table 2.4). In August, the average daily NEE from the terrestrial environment was -5.5 Mg C day^{-1} compared to 0.034 Mg C day^{-1} emitted by the stream network. Thus, stream emission accounted for only 0.62% of watershed NEE in August. In

November, the average daily NEE was -2.2 Mg C day^{-1} compared to 1.2 Mg C day^{-1} emitted by the stream.

Table 2.4 Total Carbon Emissions and Emission Comparison

Month	Location	Total C (Mg C day^{-1})[b,c]	Mean flux (g C m^{-2} day^{-1})	Median Flux (g C m^{-2} day^{-1})
August	Stream network [a]	0.034 [0.030-0.053][d]	2.86	1.00
	Watershed	-5.5	-0.67	0.10
November	Stream network [a]	1.22 [1.03 -1.47][d]	42.8	29.5
	Watershed	-2.2	-0.35	0.50

a. A mean gas transfer velocity (k_{600}) of 31.0 m day^{-1} (August) and 96.3 m day^{-1} (November) was used for predicting the C emissions from the stream.
b. A stream network area of 0.01 km^2 (August) and 0.04 km^2 (November) was used to scale the mean flux and determine the total C emissions per day from the stream.
c. A watershed area of 6.2 km^2 was used to scale the mean flux and determine the total C removal per day from the watershed.
d. 95% confidence interval for the stream network model emissions estimates. A description of how these values are obtained in included in the Supplementary Information (Supplementary Table 2.3).

Discussion

Combining our observations and the stream network model we found:

- The November time period had a much greater total carbon emissions from the stream network than the August time period (1.22 Mg C day^{-1} vs. 0.034 Mg C day^{-1}).
- The November time period had a much higher discharge (1.9 m^3 s^{-1} vs. 0.005 m^3 s^{-1}) and a larger cumulative stream network area (0.04 km^2 vs 0.01 km^2) than in August.
- In November, the highest pCO_2 concentrations were near the network origins, while in August high pCO_2 occurred in higher order streams.
- In November, the stream emissions accounted for a much larger percentage of the terrestrial sink than in August (54% vs. 0.62%).

Seasonality of Carbon Emissions

Despite the pCO_2 hotspots observed in August, the November time period had a much greater total carbon emissions from the stream network than the August time period (1.22 Mg C day^{-1} vs. 0.034 Mg C day^{-1}). We identify two factors contributing to the greater emissions: (1) a larger stream network length and area in November, and (2) a greater discharge in November leading to both higher CO_2 inputs and gas exchange rates.

Increased stream network area increased carbon emissions. In November, stream network area was 4 times higher than is August (0.04 km^2 vs. 0.01 km^2). The greater surface area increased the opportunity for carbon emissions because total network emissions are equal to areal flux times the surface area of the stream network. Additionally, with an increase in reach length, November had more headwater locations that receive the direct input of high concentration pCO_2 groundwater (Figure 2.3). Martha Creek was composed of 53% of zero order streams in November compared to 42% of first order streams in August by length.

Additionally, an increase in discharge contributed to an increase in carbon emissions. In November stream flow was 380 times greater than in August (1.9 vs. 0.005 $m^3\ s^{-1}$). This large increase in flow has significant implications for the total carbon emissions from the stream. Flux is calculated as a function of the gas transfer velocity, which was ~3 times larger on average in November than in August (96 vs. 31 m day^{-1}). The gas transfer velocity is calculated as a function of stream velocity in the model; the stream velocity was ~6 times larger on average in November than August (0.32 ± 0.2 m s^{-1} vs. 0.053 ± 0.05 m s^{-1}). Higher flows also represented increased hydrological connection with terrestrial soils, thus increasing CO_2 delivery to the stream.

Quantifying these seasonal variations is necessary for understanding the overall carbon flux from headwater streams, and these variations will likely differ between ecosystems. Crawford et al. (2017)[14] found the influence of seasons on pCO_2 concentrations varied substantially among six headwater catchments in different ecosystems with baseline concentrations varying 12-44%. Studies have also observed pCO_2 responses to increasing discharge from storm events vary between ecosystems with storm events both increasing and decreasing concentrations[14, 27]. Seasonal carbon emission variations covary with changes in groundwater inputs and in-stream respiration[15, 71]. Our results demonstrate the importance of considering not only the spatial but also the temporal changes in carbon accounting of headwater streams, especially in climates with distinct dry and rainy seasons.

Stream Network Model

The non-adjusted stream network model did not capture all of the concentration variations observed in the stream. The model predicted high pCO_2 at the headwaters of the network followed by rapid decays within ~10^1-10^2 m of the stream origins. Our observations indicate there are additional inputs in the stream network the original model is not accounting for, particularly in August under low flow conditions (Figure 2.5). The model assumes a constant input of groundwater into the stream network at each point. We hypothesize that this assumption is an oversimplification and that these additional inputs are from hotspots of higher groundwater inputs. Previous studies show that groundwater inflows can result in a pulse of pCO_2 followed by a sharp decrease in concentrations[7, 13, 17]. These inputs are most likely groundwater derived; in-stream primary production is typically not the dominant source of pCO_2 in small streams relative to external inputs[18]. The rate of NEP in Martha Creek was modeled as 0.41-1.1 g CO_2 m^{-2} day^{-1},

which accounted for 0-10.3% and 0-2.57% of the pCO_2 predicted by the stream network model in August and November, respectively. At points of higher measured pCO_2 concentrations within the network in August, we see indicators that these locations are receiving groundwater inputs indicated by lower temperature (14-32% difference) and changes in specific conductivity (9-70% difference) compared to the surrounding points (Supplementary Figure 2.6).

The stream network model does not incorporate carbonate equilibrium. We assumed that additional CO_2 inputs from speciation would be small at alkalinities >2 meq/ L^{-1} [19, 38], which was recorded at all sample sites in both August and November. At a higher pH (7 or higher) pCO_2 and H_2CO_3 dissociates into its ionized form and can reduce the rate of CO_2 emissions to the atmosphere[72]. We observed a lower pH in the groundwater (5.6-6.0 in August and 6.1-6.2 in November) compared to the stream water (median 7.0 in August and 7.2 in November). We acknowledge the model may be missing this removal of pCO_2 from carbonate equilibrium, although incorporating the measured pCO_2 concentrations into the model could provide this adjustment.

The models that included the measured pCO_2 concentrations as inputs had carbon emissions 415% higher from the stream network in August and 12.2% lower from the stream network in November. In November, we were unable sample up to the origins of the stream network in many instances due to the terrain and conditions (Figure 2.3). It is possible we missed points with higher pCO_2 concentrations than the model predicted at these locations that would elevate network emissions estimates. However, the samples in November had less variation in the main stem of the stream and fewer hotspots than in August. This pattern could be caused by increased gas evasion with higher flow[14, 27]. Many of the measured concentrations were lower than the

modeled concentrations in November; this fact could be due to dilution by overland flow and direct precipitation during the November storm event, which would likely be lower in dissolved pCO_2 [13]. Deeper flow paths with high pCO_2 concentrations may have dominated stream network inputs under low flow conditions in August[7, 14, 68].

Saccardi and Winnick (2021)[38] found the stream network model had a tighter model-data relationship ($R^2 = 0.70$) at the East River watershed in the Colorado Rocky Mountains in their study then we found in the Martha Creek watershed. The study was conducted at the East River watershed during higher flow (1.23-3.25 m^3/ s^{-1}). The stream network model appears to predict pCO_2 with more accuracy during high flow conditions (at Martha Creek $R^2 = 0.23$ in August and $R^2 = 0.61$ in November) than during base flow when higher groundwater inputs may be less dominant due to overland flow and higher gas exchange.

Impact of Gas Transfer Velocity

Accurately characterizing the gas transfer velocity (k_{CO2}) and the air–water gas exchange velocity (k_{600}) is challenging and has implications for the total carbon emissions calculated from Martha Creek and other headwater streams. The air–water gas exchange velocity varies spatiotemporally in headwater streams with surface water turbulence[34, 37, 51]. Generally, air–water gas exchange velocities scale with discharge, flow velocities, and slope[51]. As a result, air-water gas exchange has the potential to change greatly during different flow regimes at a site.

Regression predictions for k_{600} [20, 51] were much higher than those measured by the NEON gas exchange experiments within the NEON reach (Table 2.3). While we are unable to compare measured values to the gas-exchange upstream of the sensors, it is possible that the regression

equations are also overpredicting the gas transfer velocities, leading to the discrepancy we see between the modeled and measured pCO_2. Our prediction of the k_{600} has implications for our understanding of carbon emissions from streams. Depending on which regression we chose, the total emissions from the stream network ranged from 0.031-0.051 Mg C day^{-1} in August and 1.20-1.42 Mg C day^{-1} in November.

Small streams have high variability in the gas transfer velocity within a reach[21, 37, 73, 74]. With these spatial heterogeneities, scaling these velocities has proven difficult; with widely used regression relationships overestimating the gas transfer velocities in a headwater stream at higher stream velocities and underestimating the gas transfer velocities at lower stream velocities[34]. Temporally, discharge has a positive relationship with gas exchange (k_{600})[21, 22, 36], although increased flow can decrease gas exchange if turbulence declines[37]. It is clear that gas-exchange is highly localized both among sites and within a site. The prediction of the gas transfer velocity is a limitation in this study and in nearly all research attempting to predict carbon flux from streams at scales where direct measurements are not possible.

Implication for Total River and Landscape Carbon Emissions

Our work shows how seasonality drives huge variation for carbon emissions in a headwater stream network, especially in a climate characterized by wet and dry seasons. When Martha Creek had high flow, carbon emissions from the stream network were > 26 times greater per day than when the stream is under low flow conditions. In the Pacific Northwest, these higher flow conditions are typical in headwater streams in November through March, while drier conditions prevail through the summer months. We also noted the importance of the size of the stream reach for carbon emissions; cumulative stream network length in November was larger than in August

(19.2 km vs 7.9 km) which in turn increased the total carbon emissions from the stream network (1.22 vs 0.034 Mg C day^{-1}). This increase in stream area has implications for carbon accounting in this region and other regions with intermittent streams.

These longitudinal and lateral stream size changes, which were calculated as a function of stream area, can strongly affect the amount of carbon emissions from a stream. Headwater stream locations and extents are often not well documented because they are usually based on topographic maps with limited spatial accuracy[25, 75]. Many of these streams are also not correctly classified as perennial (flowing year round), intermittent (flowing for part of the year with sustained groundwater inputs), or ephemeral (flowing in direct response to precipitation)[25, 26]. These nonperennial stream lengths constitute most headwater stream length in forested areas[25]. Many of these streams expand and contract seasonally in response to runoff and evapotranspiration[24]. Topographic maps tend to overestimate streamlines in temperate regions and underestimate streamlines in arid regions[76, 77]. The NHDPlus streamlines used in this study to define the streamlines overestimated the Martha Creek stream network area and were adjusted based on field observations. Future work should focus on examining how the accuracy of headwater stream locations and extents affects carbon emission predictions in watersheds in different ecosystems.

In this study, we assume that the dry streambeds at Martha Creek do not contribute carbon emissions to the atmosphere. However, dry streambeds of temporary streams can be active sites of CO_2 release to the atmosphere, although emissions are generally lower than flowing waters[78, 79]. We acknowledge these emissions may be missing from this study, particular during the August time period, but our focus was on flowing waters. Globally, carbon emissions estimates

from streams may underestimate emissions by not including dry streambed emissions; however, emissions may also be overestimated by assigning streams with intermittent flow to be permanent[79].

In addition, terrestrial NEE was lower in winter (85% lower in November than August), further increasing the importance of these stream network emissions in the winter months when comparing to the terrestrial sink. On the west coast of the United States, this decreased terrestrial NEE typically occurs during winter months, which are also characterized by increased precipitation and flow and reduced incoming solar radiation.

During both seasons, pCO_2 was highest at the headwaters of the stream network, consistent with past studies[17, 38, 80]. In August, pCO_2 also peaked in higher-order stream segments in addition to the headwaters. We hypothesized that these higher concentrations are due to additional groundwater inputs that become more prevalent at lower flow, combined with low gas transfer velocities due to the low flow. Despite these higher inputs, total carbon emissions were 97% lower in August. The size of the stream network length and flow (both higher in November) proved to be the most important factors for emissions. These higher inputs also indicate that single point measurements likely do not capture the heterogeneity of pCO_2 in headwater streams. Integrating a single measurement over multiple stream orders and through time may result in grossly underestimated or overestimated carbon emissions derived from the stream.

Conclusions and Next Steps

Quantifying carbon emissions from headwater streams presents ongoing challenges especially with regards to stream network spatiotemporal heterogeneity. Our results highlight the

importance of considering heterogeneity on both spatial and temporal scales. Headwater locations were consistent hotspots during two seasons, while other locations in higher stream orders emerged as hotspots during low flow season. Stream network models represent a powerful approach to accounting for this heterogeneity, although quantifying the gas transfer velocity remains difficult and drives high uncertainty in emissions estimated.

Our results also demonstrate the need to understand the nonperennial nature of streams when calculating carbon emissions. Many current estimates of carbon emissions from headwater streams depend on stream network maps derived from topographic data and geospatial products[3, 9, 81]. Fritz et al. (2013)[76] found that flow classification (perennial, intermittent, and ephemeral) from existing geospatial products only agreed with 50% of their field determinations across 300 headwater streams. These static products do not always represent the variability in stream network reach[82]. Increasing stream network area contributed to the 3500% increase in CO_2 emissions in the winter. The stream network can emit a large percentage of the forest NEE in the winter months because of both higher emissions and lower forest NEE and annual estimates of stream network emissions must therefore consider the flow regime throughout the year. Future work should focus on how stream permanence combined with seasonality influences carbon emissions in other ecosystems.

Acknowledgements

We thank Abby Nesper, Hazel Sanders, Benjamin Lloyd Miller, Anthony Stewart, Fenix Garcia Tigreros, and Gabriel Wisswaesser for field and laboratory support. We also thank Kenneth Bible, Benjamin Vierra, Matt Schroeder, Chris Burton, and Alex Keithline for help with site

access to the Wind River Experimental Forest. This work was supported by the National Science Foundation (Award #1926426).

Open Research

Additional information about this work is available in the Supplemental Information. The stream network model code is available in the Github repository Martha Creek Stream Network Model published on Zenodo available at https://doi.org/10.5281/zenodo.7651398 [83]. Additional data are available on the Environmental Data Initiative repository at https://doi.org/10.6073/pasta/556872ebc0fdb9dde5b0fddf4e778378 [84].

Supplementary Information

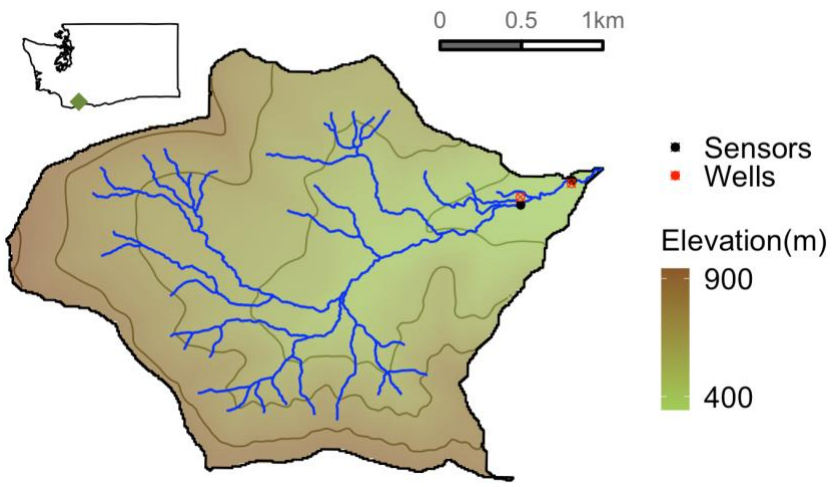

Figure S2.1. Map of Wells 3 and 6 used for groundwater data in the Wind River Experimental Forest**.**

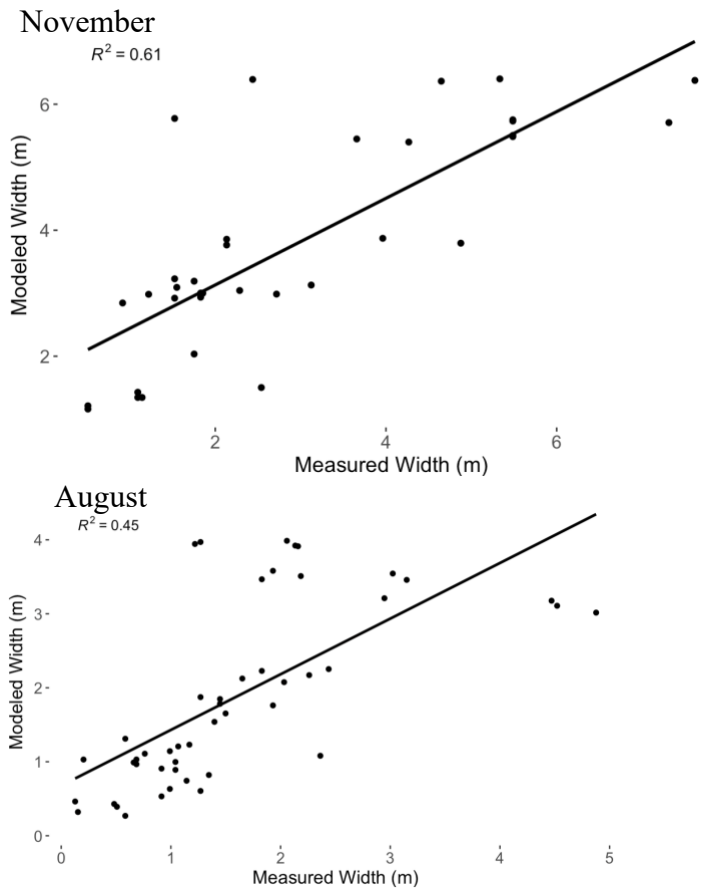

Figure S2.2. Measured widths compared to modeled widths.

Figure S2.3. Temperature and stream order used in the stream network model. Determined as average temperature measured for each order in field.

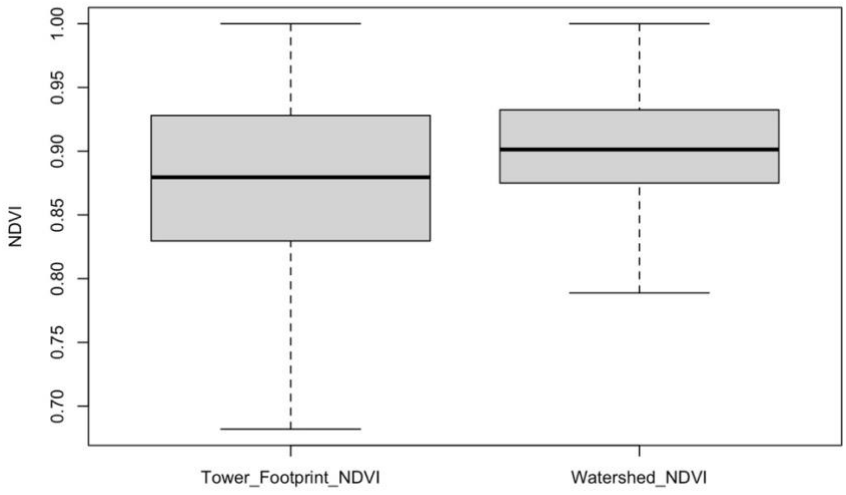

Figure S2.4. Distribution of the NDVI of the footprint of the eddy flux tower compared to the distribution of the NDVI of the Martha Creek Watershed.

August

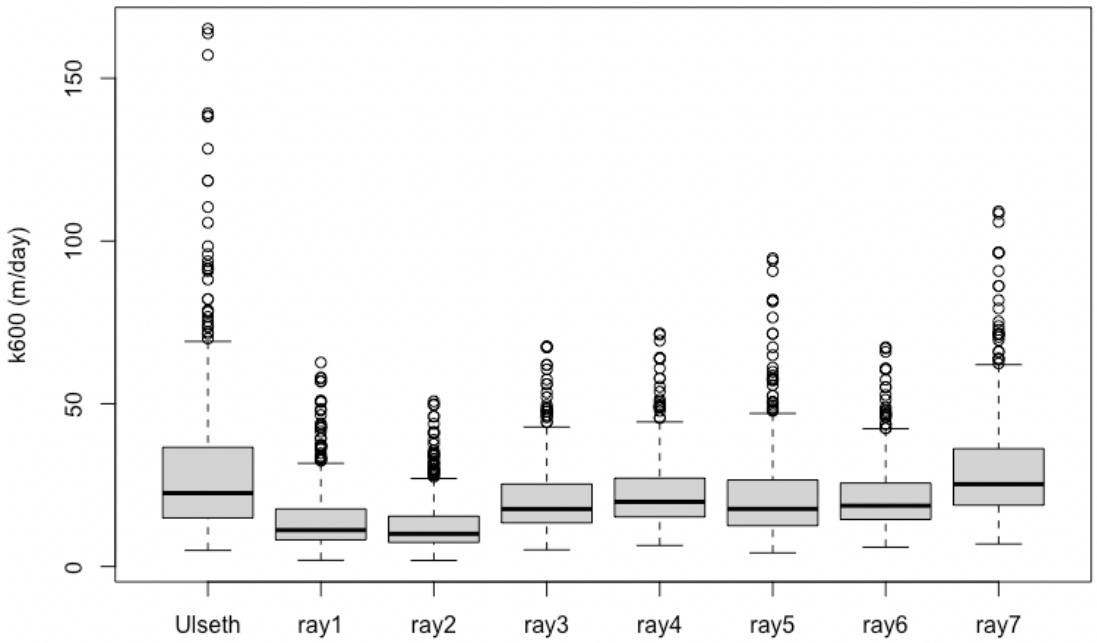

November

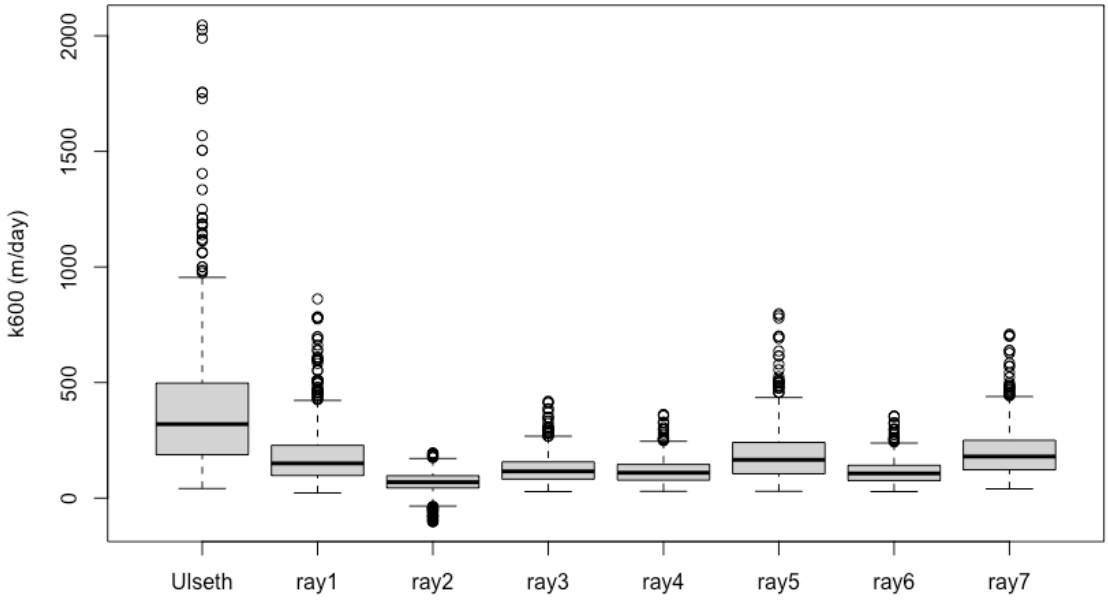

Figure S2.5. Range of values found for the gas transfer velocity (k600) for both August and November for the multiple regression relationships tested where ray are the seven equations from Raymond et al. (2012)[51] and Ulseth is from Ulseth et al. (2019)[20].

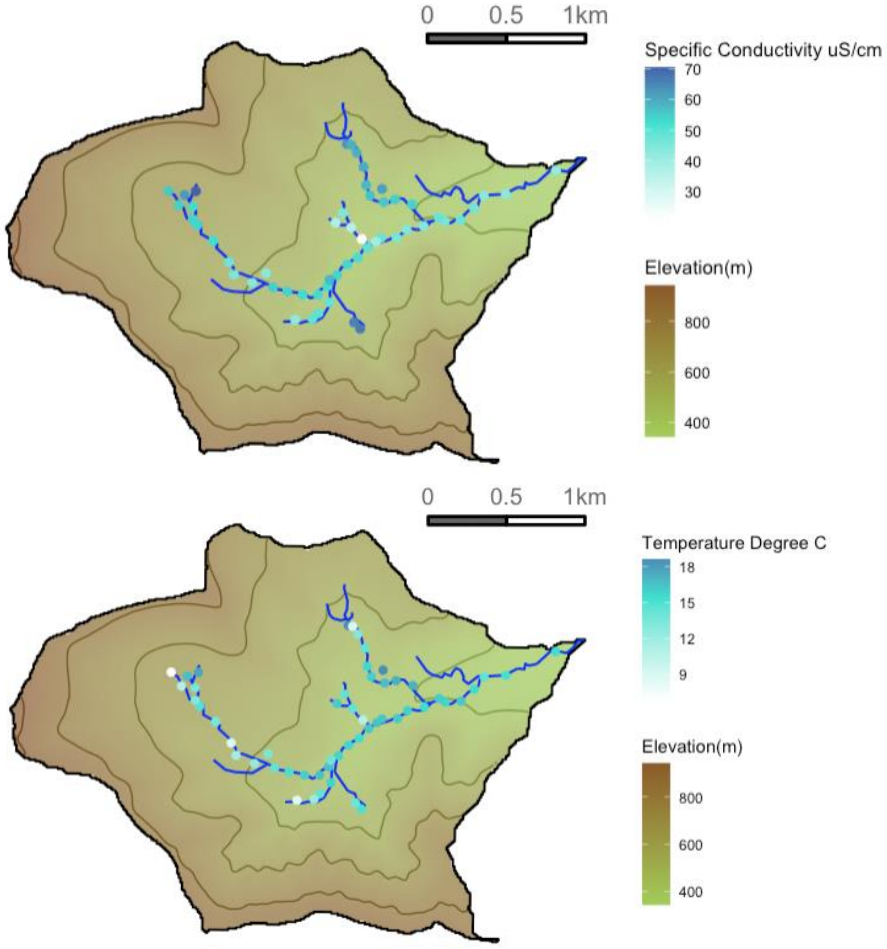

Figure S2.6. Map of measured specific conductivity and temperature in August 2021.

Regression Model	Fit of model pCO_2 compared to measured pCO_2 (R^2)	
	August	November
Raymond et al. (2012) Equation 1	0.19	0.61
Raymond et al. (2012) Equation 2	0.23	NA[1]
Raymond et al. (2012) Equation 3	0.23	0.61
Raymond et al. (2012) Equation 4	0.13	0.61
Raymond et al. (2012) Equation 5	0.14	0.60
Raymond et al. (2012) Equation 6	0.16	0.59
Raymond et al. (2012) Equation 7	0.15	0.61
Ulseth et al. (2019)	0.13	0.58

1. This relationship predicts $-k_{600}$ with high discharge.

Table S2.1. Fit of model pCO_2 compared to measured pCO_2 (R^2) for different regression equations.

	Mean gas transfer velocity (k600, m/day)	**Stream Network Area (km^2)**	**Total C (Mg C /day)**	**Mean flux (g C /m^2/day)**	**Median Flux (g C /m^2/day)**
August	31.0	1.40	0.0066	1.48	0.37
Adjusted August	31.0	1.40	0.034	2.86	1.00
November	96.3	3.25	1.39	45	30.3
Adjusted November	96.3	3.25	1.22	42.8	29.5

Table S2.2. Total Carbon Emissions and Emission Comparison between Model Run

	August (Mg C day^{-1})		November (Mg C day^{-1})	
Variable	Lower (5)	Upper (95)	Lower (5)	Upper (95)
Groundwater pCO_2	0.033	0.035	1.18	1.26
NEP	0.033	0.035	1.21	1.22
Gas exchange	0.031	0.051	1.07	1.42
All variables	0.030	0.053	1.03	1.47

Table S2.3. Uncertainty of Carbon Emissions from Stream Network Model determined based on Input Variables

To determine the uncertainty of carbon emissions from the stream network model, we ran the model by varying the three input variables: groundwater pCO_2, net ecosystem production (NEP), and gas exchange between their lower and upper bounds. We also ran the model with all of the lower bounds and all of the upper bounds to determine the uncertainty with all variables. The uncertainty of groundwater pCO_2 was determined based on measurement replicates. The uncertainty of net ecosystem production was reported by the program streamMetabolizer. The uncertainty of the gas exchange was determined by running the regression model that produced the lowest emissions (Raymond et al. (2012)[51] equation 4) and the highest emissions (Ulseth et al. (2019)[20].

Chapter 3 Hydrologic regimes shape stream network CO_2 dynamics and emissions

Hydrologic regimes shape stream network CO_2 dynamics and emissions

Hannah Conroy[1], Erin R. Hotchkiss[2], Frances M. Iannucci[2], Ashif H Abir[5], Kaelin M Cawley[3], Keli Goodman[3], Robert Hensley[3], Jeremy B. Jones[4], Kristin Kraus[4], Wilfred M. Wollheim[5], David Butman[1]

[1]University of Washington

[2]Department of Biological Sciences, Virginia Polytechnic Institute and State University

[3]National Ecological Observatory Network, Battelle

[4]Department of Biology and Wildlife and Institute of Arctic Biology, University of Alaska Fairbanks

[5]Department of Natural Resources and the Environment, University of New Hampshire

Key Points

- A disproportional amount of stream carbon emissions and export occur during high discharge periods
- Accounting for stream permanence results in small changes in total annual emissions
- CO_2 sensors will be limited in their representative of entire headwater stream network

This chapter is in prep to submit to Global Biogeochemical Cycles:

Conroy, H. D., Hotchkiss, E. R., Iannucci, F. M., Abir, A. H., Cawley, K. M., Goodman, K., Jones, J. B., Kraus, K., Wolheim, W. M., Butman, D. (2025). Hydrologic regimes shape stream network CO_2 dynamics and emissions [in prep].

Abstract

Understanding the balance between terrestrial carbon sequestration and aquatic carbon exports and emissions is crucial for assessing landscape carbon budgets. Headwater streams are hotspots of carbon emissions, often exhibiting higher rates of exchange per unit surface area than surrounding terrestrial environments. However, accurately quantifying and upscaling emissions remain challenging due to their high spatial and temporal variability. Stream carbon dioxide (CO_2) emissions estimates typically rely on static stream network maps derived from topographic data, missing dynamic changes in emissions linked to varying flow conditions. We modeled carbon emissions from five headwater stream networks in different biomes, incorporating stream network extent to account for dynamic flow and a stream network model to account for spatial and temporal variations in CO_2 emissions. We found that while accounting for the extent of the stream network due to drying does not change modeled annual emissions substantially (0.06-4.3%), it does change the timing and spatial distribution of emissions and CO_2 concentrations. When incorporating stream permanence, our predictions for CO_2 concentrations at the network outlet increased by 32%. Across all stream networks, discharge was the main driver of emissions with 50% of carbon emissions occurring in the top 3-29% of discharge conditions. Spatially, areal emissions in first order streams were on average 1.3-2.7 times higher than the remainder of the network due to both high gas exchange resulting from increased slope and from a tight connection to the terrestrial environment and high groundwater concentrations. Our results show that to better estimate annual emissions at a watershed scale, sampling campaigns should focus on spatial and temporal hotspots: headwaters and high discharge events.

Introduction

Accurate accounting of carbon storage and flux in terrestrial ecosystems is essential for understanding the global carbon cycle. While terrestrial ecosystems are often net sinks of carbon dioxide (CO_2), surface waters within the landscapes export carbon, as particulate organic carbon (POC), dissolved organic carbon (DOC), and dissolved inorganic carbon (DIC), downstream to the oceans. Surface waters also emit a large portion of this transported DIC as CO_2 to the atmosphere. Reconciling the magnitude of terrestrial carbon sequestration and aquatic exports and emissions is necessary for determining landscape carbon budgets[85]. Streams and rivers have been recognized as a hotspot of carbon emissions, because they are typically super-saturated in CO_2 relative to the atmosphere and have higher rates of exchange per surface area than the surrounding land[4, 6, 86]. In addition, streams and rivers can emit more CO_2 to the atmosphere than is ultimately exported downstream to the ocean, with headwater streams emerging as hotspots for these emissions because of their connectivity to the terrestrial environment and high turbulence[3, 15].

Estimates of carbon emissions often exclude seasonal dynamics or do not provide differentiation between high and low flow periods[3, 15]. Globally, CO_2 emissions from streams and rivers vary between 112 and 209 Tg of carbon per month[12]. CO_2 emissions from headwater streams can increase during high discharge events, including snowmelt and rainstorms[34, 35, 78]. High discharge events may disproportionately contribute to both emissions and downstream carbon export, with the majority of exports often occurring during a few short high-flow events[21, 34, 87]. Capturing high discharge events can be challenging because they are often sporadic and short lived, and

may be missed during discrete sampling. In addition, sampling during high discharge events can be challenging due to the weather and terrain that often accommodate higher discharge[88].

Seasonal changes in carbon emissions are partially driven by the sources that contribute to in-stream CO_2 concentrations (pCO_2) within a stream network. pCO_2 can be supplied to the stream by groundwater, direct soil pCO_2 in runoff, and in-stream generation from the respiration of external and upstream carbon inputs[17, 18, 28]. Groundwater pCO_2 is typically high (more than four times higher than in the stream) and can be a large source of stream pCO_2 because headwater streams are well-connected to the subsurface where the majority of the streamflow originates[14, 17, 89]. Groundwater inputs into a stream network can be controlled by flow, with higher flow rates leading to greater inputs of high pCO_2 groundwater[21, 22]. Seasonal snow melt can also increase hydrological connectivity to high pCO_2 soil layers increasing pCO_2 within the stream; it can also decrease pCO_2 by diluting gas concentrations[17, 90]. When a stream is ice covered in the winter, higher pCO_2 may also build up from respiration where snow acts as an insulator[91]. In-stream metabolism can also supply a source of pCO_2 to stream networks, although metabolic contributions are usually smaller relative to groundwater inputs, especially in headwaters[18]. Stream metabolism can vary seasonally with changes in temperature, light availability and nutrient availability. All of these drivers can be influenced by discharge, acting to stimulate or suppress metabolic processes through delivery of nutrients or flooding scouring of biofilms[23, 62, 92].

If both the gas exchange velocity and the source of pCO_2 are high, hotspots of CO_2 evasion will emerge[93]. Carbon emissions from headwater streams are also a function of the gas exchange velocity, which scales with discharge and will vary within a network with changes in flow,

turbulence, morphology, and slope[36, 37, 51]. The source of pCO_2 and the gas exchange velocity will vary in space along a stream network, seasonally within a watershed, and across different biomes; this makes estimating overall CO_2 emissions difficult within and across stream networks[37, 88].

Finally, carbon emissions are a function of stream area. Many headwater stream networks expand and contract seasonally in response to runoff and evapotranspiration, so the longitudinal and lateral changes in wetted stream area will alter total carbon emissions from a stream network[248894]. Flow also connects streams longitudinally, laterally and vertically, influencing the delivery of high pCO_2 from groundwater inputs[94]. Additionally, CO_2 emissions can be high during the rewetting processes in dry and disconnected streams, when pCO_2 builds up in the soil and stagnant pools are flushed during precipitation events[94-96]. Headwater stream locations and extents are often not well documented because they are usually based on topographic maps with limited spatial accuracy[25, 75]. Temporary stream lines within headwater streams can comprise more than 50% of the total drainage network length within stream networks[95, 97]. Many streams are also not correctly classified as perennial (flowing year round), intermittent (flowing for part of the year with sustained groundwater inputs), or ephemeral (flowing in direct response to precipitation)[25, 26]. Surface area can also be lost due to winter ice coverage in some biomes[12]. Current estimates of carbon emissions from headwater streams usually depend on stream network maps derived from topographic data and geospatial products, which may not account for changes in stream area during different flow conditions[9, 12, 81]. Accounting for dynamic stream network extent is likely essential for accurately estimating carbon emissions and export from streams.

Few studies to date have explicitly examined the influence of stream permanence on carbon emissions from headwater streams, especially during low flow when stream networks shrink. Additionally, there is a need to incorporate variability in carbon emissions at the event scale and include high-flow periods that yield the highest land to water fluxes. Analyzing carbon emissions seasonally across a range of biomes is critical to identify the heterogeneity of CO_2 emissions in both space and time. In this study, we combine modeled estimates of stream permanence for headwater streams with a spatially explicit stream network model to examine the spatial and temporal controls on annual carbon emissions and export from stream networks in five different biomes with different climate, geology, and topography.

Methods

Stream Networks

We selected five stream networks that each include one stream site monitored by the National Ecological Observatory Network (NEON), a continental-scale observation facility that collects comprehensive standardized aquatic and terrestrial data across a range of ecosystems in the United States (Figure 3.1). The streams were chosen because they had nearby NEON terrestrial monitoring sites and represent a range of climate, geology, and topography (Figure 3.1, Table 3.1). At each stream, NEON collects continuous, sensor-based measurements that includes temperature of surface water and water level used to estimate continuous discharge[98, 99]. The stream networks also have riparian near-stream, shallow groundwater wells equipped with sensors that measure elevation and temperature of groundwater[54, 100]. Grab samples of water chemistry including DOC and DIC are collected by NEON 26 times per year for surface

water[101]. Grab samples of dissolved gas[102], including CO_2, are collected by NEON in conjunction with this water chemistry sampling.

As part of our work to characterize high-frequency pCO_2 dynamics at five streams across different biomes of the U.S., we installed Eosense pCO_2 sensors at the NEON downstream sensor locations from 2022-2023. Data collected at 1-minute frequency were aggregated to 15-minute intervals to reduce noise. Sensor CO_2 concentrations were corrected to match grab samples collected by NEON via linear regression[102]. The relationship between grab sample and sensor CO_2 concentrations was not significant at Martha Creek; therefore, we corrected the sensor data using the average difference between sensor and grab sample concentrations. We also collected additional shallow groundwater samples for pCO_2 to cover a range of flow conditions from the NEON groundwater wells in stream riparian zones. For all sites except Caribou Creek, we sampled wells for pCO_2 using a headspace equilibrium method with a peristaltic pump after the well was flushed the length of the tubing and measurements restabilized (as described in Conroy et al., 2023[88], Text S3.1). At Caribou Creek, groundwater pCO_2 samples were collected from four of the NEON groundwater well sites using a soil sipper needle fit with tubing and an airtight syringe. The soil needle was inserted to thaw depth to retrieve a headspace-free groundwater sample from the active layer and the sample was processed using the same headspace equilibration techniques as the other stream sites.

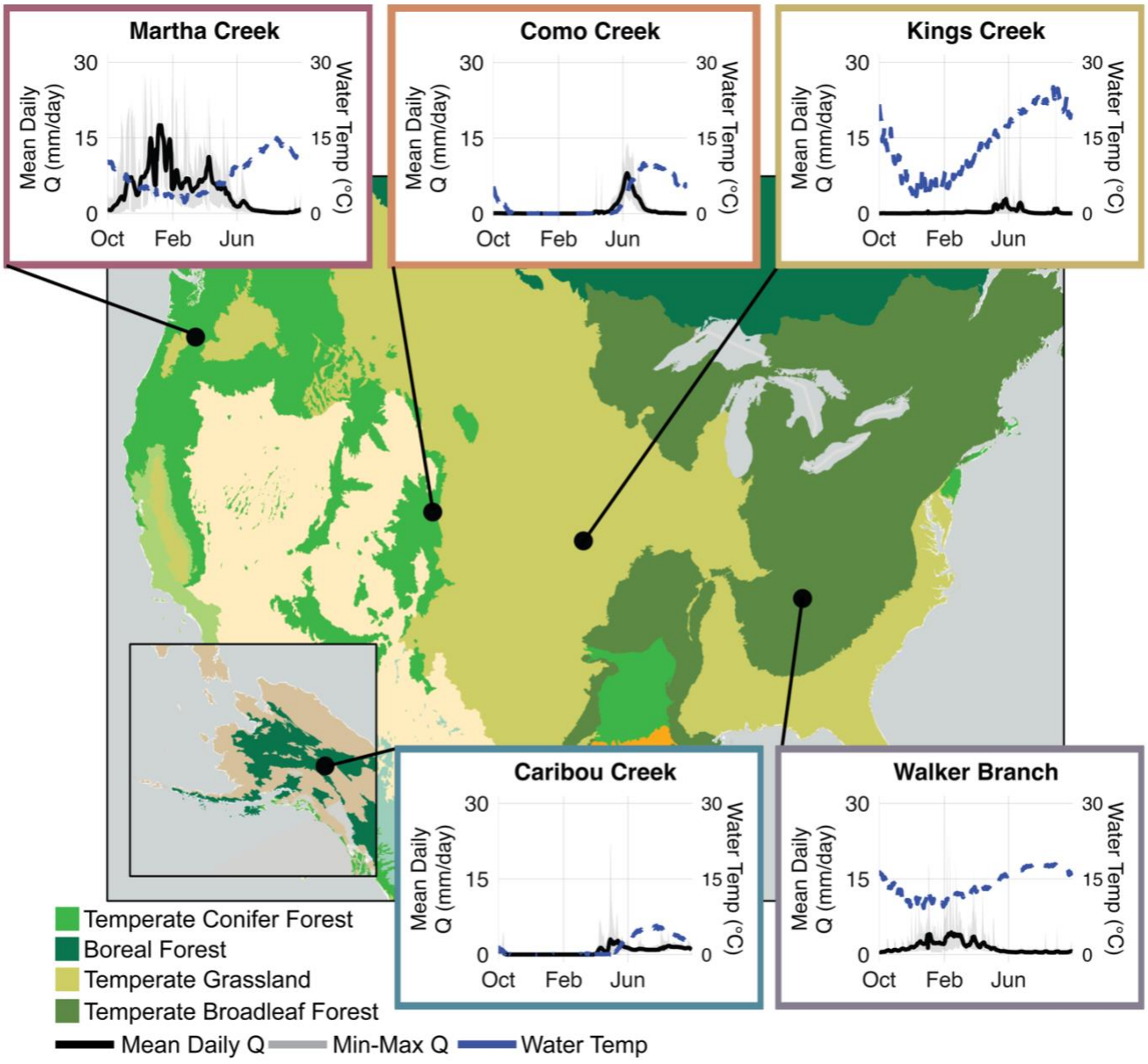

Figure 3.1 Study stream networks located at five National Ecological Observatory Network stream monitoring sites throughout the United States. Plots show the average daily discharge (Q; mean from 2018-2023) for each site over a water year in black with the minimum and maximum discharge from the six-year time period highlighted in grey. Average daily water temperature for the water year shown in blue.

Spatial Variability in Water Chemistry

We conducted synoptic sampling campaigns along three of our five stream networks (Martha Creek, King's Creek, and Caribou Creek) to examine how pCO_2 changes along a stream network and validate our spatial model outputs with measurements. We sampled two of the stream networks twice, (Martha Creek and King's Creek) to capture dynamics during low and high flow and validate the temporal dynamics of our spatial model outputs. Martha Creek was longitudinally sampled over two five-day sampling campaigns (low flow in August 2021 and high flow November 2021) as described in Conroy et al. (2023)[88]. We repeated this sampling campaign at King's Creek (low flow in August 2022 and high flow in May 2023) and at Caribou Creek (for typical summer flow in July 2022). We attempted to capture the high spring flows that typically occur at King's Creek, but we note that spring 2023 was exceptionally dry. Samples were taken at 100m intervals along the stream reach beginning at the NEON sensor location, which we fixed as the outlet of each network model. We took pCO_2 measurements using a headspace equilibrium method described in Text S3.1. Results for the sampling campaigns are shown in Table 3.1. We used these sampling points to compare to our stream network model results. Como Creek and Walker Branch were not sampled due to time constraints.

Table 3.1 Stream Network Comparisons

Stream Network	Location	Elevation (m)	Climate	Mean water temperature (°C) [98,a]	Flow regime	Mean annual precipitation (mm)	Sensor pCO_2 (umol L^1)[a]	Sampling period	Sampling mean discharge (m^3 s^{-1})	# of samples	Longitudinal sampling pCO_2 (umol L^1)[a]
Walker Branch[103] (WALK)	Anderson County, TN	260	Humid Subtropical	13.9 (2.1 – 20.3)	Highest flows in winter and spring	1340	51 (37 – 100)	Not sampled	NA	NA	NA
Martha Creek[41] (MART)	Skamania County, WA	340	Temperate Rainforest	6.87 (-4.1 – 25.4)	Wet winter, dry summers	2330	51 (28 -77)	August 2021	5×10^{-3}	55	61 (13 – 280)
								November 2021	1.9	45	37 (12 – 230)
Caribou Creek[104] (CARI)	Fairbanks North Star Borough, AK	230	Continental subarctic	3.82 (-0.6 – 9.4)	Ice-covered winter streamflow, seasonal snow melt pulse	260	80 (55 – 317)	July 2022	0.2	61	45.0 (17 – 260)
Como Creek[105] (COMO)	Boulder County CO	3020	Continental alpine	3.2 (-0.1 – 13.3)	Ice-covered winter pools, seasonal snow melt pulse	840	59 (18 – 138)	Not sampled	NA	NA	NA
King's Creek[106] (KING)	Riley County, KS	320	Continental Tall-Grass Prairie	15.2 (-0.5 – 32.1)	Flashy and impermanent with high flows during spring rains	860	390 (0 – 810)	August 2022	2.0×10^{-3}	55	240 (93 – 590)
								May 2023	0.08	62	155 (71 – 400)

a. Parentheses indicate range of measured values.

Modeling Stream Permanence

We used the Watershed Erosion Prediction Project Model (WEPP) to predict how surface water presence might change seasonally and with discharge at each of the stream networks[107]. In a previous study, WEPP correctly classified annual streamflow permeance of a stream network for 83% of the reaches in both a humid coastal climate and arid climate in western and southeastern Oregon[107]. The WEPP model is a process-based hydrology model that simulates surface and subsurface hydrology[108, 109]. WEPP requires input of climate, slope, soil, and vegetation and outputs a continuous daily water balance of surface runoff, subsurface lateral flow, evapotranspiration, total soil-water, percolation, and snow accumulation and melt[108]. While we were limited in our observations of surface water presence to validate the WEPP model at our networks, we treated the WEPP model as a basis for exploring how stream networks in different biomes may potentially expand and contract annually.

We ran the WEPP model using WEPPCloud, the online implementation of WEPP[108] (Text S3.2). We manually calibrated the models using realistic values for each ecosystem from the literature (Text S3.3). The best calibration of the WEPP model for each stream network was determined by selecting runs that resulted in the largest Nash-Sutcliffe Efficiency (NSE)[110] and smallest percent bias (PBIAS) when compared to discharge at the NEON gages, using the hydroGOF package in R[99, 111]. We also examined the natural log of NSE (NSE log Q) to give a better metric for model fit during periods of low flow[107]. We kept all runs with NSE values greater than 0.2 and PBIAS values below 25%, as previous modeling studies indicate that these thresholds represent satisfactory hydrological model results[107, 112, 113]. We also chose to keep model runs with the greatest value of log NSE. Hafen et al. (2023)[107] kept model runs with NSE<0.3 by maximizing

log NSE because identifying non-permanent channels depends on accurate simulation of these zero flow periods[113]. We also justify using lower NSE values than those typically used in hydrological models by emphasizing that we employed the WEPP model as a tool for understanding how stream network expansion and contraction influences carbon emissions. The resulting NSE, PBIAS, and NSE log Q for each stream network were determined satisfactory for Martha Creek, Como Creek, Walker Branch, and King's Creek but not Caribou Creek (Table S3.2, Figure S3.1). We were not able to produce a WEPP model for Caribou Creek due to constraints on the data available for running the WEPP model in Alaska. However, we know from field observations at Caribou Creek that the highly incised stream channel likely has minimal expansion and contraction during non-frozen periods and therefore assumed the stream network lines to be constant from May – September. Using the WEPP model for all networks except Caribou Creek, we analyzed daily streamflow estimates for each stream network reach to identify periods when reaches were wet or dry, with zero streamflow indicating a dry reach. This exercise allowed us to obtain a daily estimate of stream network extent for each watershed for 2018-2023 (Figure S3.2).

Stream Network Models

We used the process-based stream network model originally developed by Saccardi and Winnick (2021)[38] and updated by Conroy et al. (2023)[88] using a priori parameterization based on the available NEON field measurements instead of calibration. The network model predicts CO_2 concentrations along each stream network based on the advection-reaction equation for solute transport:

$$\frac{\partial C}{\partial t} = -v\frac{\partial C}{\partial x} + \frac{1}{A}\frac{\partial Q}{\partial x}(C_{gw} - C_i) - k_{CO_2}(C - C_{atm}) + \frac{-NEP}{h}$$

(3-1)

We solved the equation assuming steady state conditions and using a backwards-difference finite approximation scheme at each point along the stream:

$$0 = -v\frac{C_i - C_{i-1}}{\Delta x} + \frac{1}{A}\left(\frac{\Delta Q}{\Delta x}\right)(C_{gw} - C_i) - k_{CO_2}(C_i - C_{atm}) + \frac{-NEP}{h}$$

(3-2)

where the concentration of CO_2 at each point (C_i; µmol m^{-3}) is a function of the concentration upstream (C_{i-1}; µmol m^{-3}), atmospheric and groundwater CO_2 (C_{atm} and C_{gw}; µmol m^{-3}), and internal production represented as stream net ecosystem production (NEP; see below). Additional inputs into the model at each point include the flow at the outlet of the stream network (*Q;* m^3 s^{-1}), velocity at each point (v_i; m s^{-1}), the stream cross-sectional area at each point (A_i; m^2), and the gas transfer velocity at each point *(*k_{CO2}; m day^{-1}).

As in Conroy et al. (2023)[88], we calculated flow at each point (Q_i; m^3 s^{-1}) based on conservation of mass within the drainage basin (Text S3.3). We performed multiple stream network model runs with different flow inputs. We used the WEPP modeled predicted discharge for model runs determining the impact of stream permanence. We also ran the model with daily discharge at the downstream NEON gage to directly compare emissions to carbon exports (DIC, DOC). For King's Creek, we used USGS discharge data for a more complete discharge dataset for the 2018-2023 time period[114].

We estimated the stream cross-sectional area (A, width × depth; m^2) at each point using scaling relationships with width (w) and depth (h) with Q_i [9, 88] (Text S3.4). Velocity was also estimated

using these scaling relationships[9, 88] (Text S3.4). Daily water temperature and daily atmospheric CO_2 were estimated from daily averages of NEON surface water temperature and atmospheric CO_2 isotopes[98, 115].

For the groundwater pCO_2, daily groundwater estimates were derived for each stream network from our project's groundwater sampling during different flow periods and assumed to apply throughout the river network. Groundwater pCO_2 was averaged across wells when multiple wells were sampled and were interpolated using the spline function in R to get a daily estimate (Figure S3.3). Uncertainty for daily estimates were determined using bootstrap resampling, and confidence intervals are calculated as the standard deviation of the bootstrap predictions around the interpolated values. The initial condition for C_i was set to the daily estimate of groundwater pCO_2 for the stream network. Groundwater pCO_2 concentrations were assumed to be constant throughout the stream network on a given day, and concentrations were multiplied by runoff based groundwater inputs of discharge, assuming constant gaining conditions.

For NEP, we used estimates from the literature available for each NEON reach for GPP and ER[116] for Martha Creek, Caribou Creek, Como Creek, and King's Creek. NEP is the difference between gross primary production (GPP) and ecosystem respiration (ER) and is typically negative in streams because ER exceeds GPP when supported by external organic carbon subsidies[55]. It is thus represented here by -NEP to impose a positive CO_2 flux when negative:

$$NEP = GPP - |ER| \quad \textbf{(3-3)}$$

We calculated NEP across the GPP and ER time series from Marzolf et al. (2025)[116]. To reduce uncertainty associated with daily NEP estimates, we ran the stream network models using the

median NEP values from the time series for each reach. To capture uncertainty in our emissions estimates, we used the interquartile range of NEP values, specifically the 25th and 75th percentiles for the lower and upper range of NEP. We assumed that NEP was spatially and temporally constant throughout the stream network, after running checks that our annual emissions would be similar to incorporating daily NEP predictions for networks (Table S3.3). We acknowledge that NEP will change across headwater stream networks in both space and time[117, 118], but our approach attempted to estimate a reasonable metabolism contribution at each stream network.

For Walker Branch, we also obtained minimum, maximum, and median NEP from previous literature in the west fork of the stream network upstream of the NEON reach[119]. We used the Roberts et al. (2007)[119] estimates for our primary model runs at Walker Branch because these estimates better represent the headwaters of the network. Based on observations in the field, the NEON upstream sensor is downstream of a confluence and an actively flowing tributary enters just above the downstream NEON sensor which will bias metabolism estimates[55]. We compared the Walker Branch stream network model runs using the Roberts et al. (2007)[119] metabolism estimates to runs using the Marzolf et al. (2025)[116] estimates to examine how using NEP estimates from different locations within a stream network may affect results.

The stream network model requires a gas exchange velocity input (k_{600}; m day^{-1}) to estimate emissions from concentrations. Gas exchange varies throughout a network because it scales with velocity, discharge, and slope[34]. To account for this heterogeneity in the air-water gas exchange, we ran the stream network model with estimates from eight different physical model regression equations[20, 51] (Figure 3.2). We compared these regression models to gas exchange experiments

performed by NEON. NEON performed gas exchange experiments with an inert gas (SF_6) at each stream network at the NEON reach (between their two sensor locations) from 2018-2021[66]. The experiments were performed during a range of discharge conditions at each NEON reach, and the relationship between discharge and k_{600} was estimated using a multilevel Bayesian model of exponential decline in SF_6 with distance as the downstream model[64, 120, 121]. We compared the k_{600} derived from gas exchange experiments to the k_{600} predicted by the physical regression models[20, 51] for the NEON stream reach between the sensor locations. For each reach, we selected the regression model that resulted in k_{600} values most similar in magnitude to the gas exchange experiments (Table S3.4). When there was a large discrepancy between the two models, we used the equations from the NEON gas exchange experiments[121, 122] for stream segments with slope similar to the NEON sensor location.

The gas transfer velocity (k_{CO2}; m day^{-1}) was then calculated from k_{600} using a temperature-corrected Schmidt number for CO_2 (sc_t) and a scaling factor of 0.5: [51, 67]

$$k_{CO_2} = \frac{k_{600}}{(600/sc_t)^{-0.5}} \quad \textbf{(3-4)}$$

The Schmidt number for CO_2 was calculated from the stream temperature (T; K) as follows: [123]

$$sc_t = 1923.6 - 125.06T + 4.3772T^2 - 0.0857T^3 + 0.00070284T^4 \quad \textbf{(3-5)}$$

Model flow scenarios

We performed multiple model scenarios to 1) test for the impact of stream permanence and 2) to get a best estimate of emissions with measured discharge (Table 3.2). We performed four model

runs at Walker Branch, Martha Creek, Como Creek, and King's Creek, and one model run at Caribou Creek (due to observations in the field that Caribou Creek has minimal expansion and contraction) at daily timescales from 2018-2023. For Caribou Creek and Como Creek, we ran the model from May-September and May-October, respectively, to capture when the stream was not covered by ice. The model scenarios were as follows:

- Modeled discharge static model
- Modeled discharge dynamic model
- Measured discharge static model
- Measured discharge dynamic model

Table 3.2 Description of combined stream network model scenarios

Model Run	Model purpose	Discharge source	Stream lines source	Stream Networks
Modeled-static	Test impact of stream permanence	Modeled by WEPP	WEPP modeled network lines	MART, WALK, COMO, KING
Modeled-dynamic	Test impact of stream permanence	Modeled by WEPP	NHDPlus network lines	MART, WALK, COMO, KING
Measured-static	Test emissions estimates based on measured discharge	Measured at NEON gage	NHDPlus network lines	All
Measured-dynamic	Check WEPP results	Measured at NEON gage	NHDPlus network lines modified based on a threshold of zero flow (0.003 m^3 s^{-1})	MART, WALK, COMO, KING

For the modeled-static scenarios, stream network lines were derived from NHDPlus[39], and we assumed streamlines from the NHDPlus dataset were constant on a daily basis. For the modeled-dynamic scenario, we modified the network lines based on the WEPP model results: when a

streamline from the WEPP model was not flowing, the streamline was not included in the stream network model. We used these two model scenarios a basis for characterizing the role of stream permanence on stream network emissions by comparing the difference between the total annual emissions from each stream network with and without accounting for changing network size.

For the measured-static scenarios, we ran the stream network model using constant streamlines from the NHDPlus dataset. We used this network run to ensure annual emissions estimates based on estimated discharge values were similar to the model runs using modeled discharge. The measured-dynamic scenario was run with measured discharge and a different metric for stream permanence where stream lines were determined to be flowing based on a threshold of zero flow. Using hydraulic geometry, we estimated a discharge value for each stream reach based on the measured discharge at the gage. If this estimated discharge was less than 0.003 $m^3 s^{-1}$, we assumed this stream reach was not flowing. The threshold was based on the minimum daily value a USGS gage can report[124]. There is limited methodology for selecting a zero-flow threshold in the literature[125], so we used this model only to determine if a different stream permanence metric would result in similar results to the modeled-static scenarios. We compared these results with the modeled-dynamic scenarios to ensure similar effect of stream permanence on annual emissions. We found comparing the measured-dynamics scenarios to the measured-static scenarios resulted in similar percent difference between annual emissions estimates to comparing the modeled-dynamic run and the modeled-static run (Table S3.5).

To run the stream network model, networks were broken into points ~20 m apart (Equation 3-2). Stream slope at each point was calculated from a digital elevation model of the area[40, 126]. Table 3.3 includes a description of each variable used in the model for each stream network.

Table 3.3 Daily average range of model inputs for each stream network

Variable	Description	Spatial variability across network	WALK	MART	CARI	COMO	KING	Data source
$\boldsymbol{T}$	Water temperature (°C)	Constant	9.2 – 18 (14)	2.2–15 (6.7)	0–5.7 (3.9)	0–10 (6.0)	3.4–25 (14)	Daily NEON sensor data
$\boldsymbol{Qi}$	Discharge at each point ($m^3\ s^{-1}$)	Varies	2.0 x 10^{-3}–0.32 (8.7 x 10^{-3})	0–3.6 (0.13)	0.14–4.0 (0.40)	0–0.60 (0.01)	0–5.4 (0)	Calculated from conservation of mass from measured or modeled discharge at gage.
$\boldsymbol{NEP}$	Net ecosystem production (g $CO_2\ m^{-2}\ day^{-1}$)	Constant	2.6–5.3 (3.6)	0.10 – 0.47 (0.22)	1.9 – 5.3 (3.5)	0.6–0.68 (0.21)	0.18 – 1.4 (0.57)	Estimated from literature*. Minimum and maximum values used to determine uncertainty. Median used for all other runs.
$\boldsymbol{C_{gw}}$	Groundwater pCO_2 (ppm)	Constant	2.2 x 10^3–6.8 x 10^3 (5.3 x 10^3)	1 x 10^3–2.6 x 10^4 (1.4 x 10^4)	2.0 x 10^4–3.4 x 10^4 (3.1 x 10^4)	8.2 x 10^3–1.9 x 10^4 (1.2 x 10^4)	2.2 x 10^4– 2.8 x 10^4 (2.6 x 10^4)	Interpolated to daily values from monthly groundwater samples for a single year.
$\boldsymbol{s}$	Stream slope (m m^{-1})	Varies	0.002–0.19 (0.02)	0.017–0.78 (0.16)	7 x 10^{-4}–0.57 (0.07)	3 x 10^{-4}–0.48 (0.06)	0–0.23 (0.02)	Digital elevation model
$\boldsymbol{k_{600}}$	Modeled air–water gas exchange velocity (m day^{-1})	Varies	0.38–33 (3.4)	0.44–410 (35)	0.97–370 (32)	1.4–190 (6.3)	0–230 (0)	Calculated from slope, velocity, and discharge.
$\boldsymbol{k_{CO_2}}$	Modeled gas transfer velocity of CO_2 (m day^{-1})	Varies	0.31–28 (2.9)	0.27–280 (24)	0.62–295 (27)	0.022–80 (5.3)	0–195 (0)	Calculated from k_{600} and the Schmidt number.

*116 for MART, CARI, COMO, and KING. 119 for WALK.
Values represent range during model period from 2018 – 2023. Median values are in parentheses. Caribou Creek and Como Creek were modeled only for months May – September and May-October, respectively, to capture non-frozen periods.

The model generates daily pCO_2 values at each point along the stream network. We evaluated its performance by comparing model outputs to our measured data, including CO_2 sensor values at the network outlets and synoptic pCO_2 samples collected across the networks on specific sampling days at Martha Creek, King's Creek, and Caribou Creek. Daily modeled pCO_2 at the sensor locations was compared to observed values to assess temporal accuracy, while synoptic measurements were used to evaluate the model's spatial performance across the networks.

Our model used an a priori approach, relying on available data as inputs to the stream network model without calibration. Exploring how adjustments to these inputs improve the fit to observed pCO_2 values can reveal key processes or parameters missing from the current model structure. To examine the sensitivity of our models to changes in groundwater pCO_2 (C_{gw}) and the gas exchange velocity (k_{600}) on an annual scale, we used the *optim* function in R[127]. The optimization minimized the mean absolute error (MAE) between modeled and observed sensor pCO_2 concentrations, using a range of multiplier values for each parameter. In each case, C_{gw} and k_{600} were scaled uniformly across the entire time series and stream network. We used these results to determine how much annual emissions changed when fitting either C_{gw} or k_{600} to match sensor pCO_2 observations. To understand what our model was missing spatially, we ran the models for the sampling periods (on a daily scale) by including our measured pCO_2 values[88] (Figure S3.7). We set the C_i of the points in the model that were located at our sampling locations equal to that of our sampled concentrations. The model was then allowed to run sequentially with these known concentrations as inputs. We compared this adjusted model to the preliminary model runs. Finally, to estimate uncertainty of carbon emissions from the model based on our inputs, we ran each measured-static model with the low and high end of our estimated carbon inputs into

the model (groundwater and NEP inputs) to get a range of possible carbon emissions from each stream network.

Carbon Losses from Stream Networks

To estimate total carbon losses from the five stream networks, we used the DOC and DIC grab samples collected by NEON. We interpolated daily DOC and DIC values using the daily discharge from NEON and the macrosheds package in R[128]. We downloaded the daily discharge, DOC and DIC data manually to ensure consistent NEON releases and used the *macrosheds* R package to estimate annual export. Annual export of DOC and DIC were estimated as the sum of daily export concentrations multiplied by the mean daily discharge. Error for DIC and DOC fluxes was propagated with the macrosheds package based on the measurement uncertainty provided by NEON[128]. For Walker Branch, DOC export was only estimated for 2022-2023 due to quality issues from 2018-2021 on the NEON data portal. Since DOC and DIC were sampled at sub-daily frequencies, interpolation introduces some uncertainty, particularly during high-flow events when concentration-discharge relationships may be nonlinear. We acknowledge potential biases could arise from underestimating peak concentrations or missing episodic pulses. Annual export was divided by the watershed area of each stream network to obtain areal estimates of carbon yields. To compare the DIC and DOC exports to CO_2 emissions, we obtained a yearly estimate of total annual emissions from the stream network models and normalized by the watershed area of each network. To show how discharge events contributed to emissions, we compared cumulative CO_2 emissions to the distribution of discharge at each stream network by creating Lorenz curves of temporal inequality[129, 130].

Results

The role of stream permanence in emissions estimates

Using the modeled-static scenario runs, we determined the percent of time the full stream network was flowing (Table 3.4), with the exception of Caribou Creek, where we did not model stream permanence, and assumed the network was at full surface coverage during 100% of the monitoring season based on field observations. The four remaining stream networks had large drying periods for at least a portion of the network. King's Creek had the most intermittent stream network; it was only at full network size 1% (range: 0.3-2.7%) of the time, while Martha Creek was at full network size for 60% (range: 54-73%) of the time from 2018-2023. Como Creek and Walker Branch were at full network size 19% (range: 8-52%) and 21% (range: 11 – 30%) of the time, respectively (noting that the modeling run for Como Creek did not include the winter months).

Table 3.4 WEPP modeled-dynamic and modeled-static scenario results

Stream Network	Full Network Size Duration[1] (%)	Minimum Network Extent (%)	Median total annual emissions from stream network (Mg C year^{-1})			Median areal emissions of stream network area[2] (g C m^{-2} day^{-1})		
			Modeled dynamic	Modeled static	% difference	Modeled dynamic	Modeled static	% difference
WALK	21	4	1.5	1.6	4.3	2.5	2.3	7.4
MART	62	0	58.89	58.93	0.07	7.4	6.6	9.6
COMO[1]	22	56	5.250	5.253	0.06	4.3	3.7	14
KING	1	0	27.6	28.1	1.9	7.4	4.6	38

1. Network extent not including frozen stream time periods; modeled from May-October.
2. Total annual emissions divided by the area of each stream network (width x length).

We compared the modeled-static scenario runs to the modeled-dynamics scenario runs to test the outcome of incorporating stream permanence. Despite periods of intermittence in the four stream networks, the difference in total average annual emissions was only 0.06-4.3% between runs (Table 3.4). We found that the modeled-dynamic scenarios, using the maximum network size all year round, only resulted in a small overestimate in emissions at all stream networks. We conclude that the majority of emissions for all of the stream networks occur when the networks are at full size (Figure 3.2.)

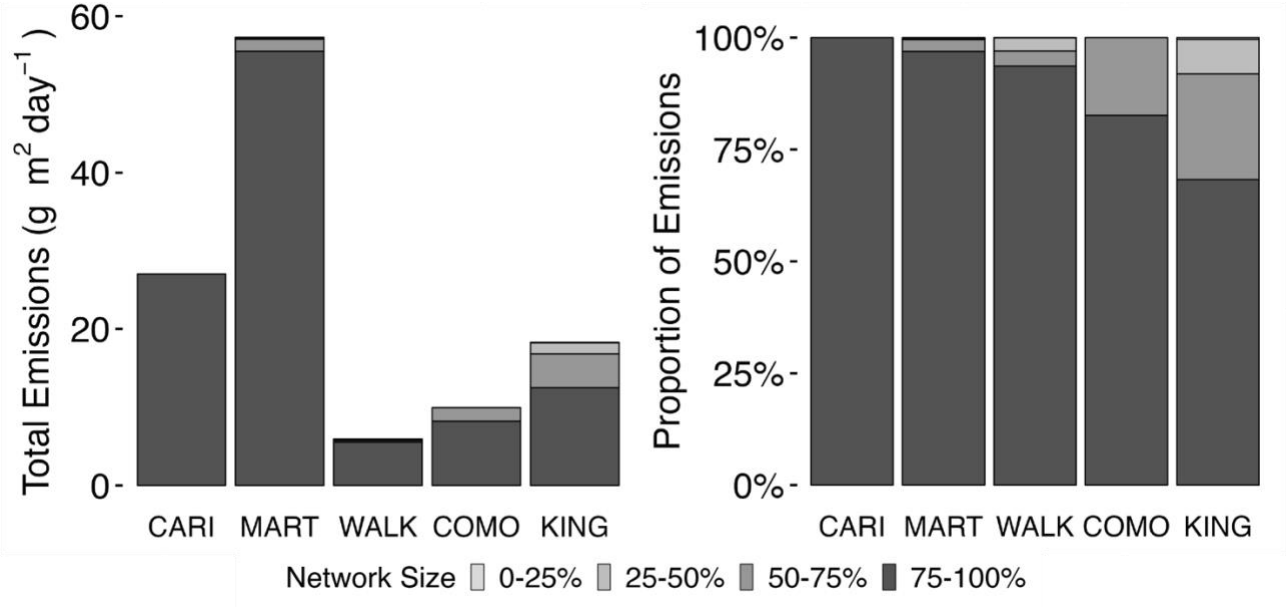

Figure 3.2 Proportion of emission that occur at varying network sizes. The majority of emissions occur when the stream networks are at full network size. The right plot shows the total emissions that occur at each stream network size. The left plot shows the proportion of emissions that occur at each network size, where the majority of emissions for each stream network when the network is at 75-100% of its maximum size. King's Creek has the smallest proportion of emissions that occur at 75-100% of network size because it is only at full network size 1% of the time. Caribou Creek, on the other hand, is at full network size 100% of the time. Emissions when the network size is 0-25% are less than 0.4% at all sites.

At the four stream networks where we tested the role of including dynamic network surface area in our network CO_2 model, we found that the areal emissions per stream network area decreased

during the modeled-static run, when the network was run at full size (Table 3.4). Incorporating stream permanence will also change the distribution of pCO_2 throughout the network. Comparing the predicted pCO_2 of the network outlet where the stream pCO_2 sensors were installed, we find that when the model incorporates stream permanence, predicted pCO_2 at the network outlet increased by 32% (Figure 3.3).

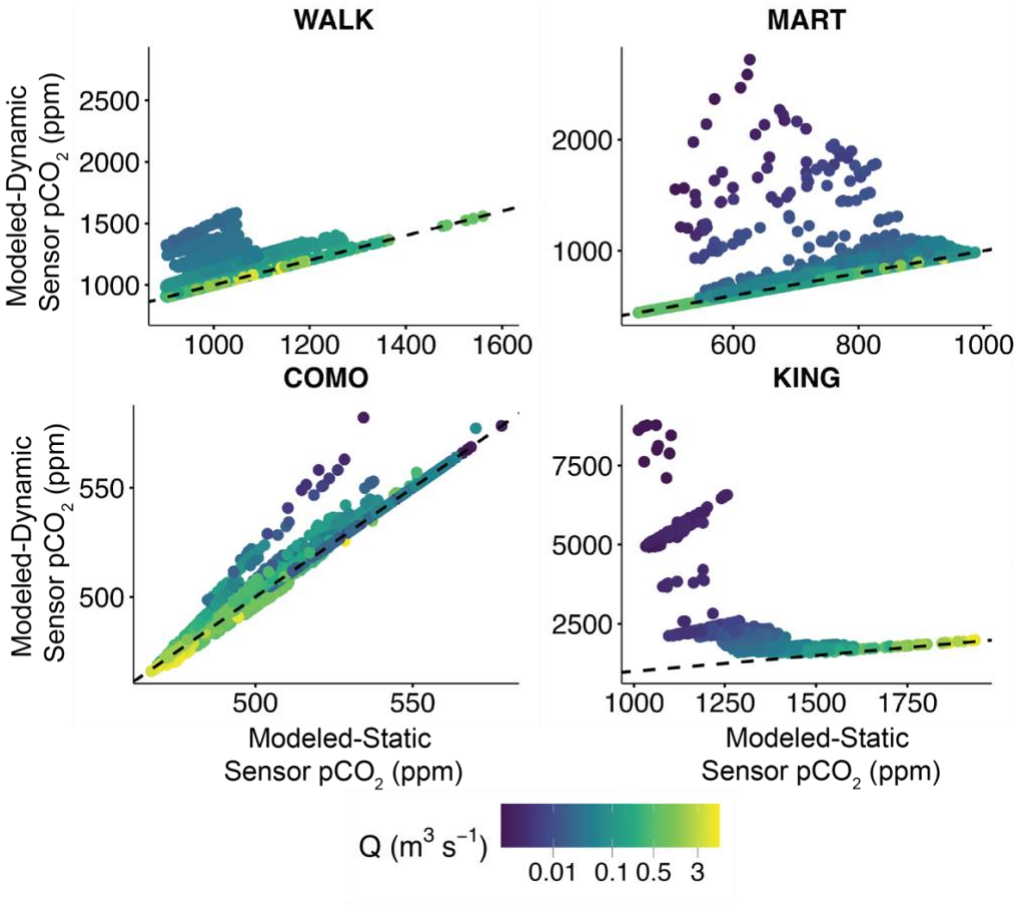

Figure 3.3 Modeled-static predicted pCO_2 at the network outlet versus modeled-dynamic predicted pCO2 at the network outlet for stream networks with modeled-dynamic scenario runs. Including periods of stream intermittence within the network results in higher pCO_2 at the network outlet for stream networks with modeled-dynamic scenario runs.

Spatial carbon export patterns

When examining spatial patterns while accounting for stream permanence, the hydrologic regime of the network and topography will determine where carbon emissions occur (Figure 3.4). At Martha Creek, the highest sloped network, emission hot spots emerge at the highly sloped headwaters when the network is at full size. A similar pattern was observed at Caribou Creek, where we assumed a full sized network during flow, with emission hotspots primarily concentrated in the steep headwaters. Hotspots near the headwaters also emerged at Como Creek, although greater variability in emissions was observed across tributaries of different slope, some of which are only active during snow melt. At Walker Branch and King's Creek, emission hotspots occurred at the headwaters and throughout the networks due to both lower slopes and contractions in network sizes.

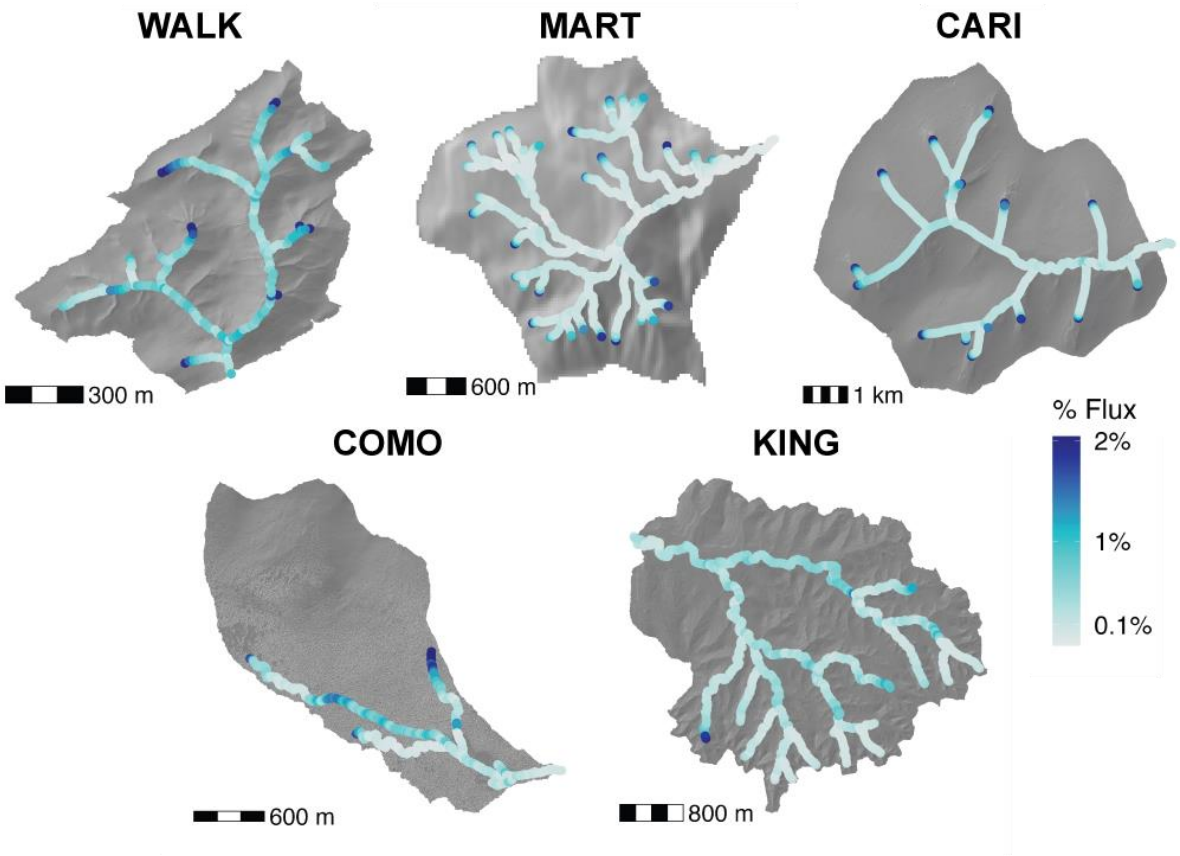

Figure 3.4 Percent of flux from each modeled point in the stream network during the 2018-2023 model time period. To create the figure, total annual emissions from each point were divided by the total annual emissions for the entire network. For Martha Creek, King's Creek, Walker Branch, and Como Creek, the modeled-dynamic scenarios are shown; for Caribou Creek, the measured-static scenario is shown. The scale bars denote the differing watershed sizes. The outlet of each network is the NEON downstream stream monitoring site used to validate modeled CO_2 and generate other parameter estimates for the network CO_2 model.

While spatial differences emerged based on the hydrology and topography of different stream networks, the majority of emissions occurred in first order streams. First order streams accounted for 56% of emissions for Martha Creek, 43% for Caribou Creek, 41% for Walker Branch, and 84% for Como Creek (Figure 3.5). King's Creek was the only network to have more emissions from second order streams (42%) than first order streams (40%). We define first-order streams as streams that have no tributaries within the network, representing the initial channels in a watershed, based on the Strahler stream order classification system. Areal emissions in first

order streams were on average 1.3-2.7 times higher than the remainder of the network. First order streams had a higher mean slope than the remaining orders at all networks. Areal emissions were most similar among stream orders at King's Creek, which along with Walker Branch had the lowest variation in slopes across the network. Conversely, the largest differences in emissions among stream orders were at Martha Creek, the network with the most drastic changes in slope across the network. Caribou Creek and Walker Branch had a higher percent of emissions from order 3 streams than order 2 streams, likely due to a greater percentage of 3rd relative to 2nd order streams in those networks.

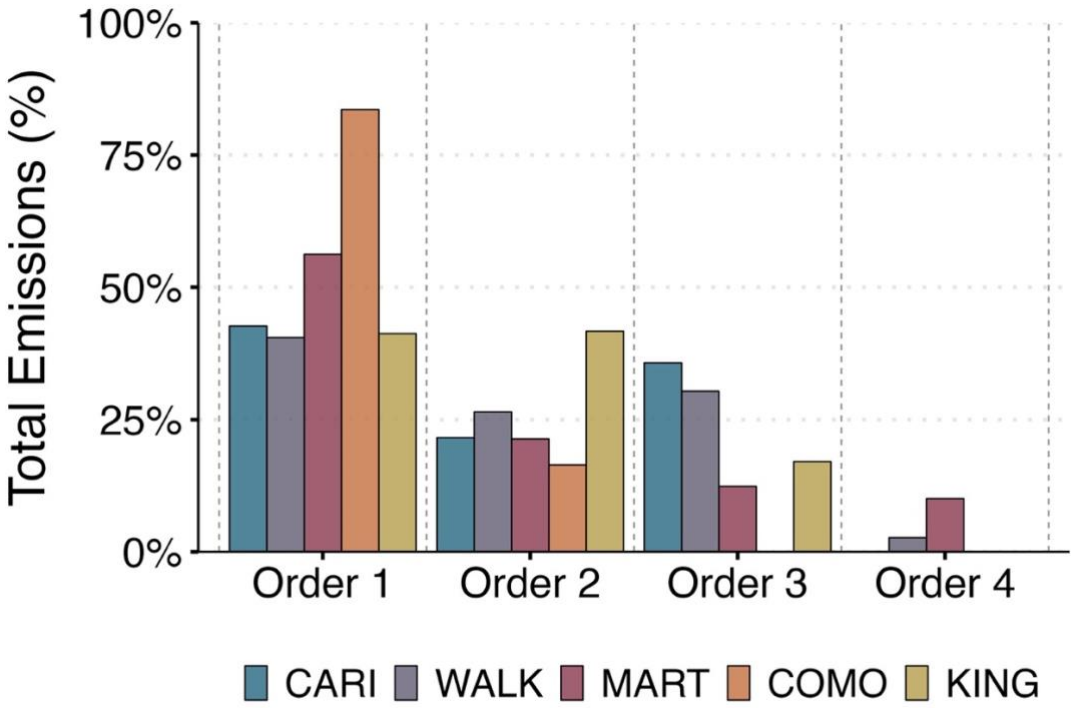

Figure 3.5 Carbon emissions percentage by stream order. The majority of emissions occur for all stream networks in first order stream segments. Martha Creek and Walker Branch are the only fourth order network. Como Creek is a 2nd order stream.

The majority of emissions from the stream network models could be attributed to inputs of groundwater; in-stream metabolism contributed a median of 30% of emissions at Walker Branch, 4.6% at Martha Creek, 3.2% at Caribou Creek, 8% at Como Creek, and 13% at King's Creek. At each stream network, in-stream metabolism had the lowest contribution for first order streams, except for King's Creek and Como Creek which both had the lowest contribution of NEP for second order streams. Running the network models with the maximum observed NEP, increased total annual emissions by 10-28%. For Walker Branch, we also compared using the metabolism estimate from the NEON reach, which was an order of magnitude smaller than the NEP estimate further up in the headwaters (0.22 g CO_2 m^{-2} day^{-1} versus 3.6 g CO_2 m^{-2} day^{-1}). Using the NEON reach estimate resulted in a much lower NEP contribution at Walker Branch from 30% of emissions to 2.6%.

Because annual emissions were similar between the modeled-static scenarios and the modeled-dynamic scenarios model runs, we show that incorporating stream permanence may not be important for annual emissions estimates. To remove the uncertainty associated with using modeled discharge as a model input, we use measured-static scenarios for the remainder of our analyses.

Stream network model results

The measured-static scenario did not provide a good fit to the sensor pCO_2 data at the watershed outlet. NSE was below 0 for all stream networks, indicating the mean sensor pCO_2 would provide a better prediction that the modeled pCO_2 (Table 3.5). The measured-static models underestimated pCO_2 for the Martha Creek, Caribou Creek, and King's Creek stream networks (percent bias = -96 to -27), while Como Creek and Walker Branch showed little bias (percent

bias = 6.6 and 1.1, respectively). The network model did capture some observed patterns in pCO_2 (Figure 3.6, Figure S3.5). At King's Creek we were limited in the number of comparable days (n = 45) with modeled and measured pCO_2 because the model was not run on zero discharge days when water is not flowing but the pCO_2 was still being measured in disconnected pools.

Table 3.5 Stream network model fit to measurements values and measurement impacts on emissions estimates

		WALK	MART	CARI	COMO	KING
Model fit to pCO_2 sensor	# days compared	421	450	325	290	45
	NSE	-1.3	-1.3	-10.6	-0.29	-12.4
	PBIAS	1.1	-27	-36	6.6	-95.7
	R^2	0.5	0.77	0.13	0.04	-0.4
	Mean absolute error (ppm)	173	280	430	382	9400
Model fit to longitudinal pCO_2 measurements	R^2	NA	0.23, 0.63 (Aug 21, Nov 21)	0.33 (July 22)	NA	0.27, 0.13 (Aug 22, May 23)
	Daily % change in emissions from sample measurements	NA	415% increase, 12% decrease	22% decrease	NA	67%, 250% increase

The model fit to pCO_2 sensor compares daily pCO_2 for the stream network models and the sensor at the stream outlet. Number of days compared is based on the number of days the sensor was installed at each stream network. The model fit to longitudinal pCO_2 measurements compares spatial model outputs to the nearest measurement points during the sampling period indicated. The daily % change in emissions from sample measurements was determined by setting C_i for points in the model that were located at our sampling locations and running the model sequentially with known concentrations as inputs. Daily % change describes how the total emissions changed incorporating our sample measurements for the sampling period.

Using an a priori approach without calibration, our model relied on available data as inputs, and examining how adjustments to these inputs affect the fit to observed pCO_2 values highlights key parameters missing from the dataset. When evaluating the sensitivity of the models to changing C_{gw} and k_{600}, we found increasing C_{gw} and decreasing k_{600} resulted in the smallest mean absolute

error when comparing the model to measured pCO_2 at the outlet for Martha Creek, King's Creek, and Caribou Creek. At Walker Branch and Como Creek, decreasing C_{gw} and increasing k_{600} resulted in the smallest mean absolute error (although only slightly) (Table S3.7). We found changing C_{gw} had a much larger impact on the annual emissions predicted by the model than changing k_{600}. For example, at Martha Creek (Figure 3.6), changing groundwater concentrations results in substantial increase in total median annual emissions (100 Mg C $year^{-1}$ versus 58 Mg C $year^{-1}$), whereas changing k_{600} resulted only in a small decrease in total median annual emissions (58 Mg C $year^{-1}$ versus 55 Mg C $year^{-1}$). The model was more sensitive to groundwater concentration changes across the stream networks (Table S3.7).

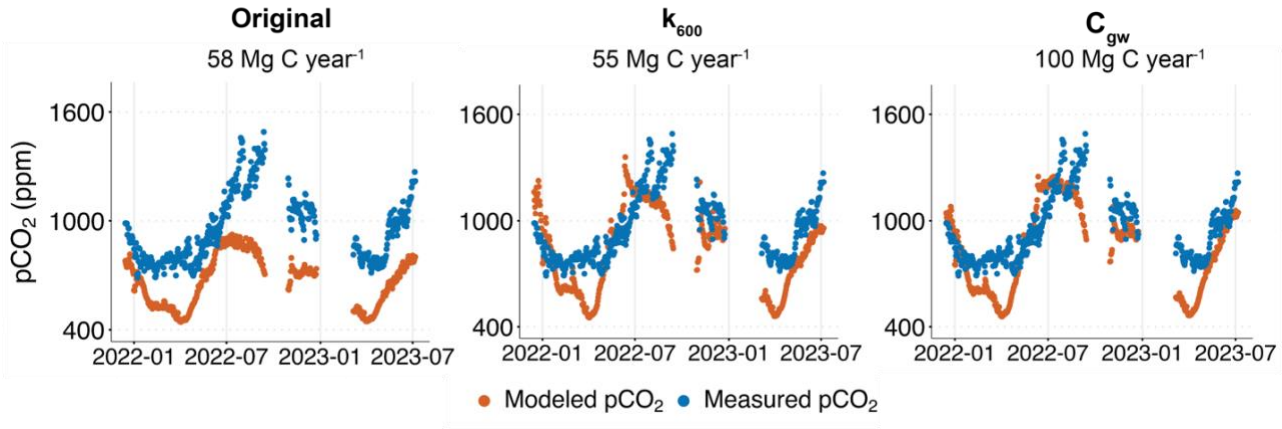

Figure 3.6 Modeled comparisons to the CO_2 sensor at Martha Creek. We ran the model by multiplying k_{600} and C_{gw} by a constant to optimize the mean absolute error. We show that both adjustments provided a better fit for the sensor pCO_2, however the groundwater adjustment resulted in a much larger increase in total annual emissions at the stream network.

For the measured longitudinal samples, the model also missed some spatial variation in pCO_2 at Martha Creek, Caribou Creek and King's Creek (R^2 = 0.13-0.63, Figure S3.6) at the sample points during the sampling period. After adjusting the model to match the sample points, we observed large increases in modeled daily emissions compared to the model without observations. Daily emissions increased 415% at Martha Creek during low flow (5 x 10^{-3} m^3 s^{-1}) in August 2021 and increased 67-250% at King's Creek during both sampling periods (August

2022 and May 2023), which also had relatively low flow ($2.0 \times 10^{-3} – 8.0 \times 10^{-2}$ m^3 s^{-1}). During high flow at Martha Creek (1.9 m^3 s^{-1}) in November 2021 and Caribou Creek (0.2 m^3 s^{-1}) in July 2022 we observed decreases in total daily emissions when adjusting the model to our measured concentrations (12-22% decrease).

Temporal carbon emission patterns

While accounting for stream permanence may not be critical for annual network carbon emissions estimates based on our model findings, discharge events drive annual emissions. Lorenz curves of cumulative emissions versus flow distribution for each stream network show that at all networks, a large fraction of total annual emissions occurred within a small fraction of time, during high discharge. We can compare stream networks by observing what fraction of emissions occurs during high flows. 50% of carbon emissions occur in the top 3% of discharge for King's Creek, the top 10% of discharge for Como Creek, top 12% of discharge for Martha Creek, the top 26% of discharge for Walker's Branch, and the top 29% of discharge for Caribou Creek (Figure 3.7). We note that Caribou Creek and Como Creek were only modeled from May–September and May–October to avoid periods when the stream was frozen.

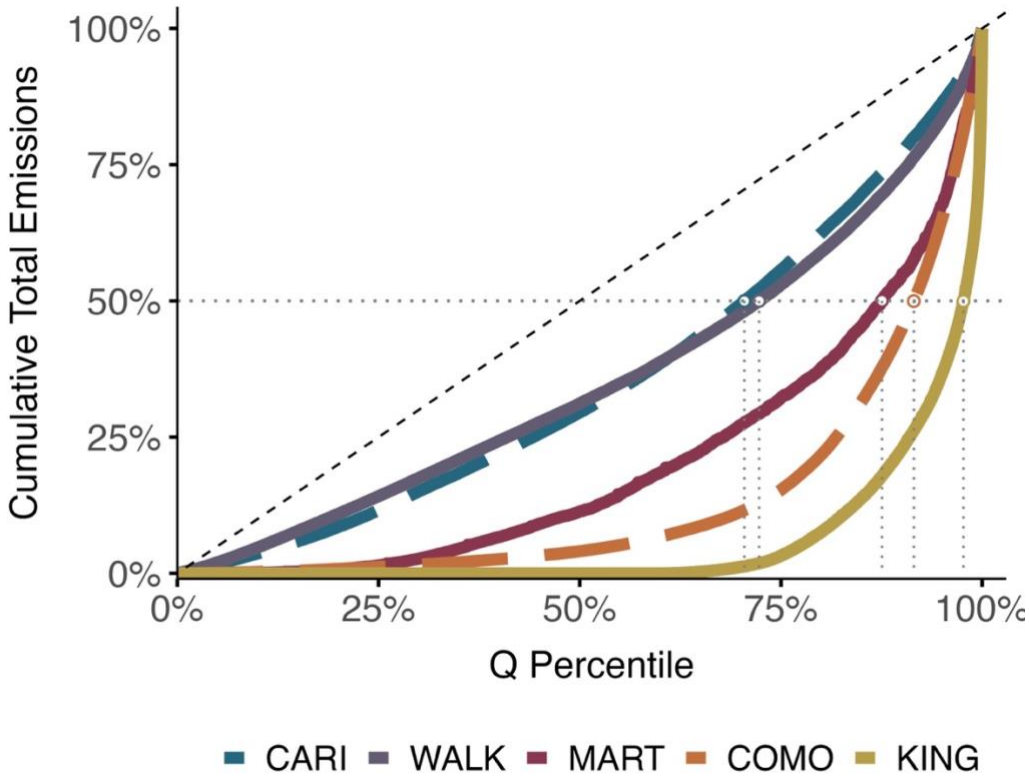

Figure 3.7 Lorenz curves of cumulative emissions with the x-axis ordinated by increasing discharge. Emissions of CO_2 are unequal, with the majority of emissions under the 1:1 line delivered at the highest discharge from all networks. Caribou Creek and Como Creek are denoted with a dashed line to note emissions were only modeled from May–September and May–October to avoid periods when the stream was frozen.

Total carbon losses from stream networks

Both CO_2 emissions from stream networks and carbon export from network outlets (together forming total carbon losses from networks) varied temporally (Figure 3.8). Total carbon losses from the networks scaled with discharge for all stream networks, with the highest carbon losses occurring when discharge was highest. The pattern of total carbon losses varied between stream networks based on the flow regimes at the networks. For example, total carbon losses peaked at Martha Creek in the winter months during the rainy season, while at Como Creek total carbon losses peaked in May when snow melt increases discharge. Each component of total carbon

losses (CO_2 emissions, DIC, and DOC) also scaled with discharge for all stream networks on a monthly scale (Figure S3.9). Each network had interannual variability across the modeled years (2018-2023) with total carbon losses ranging from 11 – 15 g m^2 $year^{-1}$ at Walker Branch (2022-2023), 11 – 30 g m^2 $year^{-1}$ at Martha Creek, 5.7 – 11 g m^2 $year^{-1}$ at Caribou Creek, 2 – 6 g m^2 $year^{-1}$ at Como Creek, and 0.96 – 33 g m^2 $year^{-1}$ at King's Creek. Across the modeled years (2018-2023), each component of total carbon losses scaled with discharge, although annual DOC export and annual discharge had a weaker relationship for Caribou Creek and Walker Branch across years (Figure S3.8).

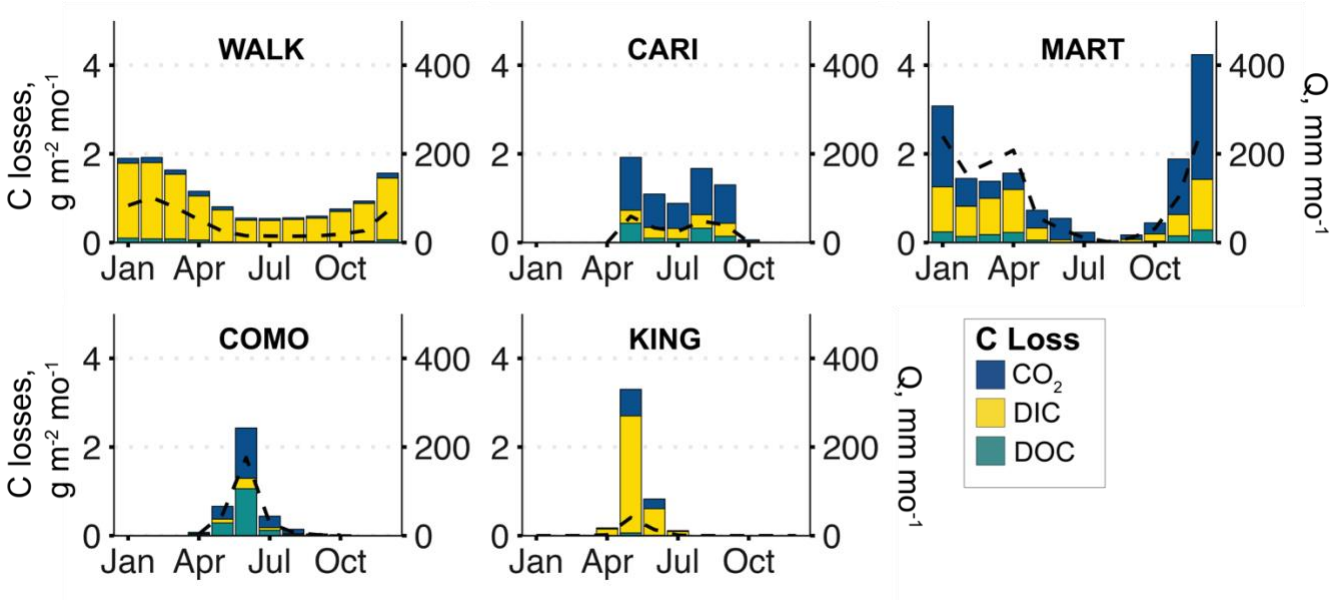

Figure 3.8 Monthly carbon exports by stream network colored by flux type: stream network CO_2 emissions, dissolved inorganic carbon (DIC) export, and dissolved organic carbon (DOC) export). Discharge is plotted on the secondary y-axis as a dashed line. Caribou Creek and Como Creek were only modeled from May–September and May–October to avoid periods when the stream was frozen.

The proportion of export and emissions of total carbon losses varied among the five stream networks (Table 3.6). CO_2 emissions represented the highest percent of carbon losses for Martha Creek (56%), Como Creek (47%), and Caribou Creek (63%), while DIC represented the highest

percent of carbon losses for Walker Branch (86%) and King's Creek (73%). DOC represented the second highest percent of carbon losses for Como Creek (40%) and Caribou Creek (16%).

Table 3.6 Total carbon losses per watershed area and proportion of total carbon losses[1]

Stream Network	DOC, g m^{-2} y^{-1}	DIC, g m^{-2} y^{-1}	CO_2, g m^{-2} y^{-1}	Sum C losses, g m^{-2} y^{-1}	% DOC to total C loss	% DIC to total C loss	% CO_2 to total C loss
WALK	0.37 (± 0.1)	10.4 (± 0.22)	1.3 (0.9–1.7)	12.0 (11–13)	3.1% (2.2-4.0%)	86% (84-88%)	11% (7.7–14%)
MART	1.4 (± 0.3)	6.0 (± 0.6)	9.2 (4.9–15)	16.5 (11–23)	8.4% (6.4-10%)	36% (32-40%)	56% (29–88%)
CARI[2]	1.1 (± 0.06)	1.5 (± 0.1)	4.4 (4.1–4.6)	6.9 (6.5–7.3)	16% (15-17%)	21% (20-23%)	63% (60–67%)
COMO[2]	1.6 (± 0.08)	0.50 (± 0.1)	1.8 (1.4–2.3)	3.9 (3.3–4.6)	40% (38-42%)	13% (10-16%)	47% (35–59%)
KING	0.06 (± 0.01)	3.7 (± 0.02)	1.3 (1.2–1.5)	5.1 (5.0–5.3)	1.1% (0.85-1.4%)	73% (72-73%)	26% (24–28%)

1. All flux estimates are provided in g m^{-2} $year^{-1}$ and normalized by watershed area. Uncertainty is provided in parentheses.
2. Carbon losses are only estimated for non-frozen stream periods – May – September for Caribou Creek and May – October for Como Creek.

The proportion of export and emissions of total carbon losses varied among the five stream networks on both a monthly basis. There was not a strong relationship between discharge and percent emissions to carbon losses or percent DIC and DOC export to carbon losses at most networks on a monthly scale (Figure S3.9). The proportion of export and emissions of total carbon losses varied slightly on an interannual basis, but was relatively consistent year to year at each network. There was a positive linear relationship (R^2 = 0.5, p = 0.18) between median stream network slope and fraction of carbon losses as CO_2 emissions to the atmosphere, although the relationship was not significant.

Discussion

Stream network model uncertainties

The stream network models parameterized a priori with field information available from the sites did a poor job of predicting pCO_2 at the outlet of the networks. When comparing our model output to measured values, model pCO_2 at the sensor locations consistently underpredicted sensor pCO_2 at three of five stream networks and showed a poor fit against the time series of observations. Spatial measurements provide potential insight into what the model might be missing: during low flow at Martha's Creek and King's Creek, measurements of network pCO_2 were also underpredicted by the model possibly attributed to some locations within the network receiving higher groundwater concentrations compared to the surrounding points[88]. Here, we assumed a constant groundwater input throughout each of the networks based on NEON wells located at one downstream point in the network; in reality, the spatial pattern of hydrologic gains and losses from groundwater inputs into stream networks will vary within watersheds, resulting in irregular pulses of CO_2 into the stream[17, 131, 132]. We also saw evidence of locations with high CO_2 groundwater pulses into King's Creek, as many of our headwater sample points occurred at known groundwater springs (Figure S3.10). Additionally, King's Creek stood out among our stream networks due to the formation of unconnected pools during low flow, which the model does not account for. Unconnected pools were particularly prevalent during the August 2022 sampling campaign. High pCO_2 build up has been observed in other intermittent streams as they contract to disconnected ponds with high rates of respiration and low gas exchange[94, 95].

During higher flow at Martha Creek and Caribou Creek, the daily models overpredicted measured pCO_2 throughout the network, although the fit was typically better during high flow.

Additionally, Saccardi and Winnick (2021)[38], using a similar stream network model, reported a stronger model-data correlation ($R^2 = 0.70$) at the East River watershed in the Colorado Rocky Mountains compared to any of these stream networks, during high flow conditions (1.23–3.25 $m^3 s^{-1}$). In Conroy et al. (2023)[88], this slight model overprediction was attributed to dilution from overland flow during direct precipitation as well as higher gas evasion that is not properly captured by the model[13, 27]. Our assumption that runoff groundwater pCO_2 was not influenced by storm events may be incorrect if dilution of pCO_2 from higher rain water proportions is occurring[133].

However, at the outlet of the network, the models underpredicted pCO_2 even during high flow at Martha Creek, King's Creek and Caribou Creek. In addition to the CO_2 sources into the network, the rate of transfer of CO_2 to the atmosphere will also regulate the distribution of the observed pCO_2. Gas exchange velocity is a function of turbulence within a stream reach and has been observed to increase with discharge[34] as well as slope[20, 51]. However the relationship between discharge and k_{600} becomes weaker in lower sloped reaches[122]. At each stream network, k_{600} was estimated with tracer-gas experiments across a range of discharges for the NEON reach but only Como Creek, the steepest NEON reach, exhibited a strong k_{600}-Q relationship[121, 122]. Notably, Como Creek also exhibited a closer agreement between measured and modeled pCO_2 at the sensor, potentially reflecting the tighter k_{600}-Q relationship. We suggest our k_{600} estimates at other stream networks using regression models might be overpredicted, causing lower modeled pCO_2 at the network outlet. Walker Branch also had a closer agreement between measured and modeled pCO_2, likely due to a more consistent slope across the entire network being similar to the low-sloped NEON reach where k_{600} was measured. While we attempted to incorporate the NEON-derived k_{600}-Q relationships at the NEON reaches for sites with a large discrepancy with

the literature regression models, predicting k_{600} remains challenging throughout the remainder of the network due to its high spatial variability, particularly in lower-order, lower-gradient streams[37]. Moreover, the slopes at NEON reaches (i.e. the outlet of each network) were consistently lower than those elsewhere upstream in the networks, which limits their representativeness when used to generate parameters for a spatially-explicit network model. Our approach of using regression relationships to estimate k_{600} based on discharge[51] remains justified for higher-sloped reaches, where the majority of emissions occur. Consequently, the NEON sensor locations equipped with CO_2 sensors do not fully represent the broader stream networks, as they predominantly capture conditions typical of lower-gradient areas.

We conclude that our models may be missing additional high-CO_2 groundwater inputs throughout the network and may be over predicting k_{600}, especially in low sloped areas. We created additional scenarios to bring modeled concentrations closer to sensor concentrations and found for the sites where pCO_2 was underpredicted by the model (Martha, Caribou, and King's Creeks) reducing k_{600} across the entire network resulted in minimal changes in annual emissions (5-48% change). In contrast, increasing pCO_2 of groundwater inputs resulted in large changes in annual emissions (72-760%). For Martha Creek and Caribou Creek, we emphasize that the reduction of k_{600} across the entire network is likely unrealistic, particularly in steep headwater streams. Ulseth et al. (2019) demonstrated that in high-slope networks (>0.1 m m^{-1}), k_{600} can exceed 100 m day^{-1} and even reach over 1000 m day^{-1}. At Martha Creek and Caribou Creek our model predicted k_{600} values of up to 500 m day^{-1} in first-order streams, where slopes ranged from 0.017–0.78 m m^{-1} (median 0.16 m m^{-1}) and 7 x 10^{-4}–0.57 m m^{-1} (0.07 m m^{-1}), respectively. While King's Creek is a lower sloped network, our modeled k_{600} fit measured k_{600} well and King's Creek does have some higher sloped reaches in the headwaters (0–0.23 m m^{-1}). We show that gas

exchange has minimal influence on the emission estimates, instead influencing where emissions will happen within the network. This suggests that groundwater CO_2 inputs play a much larger role in supporting total network emissions than gas exchange velocity and, consequently, our current measurements of shallow groundwater CO_2 may be biased low due to the representativeness of our sampling sites or methodological challenges associated with minimizing gas loss when sampling from wells.

In this analysis, we used groundwater pCO_2 ranging from 4,200 to 106,000 ppm for Caribou and Martha Creeks, values that, while high, have been observed in previous studies. For comparison, Marx et al. (2018)[134] found that groundwater pCO_2 of up to 131,050 ppm was needed to estimate stream concentrations in their model; this high pCO_2 has been measured in soils before[135]. At our sites, the highest groundwater measurement was at Caribou Creek (62,000 ppm). As we show with our spatial measurements, it is unlikely that elevated groundwater pCO_2 is uniform across the entire network as assumed in our model. If we apply our higher measured CO_2 concentrations from the August sampling period across the Martha Creek network on an annual scale, emissions increase by 24%. In addition, while we measured groundwater pCO_2 monthly across a range of flow conditions, our model assumed a fixed annual cycle of daily groundwater pCO_2 concentrations for each year, potentially overlooking event-driven shifts in groundwater connectivity and riparian soils which can vary across biomes[22, 136, 137]. It is clear that predicting groundwater DIC inputs into stream networks remains a large source of uncertainty; future work that addresses spatial variability in groundwater-surface water fluxes is critical to better constrain how these inputs change in both space and time.

At King's Creek, the model required high groundwater pCO_2 up to 236,600 ppm to match observations in the streams, which may be unrealistic. We point to other potential mechanisms for higher measured pCO_2, including the presence of disconnected pools where high pCO_2 can build up due to both lower gas exchange velocity and higher groundwater pCO_2 than used in our model[94, 95]. In addition, we show how incorporating stream permanence can result in higher pCO_2 at the outlet of the network (Figure 3.3) with less total stream area for emissions along the flow path before the outlet.

We also assessed how changes in in-stream metabolism impact emissions estimates. Our model assumed a constant NEP across the entire network, though in reality, NEP varies spatially and temporally in stream networks[118, 119]. When we incorporated daily NEP variability in networks with metabolism estimates, emissions changed only slightly (3% change, Table S3.4**)**. Spatially, ER is typically highest in headwaters and GPP will increase with drainage area, although NEP is variable across headwaters[118, 138]. This will differ between stream networks; at Walker Branch median NEP at the west fork higher up in the network (3.6 g CO_2 m^2 day^{-1}) is substantially higher than at the NEON reach (0.22 g CO_2 m^2 day^{-1}). Using the NEP estimates from further up in the headwaters increased emissions by 28% and increased overall in-stream metabolism contribution to total emissions from 2.6% to 30%. Conversely, Iannucci et al. (2024)[139] found that at Caribou Creek, NEP was similar across stream orders. Estimates from the NEON reach at the outlet of the network where metabolism contributions to total emissions are typically predicted to be higher than the headwaters[18]. Ultimately, in-stream metabolism accounted for a relatively small proportion of total emissions (4.6–30%). Even when using the maximum estimated NEP at each site, annual emissions increased by only 10–28%. Therefore, compared to

groundwater inputs, incorporating spatial and temporal variability in NEP is likely to have a smaller impact on annual CO_2 emissions estimates from stream network models.

Impact of Stream Permanence

Accounting for stream permanence had little impact on annual emissions estimates at the four modeled stream networks (0.17-4.4% difference), with the caveat that the network model did not have high predictive capabilities based on sensor outlet pCO_2 comparisons with modeled pCO_2. This was an unexpected result, particularly for a stream network like King's Creek, which our model indicated was fully wetted only 1% of the year and also had some of the highest pCO_2 concentrations among the five NEON stream sites. Stream drying coincides with low flow, which corresponds to lower gas exchange[20, 34]. The majority of total modeled emissions occur when network size is maximized during high flow. In addition, although we observed higher groundwater concentrations during low flow at most of our stream networks, low flow corresponds to decreased hydrological connection with terrestrial soils, decreasing total CO_2 delivery to the stream[88, 90]. It has been posited that accounting for an increase in areal extent of drainage networks at higher discharge leads to an increase in emissions because of both an increase in surface area and increased connectivity to the terrestrial environment[12]. Our findings indicate that changes in surface area have minimal impact on annual emissions estimates when the maximum extent of the stream network is known in headwater streams. This conclusion may shift if current predictions of stream extent are underestimating stream area. Topographic maps often overestimate stream networks in temperate regions while underestimating them in arid environments[76, 77].

We did find, however, that including stream permanence in our model runs changed areal emissions estimates, increasing areal emissions from 8-33%. The model uses the same daily discharge for each run despite the size of the stream network. Discharge throughout the network is estimated using conservation of mass (Text S3.4) so when the network is smaller, the discharge, and sometimes gas exchange depending on the slope of the network, is higher at the headwaters of the stream network, even though they are draining larger watersheds. At the headwaters of the stream networks, the initial pCO_2 is high because it is set equal to the groundwater concentration. The combination of the high pCO_2 coinciding with higher gas exchange results in higher total emissions and higher areal emissions when the stream network shrinks. A smaller stream network has less surface area available for CO_2 emissions, leading to less overall CO_2 emissions along the flow path. As a result, CO_2 concentrations remain higher in downstream reaches compared to larger networks where more evasion occurs upstream. These higher CO_2 concentrations are reflected in our modeled pCO_2 estimates at the sensor outlets, with modeled pCO_2 at the sensor increasing by 32% when incorporating stream permanence. We show that understanding the extent of the stream network is crucial for interpreting pCO_2 sensor measurements, as sensors capture the signal of upstream processes.

Finally, we acknowledge our stream network models are likely missing some emissions that could occur because of changing stream network extent. The stream network model relies primarily on sources of CO_2 to the stream, namely external groundwater concentrations and in-stream metabolism, to estimate carbon concentrations. It therefore may overlook critical periods of high pCO_2 buildup occurring in disconnected stream pools during low flow from high rates of respiration in sediments[94]. At our stream networks, disconnected stream segments during low flow have been observed at King's Creek and Walker Branch, and at Como Creek during the

winter months. When we sampled King's Creek in August, we observed disconnected flow through much of the network and consequently measured high pCO_2 in the network (2,900-18,400 ppm). This aligns with findings from previous studies of high pCO_2 accumulation in fragmented stream reaches[94, 96]. Elevated CO_2 concentrations in these fragmented pools can be mobilized during storms with increased turbulence resulting in high emissions that may contribute to the network's annual carbon emissions but missing from our high-frequency CO_2 data recorded at the outlet only when emitted upstream[17]. Additionally, in this study we did not evaluate the carbon emissions that may be emitted from dry streambeds when the network shrinks. Dry streambeds of temporary streams can act as active CO_2 release from stream networks to the atmosphere, although their emissions are typically lower than those from flowing waters[78, 79]. We recognize that emissions may be underrepresented in this study, especially at King's Creek where the stream beds are often dry.

Discharge drives carbon emissions at all stream networks

At all stream networks, we observed a disproportionate amount of emissions occurring during times of high discharge. Disproportionally high emissions during periods of high discharge have been observed before; Natchimuthu et al. (2017)[21] found the highest discharge occurring in 10% of the study period was responsible for 43% of CO_2 emissions. Our results were similar with 3-29% of the highest discharge events accounting for 50% of carbon emissions depending on the network. These findings suggest that high-discharge events are pivotal in their contribution to annual emissions, with even short-lived events playing a critical role in overall carbon dynamics across diverse stream networks.

We highlight how high discharge events become especially important when incorporating entire stream networks into emissions estimates. High discharge corresponds to higher rates of gas exchange velocity, particularly in higher sloped reaches with increased stream power and turbulence that will be active during high flow events[20, 51, 122]. These high sloped reaches are typically near the headwaters and therefore receive direct input of high pCO_2 groundwater. When gas exchange rate is high, these high pCO_2 locations will evade rapidly resulting in both temporal and spatial hot spots on evasion within the networks. These high discharge events can also result in the flushing of CO_2 from soils as the channel becomes better connected to CO_2-rich floodplains[27, 90, 140]. In our stream network models, we show that these headwater locations are usually activated during high discharge events at all stream networks. When examining where emissions occur within the networks (Figure 3.4), we show how hotspots of emissions emerge at the headwaters of each network, even when the network shrinks and headwater locations were not active for the entire model period. Estimates of carbon emissions do not always have a positive relationship with discharge, which has been attributed to lack of a Q-k_{600} relationship in some stream networks[37] or a lack of pCO_2 source to the networks[87, 93]. With spatially and temporally explicit stream network models, we show how including first order streams and the headwaters of the network can reveal locations with both steep slopes, high k_{600} and high connectivity to the terrestrial environment that will drive a strong positive relationship between discharge and emissions. Omitting these locations when estimating emissions and relying solely on measurements from higher-order stream reaches, such as those where our CO_2 sensors were located, may underestimate this relationship.

The hydrologic regime of a network will influence total carbon losses from a network

When comparing results from our five stream networks located in differing biomes, we find that the hydrologic regime controls the magnitude, form, and timing of carbon losses from streams. King's Creek exemplifies the impact of short-lived, extreme discharge events, with the highest proportion of emissions and carbon export occurring during such events in the spring months. Even though King's Creek is dry for a large portion of the year, total carbon losses from the stream network can surpass other networks with more sustained flows. This is in part due to its flashy nature where brief but large discharge events drive higher carbon losses that contribute a substantial amount to the network's annual total loss. Similarly, Caribou and Como Creeks are also limited in flow through much of the year when they are ice covered. Snowmelt pulses and other high flood events in the spring and summer drive a large portion of total carbon losses for both networks, although we focused on non-winter periods in our analysis of Caribou and Como Creeks. Both Martha Creek and Walker Branch have more sustained flows throughout the year, but higher overall base flow and more frequent storm events in the winter months drive greater carbon losses. These examples highlight how flow variability shapes carbon losses across stream networks. Capturing high discharge events is crucial for accurately estimating overall carbon losses on an annual scale. High discharge events driving carbon losses have been observed across a range of biomes[12, 87, 94, 141]. Finally, we note that we did attempt to estimate POM from the NEON data[142], however, the NEON sampling method is not set up to capture larger particles and debris and thus estimates were much smaller in magnitude than other carbon losses. POM export has also been observed to be driven by discharge events[143, 144], but we acknowledge it is a missing piece of our total carbon losses.

While discharge drives total carbon losses from each network, topography and geology will determine the form of carbon losses from the networks (Figure 3.8). We found the highest proportion of carbon emissions of total carbon losses in the highest sloped networks (Martha, Caribou, and Como Creeks). Mountainous streams with high slopes have higher areal CO_2 evasion fluxes from higher gas exchange velocities[9, 20, 145]. When examining where emissions occur in each stream network, we find that first order streams especially drove emissions in these three networks. In contrast, emissions were more spatially distributed across the Walker Branch and King's Creek stream networks, which exhibited lower gas exchange velocity due to lower slopes (Figure 3.4). Walker Branch and King's Creek also had the highest proportion of DIC export of total carbon losses. This is consistent with the carbonate bedrock in both networks, which will enhance carbonate weathering, removing pCO_2 from the water column and increasing bicarbonate[19]. Our stream network models do not incorporate the removal of pCO_2 from carbonate equilibrium, which will impact our estimation of emissions at both stream networks. The removal of pCO_2 from carbonate buffering will likely inhibit evasion[146], although Saccardi and Winnick, 2024[147], using a similar same stream network model that incorporates carbonate buffering, observed that total watershed CO_2 fluxes remained slightly elevated due to disproportionate contributions from high-gas-exchange areas where the buffering model predicted slightly higher pCO_2. DOC export was relatively low across all stream networks but had the highest relative proportions of total carbon losses at Caribou Creek and Como Creek, primarily due to elevated DOC concentrations coinciding with high discharge during snowmelt, a pattern that has been observed for boreal and mountainous streams[144, 148, 149]. When comparing our five stream networks located across diverse biomes, we conclude that hydrological regimes predominantly determine the magnitude, form, and timing of stream carbon losses; however,

accurately capturing these losses also requires considering topography, geology, and terrestrial productivity, which influence carbon dynamics and whether carbon will be evaded from a network or transported downstream.

Conclusions

Our findings underscore the pivotal role of discharge in driving lateral carbon transfer, carbon emissions, and total carbon losses by headwater stream networks across five biomes with different hydrologic regimes. Our network models demonstrated that high discharge events contributed disproportionately to annual CO_2 emissions at all stream networks. Spatially, our analysis highlighted that first-order streams consistently produced higher areal emissions compared to higher-order streams, attributed to steeper slopes and connectivity to the source of pCO_2, terrestrial soils and groundwater.

While incorporating stream permanence did not alter annual emissions estimates with our modeling approach, it determined the timing and distribution of emissions. Incorporating stream permanence also revealed how pCO_2 sensors capture the influences of upstream processes, emphasizing the need to understand the stream network extent to interpret sensor readings. We also highlight how sensors placed in low-gradient areas compared to the slope of the rest of the network are not representative when estimating annual emissions. We show that the stream network models were most sensitive to changes in groundwater concentrations; better characterization of spatial and temporal variability in groundwater concentrations will be essential for accurately predicting stream carbon emissions.

Our findings reveal that differences in biome and landscape characteristics, including topography, hydrologic regime, and bedrock type, shape both temporal and spatial patterns of carbon emissions and will determine whether carbon is emitted to the atmosphere or exported downstream. Our analysis demonstrates that while hydrologic regimes primarily control the magnitude and timing of carbon losses across stream networks, topography and geology shape whether carbon is evaded as CO_2 or exported as DIC and DOC, highlighting the need to capture both high discharge events and characterize stream network landscapes. While discharge remains the primary driver of stream carbon losses, the influence of groundwater concentrations and intermittent flow conditions create hotspots of emissions that may not be captured by sampling pCO_2 at a single site or season or even with a single CO_2 sensor. Sampling campaigns should focus on these spatial and temporal hotspots to better capture annual emissions and generate an improved understanding of carbon emissions and export. When this is not possible, spatially explicit process-based models offer an opportunity to simulate difficult to measure high discharge events as well as emissions at the headwaters of networks when terrestrial connectivity and transport are the highest.

Acknowledgments

We thank Jill Conroy, Abby Nesper, Hazel Sanders, Benjamin Lloyd Miller, Anthony Stewart, Fenix Garcia Tigreros, and Gabriel Wisswaesser for field and laboratory support. We also thank Kenneth Bible, Benjamin Vierra, Matt Schroeder, Chris Burton, and Alex Keithline for help with site access to the Wind River Experimental Forest and John Blair, Barbara Van Slyke, Walter Dodds, and Erin Seybold for help with site access and background for the Konza Prairie Biological Station. This work was supported by the National Science Foundation (Award

#1926426 and Award #1926423). The National Ecological Observatory Network is a program sponsored by the U.S. National Science Foundation and operated under cooperative agreement by Battelle. Data collected and used in this research were obtained through NEON Research Support Services.

Supplementary Information

Text S3.1. CO_2 Sampling Headspace Equilibrium Method

During our longitudinal sampling campaigns, we measured pCO_2 using a headspace equilibrium method. We equilibrated three gas-tight syringes with 30 mL of stream water with 30 mL of nitrogen gas in the field[48, 49]. The syringes were shaken for 3 minutes before injection of the equilibrated headspace into a pre-evacuated exetainer. Samples were analyzed using a Shimadzu GC-2014 Gas Chromatograph equipped with a methanizer and a flame ionization detector set to 100°C. Dissolved pCO_2 in the original water sample was calculated from a mass balance of the headspace equilibrium system using standards of known concentration, temperature measured in the field, local pressure, and the volume of water and the headspace[48, 49]. The molar quantity of carbon dioxide in the headspace is calculated as:

$$n_{headspace} = \frac{[CO_2] \times V_{headspace}}{0.08206 \times T}$$

where $[CO_2]$ is the concentration of CO_2 calculated from standards of known concentration, $V_{headspace}$ is the volume of the headspace in the vial, and T is the temperature (K). The molar quantity of carbon dioxide in the sample water is calculated as:

$$n_{water} = \frac{\alpha \times [CO_2] \times V_{water}}{0.08206 \times T}$$

where α is the solubility coefficient calculated based on the temperature[50]. The molar quantity of carbon dioxide in the headspace and water are then added together to find the total concentration.

Text S3.2. WEPPCloud Model Outputs

Our initial WEPPCloud model outputs are included here. Model outputs were downloaded to a local a local machine and modified as described in Text S3.1:

- Walker Branch: https://wepp.cloud/weppcloud/runs/misty-inversion/disturbed9002/
- Martha Creek: https://wepp.cloud/weppcloud/runs/barbarian-destructiveness/disturbed9002/#export
- Como Creek: https://wepp.cloud/weppcloud/runs/goggle-eyed-loosening/disturbed9002/
- King's Creek: https://wepp.cloud/weppcloud/runs/phlegmy-treason/disturbed9002/

Text S3. Watershed Erosion Prediction Project Model Description

The Watershed Erosion Prediction Project Model (WEPP) runs were run with WEPPCloud, the online implementation of WEPP. The WEPPCloud model summarizes land cover and soil data for each hillslope from the National Land Cover Database[150] and the NRCS SSURGO soils database[151]. We selected the NEXRAD breakpoint to build the climate files built from daily stochastic climate from weather stations nearby the sites[108, 152]. To further alter other WEPP-specific parameters, we downloaded the initial WEPPCloud runs to a local machine with the WEPP-win-bootstrap tool[108].

Once downloaded, we manually calibrated the streamflow outputs from WEPP using four WEPP parameters most critical for streamflow calibration in previous studies: (1) the baseflow coefficient, which determines the rate of the linear baseflow recession curve, (2) the deep seepage coefficient, which controls the amount of subsurface groundwater flow leaving the watershed, (3) the vertical conductivity of the restrictive layer (Ksat), and (4) the mid-season crop coefficient, a multiplier relating actual evapotranspiration to the reference ET calculated with the Penman-Monteith equation[107, 112, 153]. We determined baseflow coefficient and deep seepage coefficient had minimal impact on the WEPP model results so we set them to their

default values for each run. We estimated the vertical conductivity of the restrictive layer based literature ranges for each site of the underlying geology, where we selected a value within the range that provided the best model fit. At King's Creek, highly variable hydraulic conductivity has been observed ranging over five orders of magnitude from 3.6×10^{-2} to 3.6×10^{3} mm hr^{-1} [154]. At Martha Creek, we used a range for basaltic-andesite volcanic bedrock found in the region from 1.7×10^{-3} to 250 mm h^{-1} [155]. At the Niwot Ridge near Como Creek, variable hydraulic conductivity has been observed from 2.0 to 180 mm h^{-1} [156]. At Walker Branch, the nearby Melton Valley hydraulic conductivity has been observed from 1.3×10^{-2} to 31 mm h^{-1} [157]. To estimate the mid-season crop coefficient, we used eddy covariance data from the NEON towers using the R package bigleaf[58, 158]. Parameters are described in Table S3.1. The resulting model fit is described in Table S3.2.

Text S4. Scaling Relationships used in Stream Network Model

We calculated the flow at each point (Qi) as a function of the drainage area upstream of the point (A_i), the upstream drainage area of the gage (A_g), and the average flow at the gage during the sampling period (Q_g)[56, 57]. The constant, c is the scaling power dependency and commonly set to 1 in hydrology to assume discharge scales linearly with drainage area[56, 57]:

$$Qi = Q_g \frac{{A_i}^c}{{A_g}^c}$$

We estimated the stream cross-sectional area (A, width × depth; m^2) at each point using scaling relationships with width (w) and depth (h)[9, 38]. Velocity was also estimated using these scaling relationships[9]:

$$w = 7.104\ Q^{0.447}$$

$$h = 0.298\ Q^{0.222}$$

$$v = 0.668\ Q^{0.365}$$

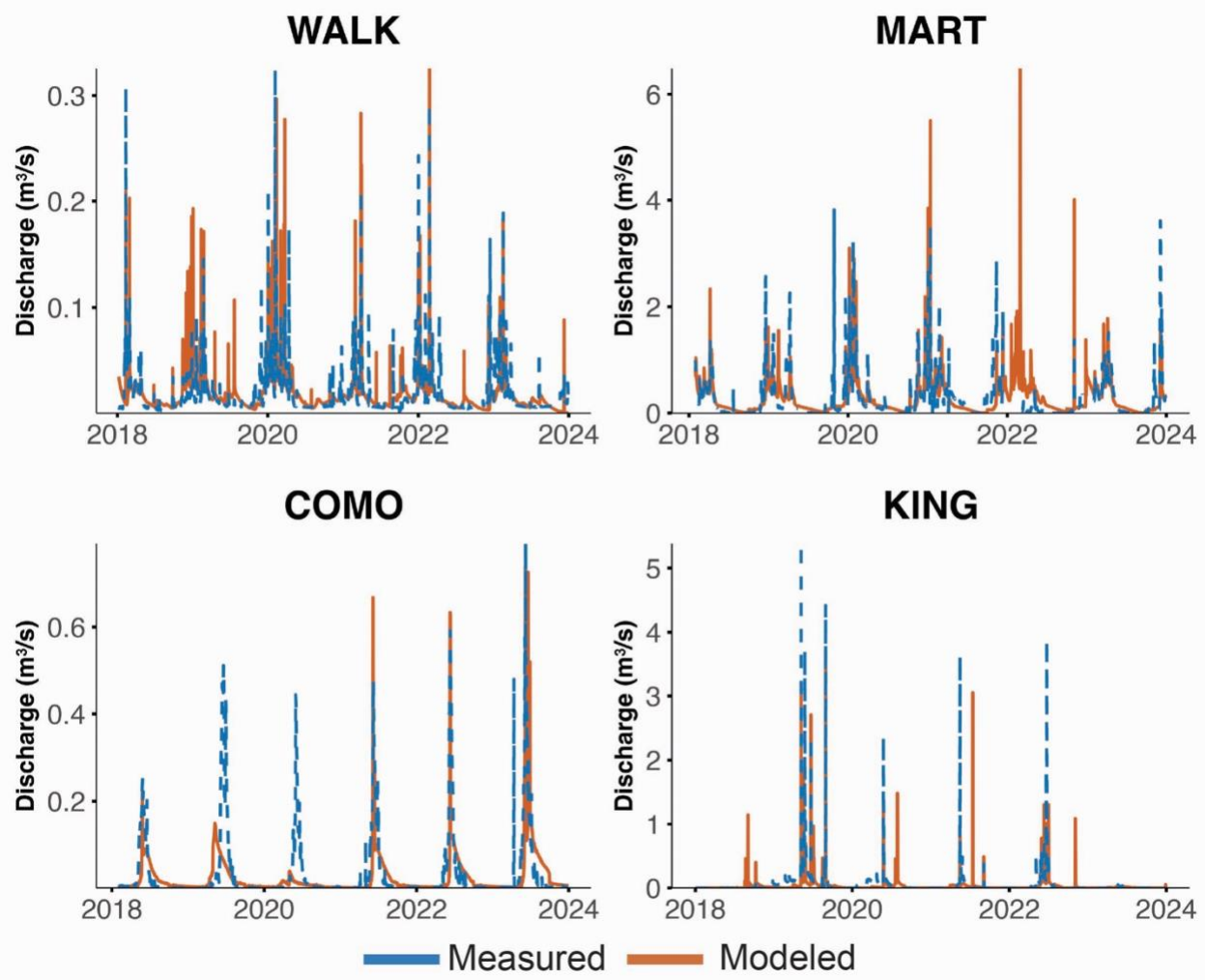

Figure S3.1. WEPP Calibration Discharge Results. Measured values are shown in blue from the NEON stream gages. Modeled values are shown in orange from the WEPP model.

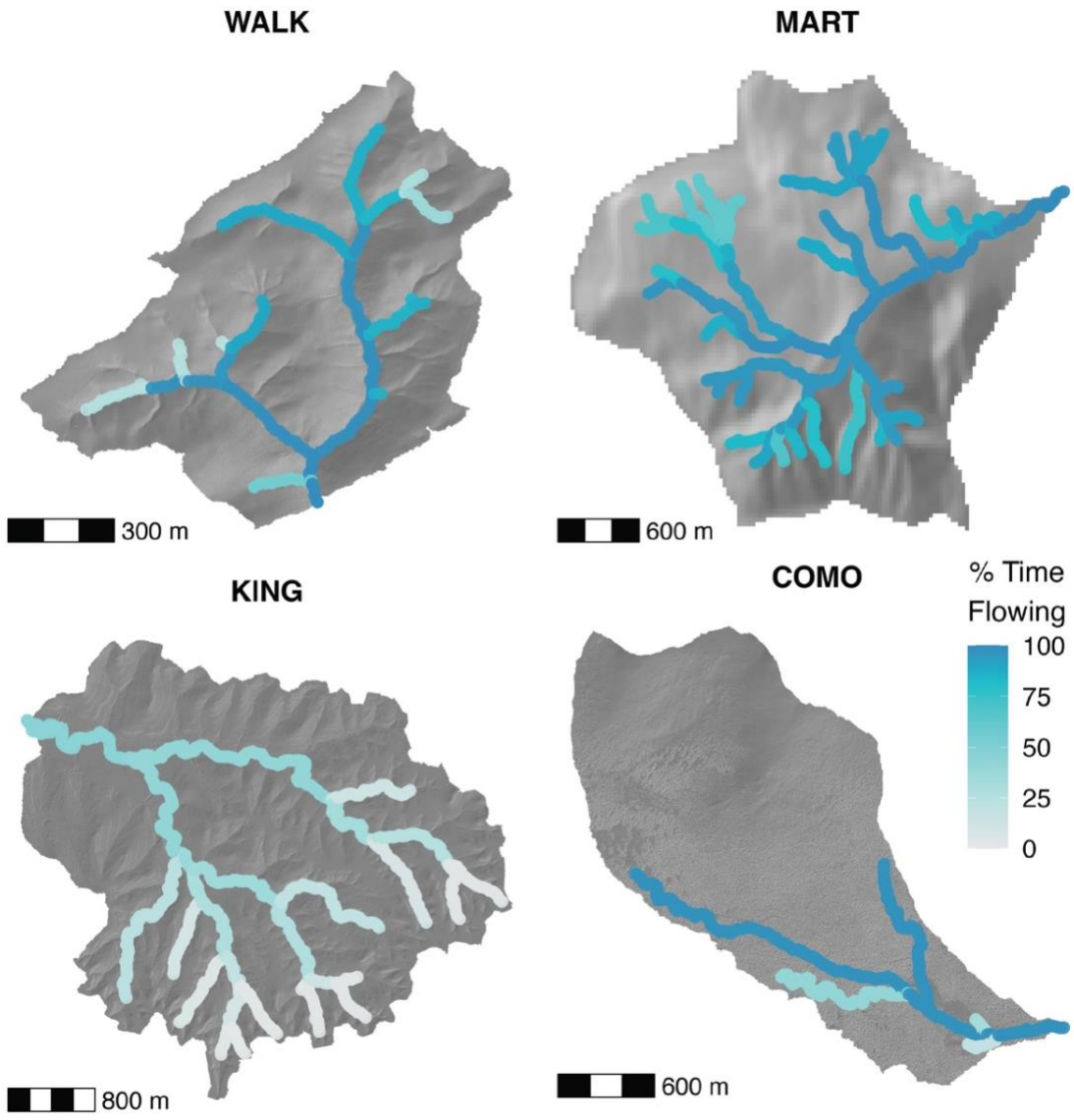

Figure S3.2. Percent of time each stream reach was flowing from the WEPP model by stream reach from 2018-2023. For Como Creek, stream flow was only estimated for non-frozen stream periods (May – October).

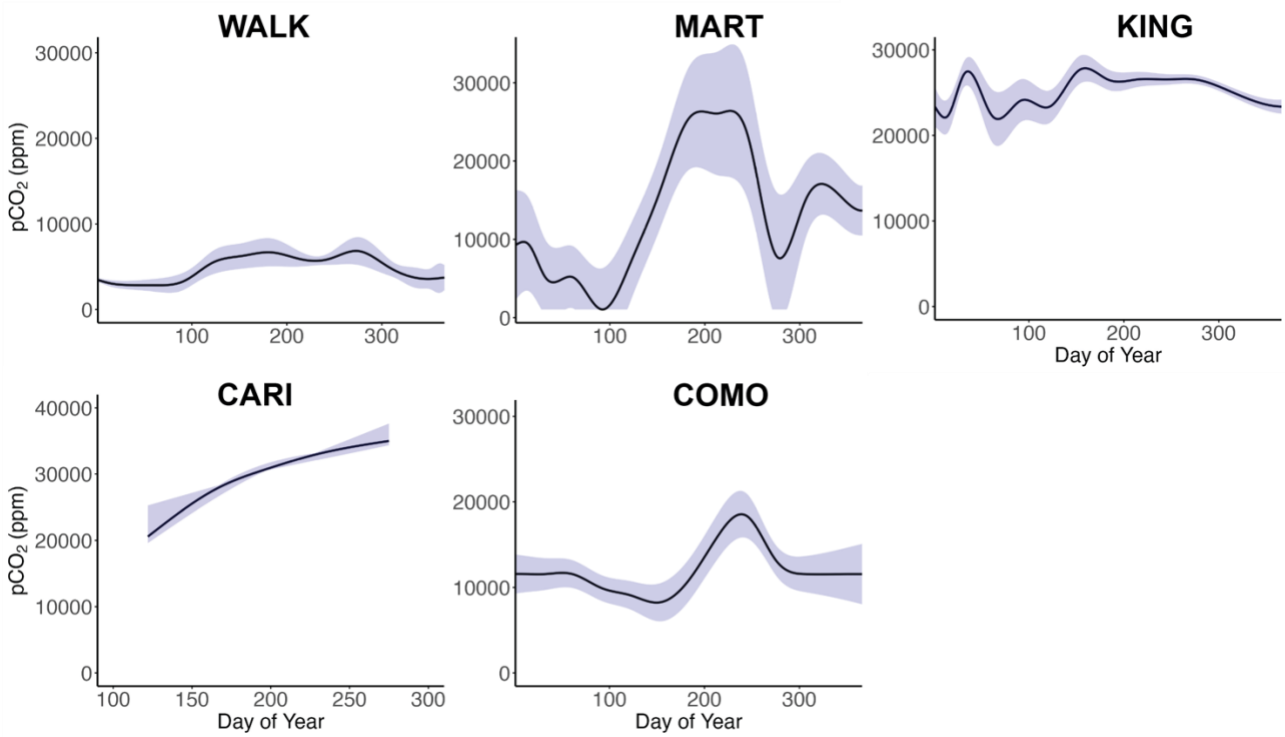

Figure S3.3. Daily groundwater pCO_2 for each site with uncertainty shown in blue. Groundwater pCO_2 was averaged across wells when multiple wells were sampled and were interpolated using the spline function in R to get a daily estimate. Estimates were determined from monthly well sampling. Uncertainty for daily estimates were determined using bootstrap resampling, and confidence intervals are calculated as the standard deviation of the bootstrap predictions aro und the interpolated values.

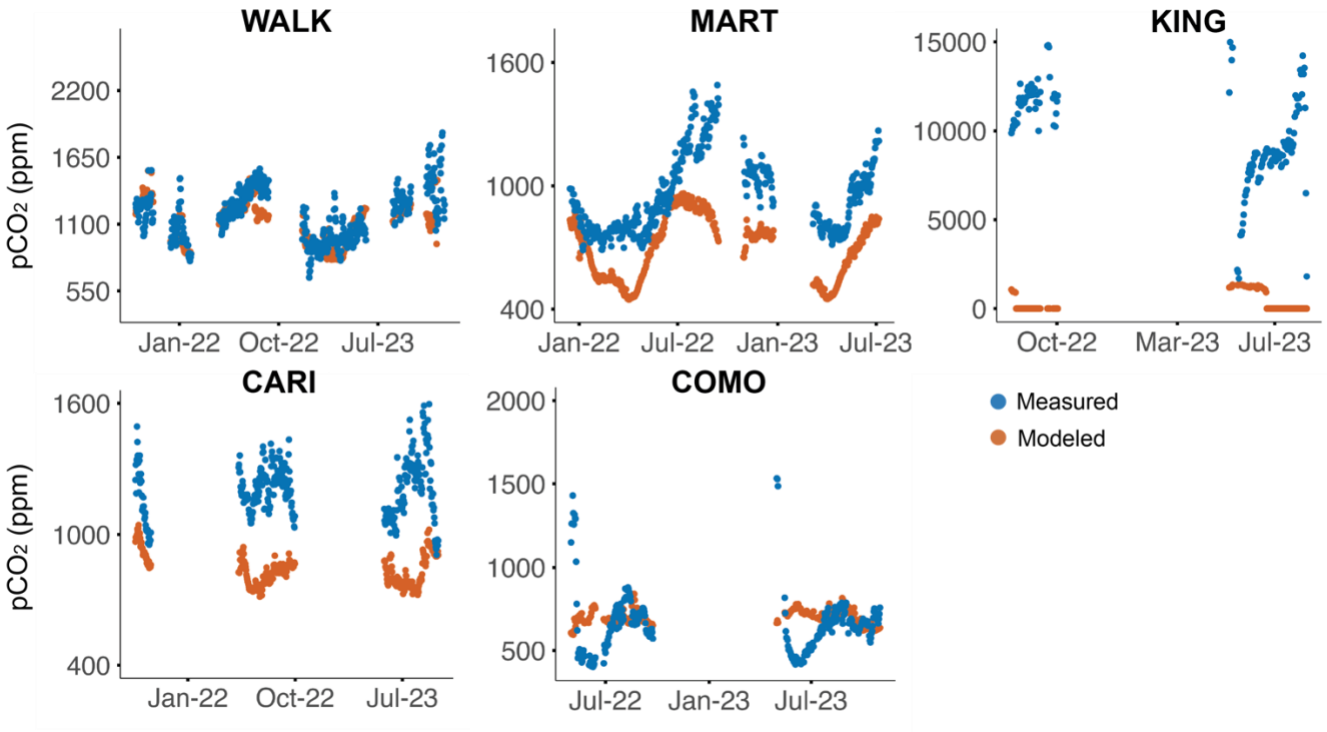

Figure S3.5. CO_2 sensor concentrations versus modeled pCO_2 at the network outlet for the modeled-static network runs. pCO_2 at Como Creek and Walker Branch had the best model fit, while pCO_2 at Martha Creek, Caribou Creek, and King's Creek were underestimated.

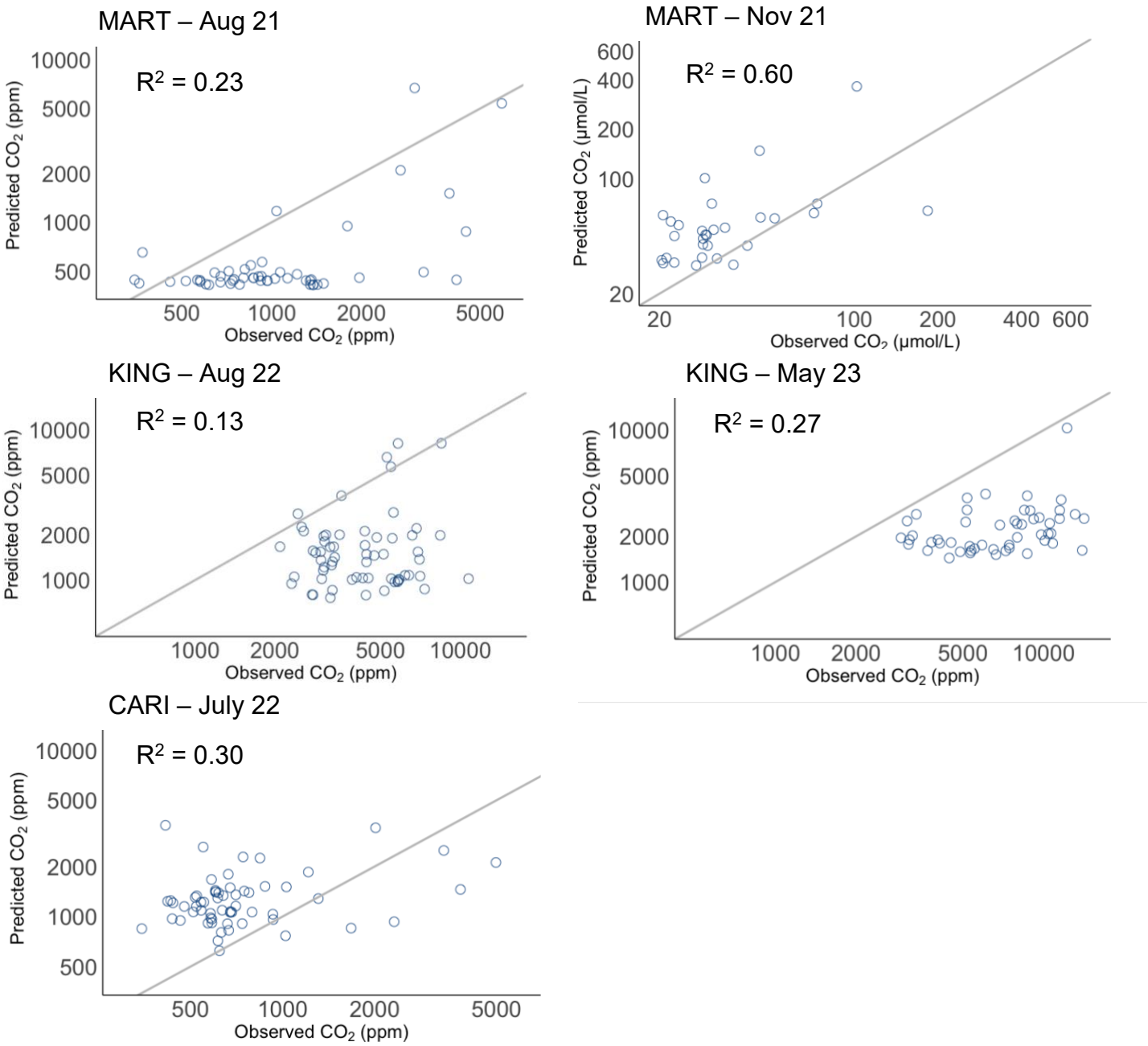

Figure S3.6. Longitudinal Sample Fits. Observed pCO_2 during the longitudinal sampling versus predicted pCO_2 from the stream network models at Martha Creek, King's Creek, and Caribou Creek during each sampling campaign.

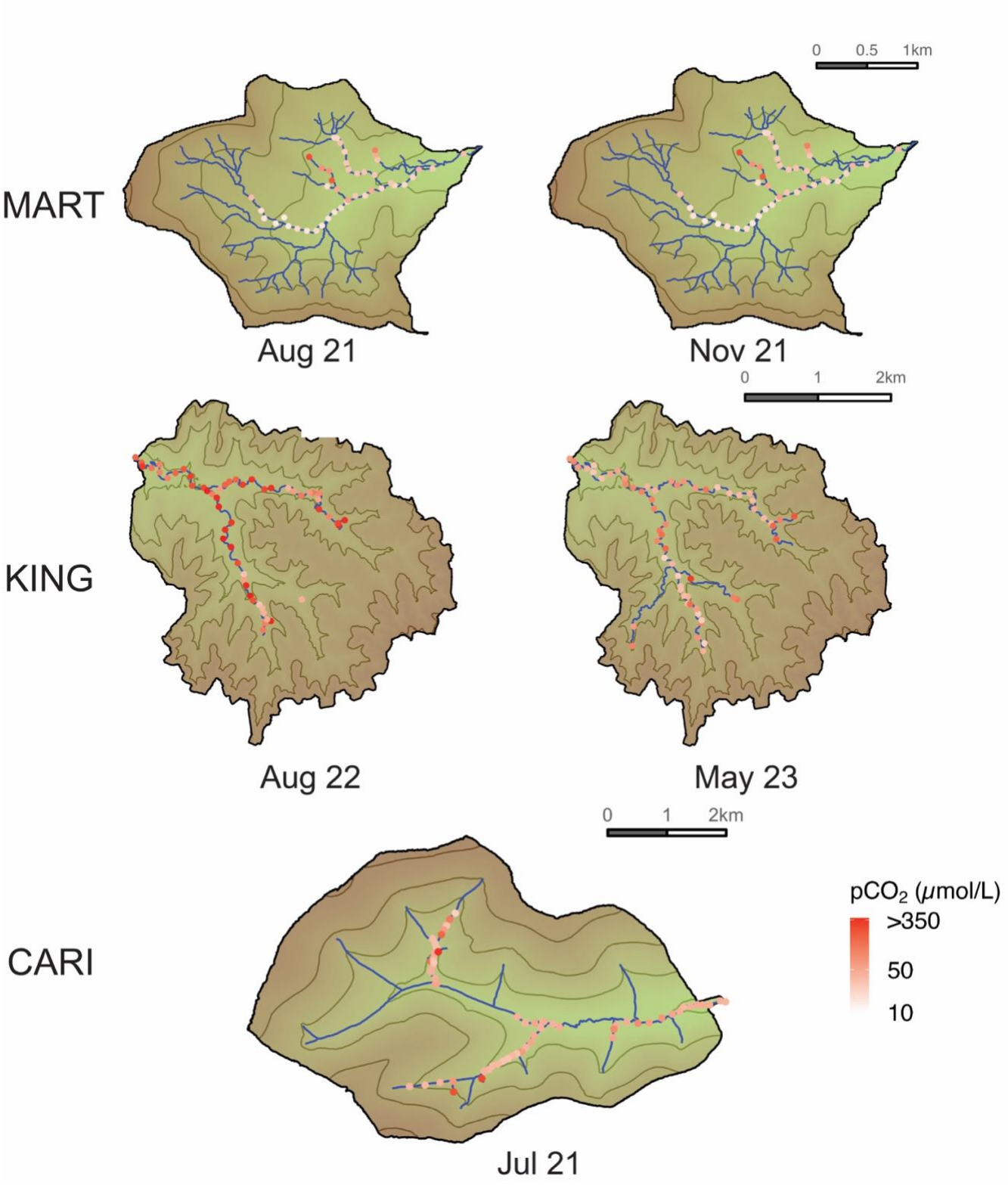

Figure S3.7. Longitudinal Sample Maps. Observed pCO_2 samples from longitudinal sampling campaigns. Sampling campaigns were conducted at Martha Creek in August and November 2021, King's Creek for August 2022 and May 2023, and Caribou Creek in July 2021.

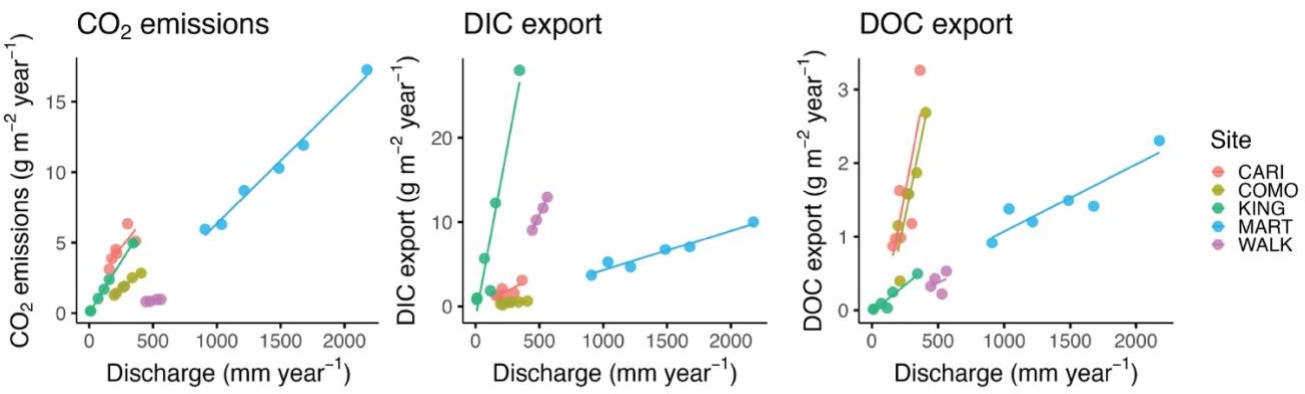

Figure S3.8. Annual emissions versus discharge. Each site is plotted from 2018-2023 versus discharge where a point represents a single year. Caribou Creek and Como Creek years only include May-Sept and April-Oct. All relationships are significant ($p < 0.05$) except at Caribou Creek and Walker Branch for DOC.

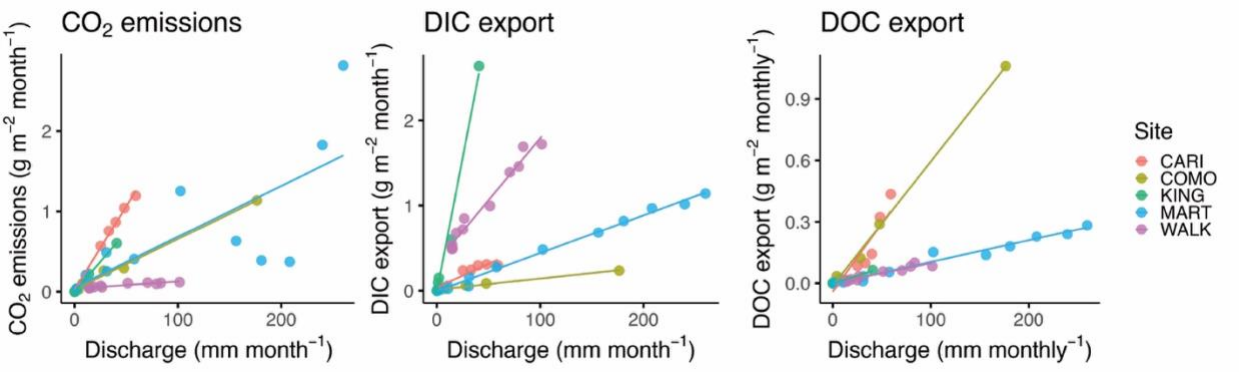

Figure S3.9. Monthly emissions versus discharge. Each site is plotted for each month versus discharge where a point represents a month. Caribou Creek and Como Creek only include May-Sept and April-Oct. All relationships are significant ($p < 0.05$).

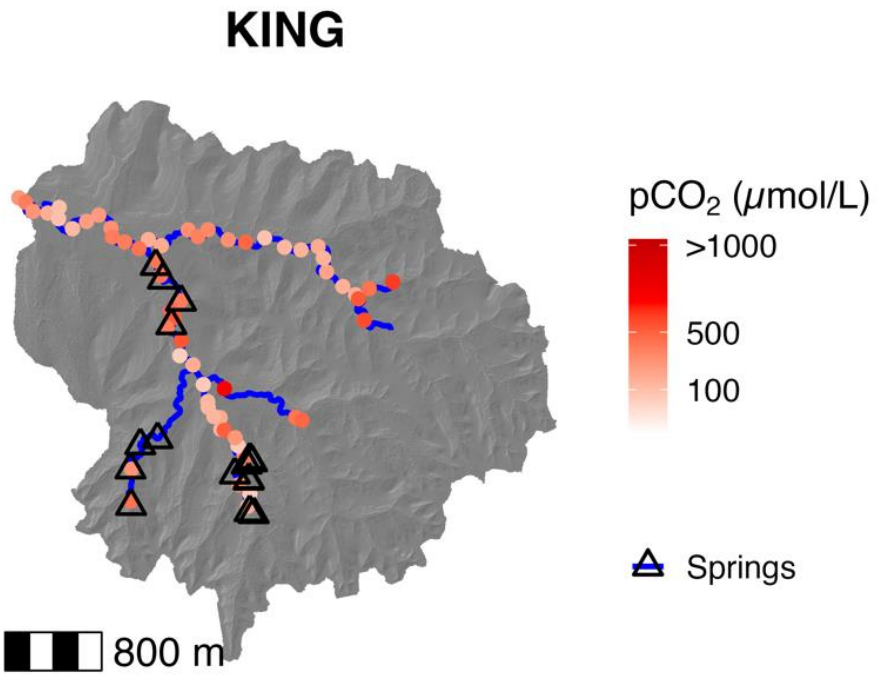

Figure S3.10. King's Creek spring locations. Locations of known springs at King's Creek compared to measured concentrations in May 2022.

Table S3.1. Calibrated WEPP parameters

Stream Network	Baseflow coefficient (day^{-1})	Deep seepage coefficient (day^{-1})	Vertical conductivity of the restrictive layer (Ksat, mm hr^{-1})	Mid-season crop coefficient
WALK	0.04	0	0.001	0.59
MART	0.04	0	0.0017	0.36
COMO	0.04	0	2	0.46
KING	0.04	0	0.01	0.50
Default	0.04	0	0.01	0.95

Table S3.2. WEPP model results

Stream Network	NSE	PBIAS	NSE log Q
WALK	0.25	-22	0.5
MART	0.51	-28.1	0.29
COMO	0.29	0.40	0.37
KING	0.51	-2.6	-24.3

Table S3.3. Changes in annual emissions estimates when incorporating daily NEP predictions from *streamMetabolizer*

Site	Annual emissions with constant median NEP (Mg C $year^{-1}$)	Annual emissions with daily NEP predictions (Mg C $year^{-1}$)	% change
Martha Creek	57.57	57.61	0.06%
Caribou Creek	152.3	152.6	0.16%
Como Creek	6.44	6.56	1.8%
King's Creek	16.4	17.3	5.5%
		Median	1%

Annual emissions with constant median NEP is the annual emissions prediction from each stream network using the median NEP as a constant input into the stream network models. Annual emissions with daily NEP predictions uses the average daily outputs of NEP from where each day of a year is assigned a different NEP input into the network model. Estimates from Marzolf et al. (2025) [116].

Table S3.4. Gas exchange velocity model selected for each site

Site	Regression model selected	k_{600} Mean (m day^{-1}) for NEON monitoring reach	
		Regression model	NEON Gas Exchange Experiments [121]
Walker Branch	Raymond et al. (2012) Equation 4	6.9 (4.64 – 26)	2.2 (0.8 – 31)
Martha Creek[1]	Raymond et al. (2012) Equation 4	16 (0.36 – 43)	0.61 (0.22 – 0.72)
Caribou Creek	Raymond et al. (2012) Equation 7	16.9 (10.6 - 48)	7.7 (6.4 – 12.0)
Como Creek	Raymond et al. (2012) Equation 1	13.9 (2.4 - 108)	8.19 (0.58 - 180)
King's Creek	Raymond et al. (2012) Equation 4	4.39 (0.99 - 16.8)	3.37 (0.47 – 19.8)

1. In the model, we used a combination of the Raymond equations and the regression model obtained from the NEON gas exchange experiments for locations with a similar slope to the NEON reach because of the large discrepancy in the two models[122].

Table S3.5. Measured-dynamic run versus measured-static run

Site	Full Network Size Duration (%)	Minimum Network Extent (%)	Median total stream network annual emissions (Mg C $year^{-1}$)			Median stream network areal emissions (g C m^{-2} day^{-1})		
			Measured dynamic	Measured -static	% difference	Measured dynamic	Measured -static	% difference
Walker Branch	3.1%	34%	1.3	1.4	8.2%	2.6	2.2	15%
Martha Creek	9.3%	0	57.0	57.5	2.1%	5.0	4.8	2.7%
Como Creek*	37%	0	6.5	6.4	0.8%	2.9	2.0	24%
King's Creek	1.9%	0	17.3	16.4	5.5%	4.6	4.3	8%

*Network extent not including frozen stream time periods.

We show using a different stream permanence measure (a zero-flow threshold) results in similar small changes in annual emissions and larger changes in areal emissions between the dynamic and static runs to using the WEPP model.

Table S3.7. Measured-dynamic run versus measured-static run

Run	WALK	MART	CARI	COMO	KING
Standard run					
Annual emissions (Mg C $year^{-1}$)	1.43	58	152	6.44	16.4
MAE (ppm)	173	280	430	220	9400
k_{600} optimized run					
Annual emissions (Mg C $year^{-1}$)	1.44	55	150	6.46	8.95
k_{600} multiplier	1.1	0.41	0.65	1.05	0.04
MAE (ppm)	104	140	75	188	3075
% change in emissions	0.7%	5%	1%	0.3%	48%
C_{gw} optimized run					
Annual emissions (Mg C $year^{-1}$)	1.3	100	288	6.0	149
C_{gw} multiplier	0.92	1.7	1.9	0.94	9.1
MAE (ppm)	112	134	78	189	2763
% change in emissions	7%	72%	89%	7%	760%

Chapter 4 Dynamic contribution by aquatic metabolism to carbon dioxide emissions from a low-land agricultural catchment

Dynamic contribution by aquatic metabolism to carbon dioxide emissions from a low-land agricultural catchment

Authors: Hannah Conroy[1], David Butman[1], Jens Fölster[2], Emma Lannergård[2], Marcus Wallin[2]

1. University of Washington, Seattle, WA
2. Swedish University of Agricultural Sciences, Uppsala, Sweden

This chapter is in prep to submit to Limnology Oceanography Letters:

Conroy, H. D., Butman, D. Fölster, J., Lannergård, E., Wallin, M. (2025). Dynamic contribution by aquatic metabolism to carbon dioxide emissions from a low-land agricultural catchment [in prep].

Abstract

Carbon dioxide (CO_2) emissions from streams are globally significant despite their limited areal extent and rival those from terrestrial ecosystems. Agricultural land represents 40% of the world's landmass; still magnitude and source dynamics of CO_2 emissions from agricultural streams are largely unknown. We used high-frequency measurements of CO_2 and dissolved oxygen in a temperate low-land agricultural catchment to estimate emissions and the contribution of in-stream metabolism. Although CO_2 concentrations were high (median 3720 µatm), emissions were low (median 4.0 g C m^2 day^{-1}) due to consistently low gas transfer velocities (k_{600}). In contrast to other systems, in-stream metabolism accounted for up to 46% of the emissions. Emissions peaked during late summer when k_{600} was lowest and CO_2 had accumulated, highlighting the importance of CO_2 supply over hydrologic drivers. We show agricultural streams exhibit distinct emission dynamics, underscoring the need to account for biological drivers in carbon budgets for human-impacted landscapes.

Introduction

Streams receive large amounts of organic and inorganic carbon from terrestrial landscapes and subsequently emit a portion of this carbon as carbon dioxide (CO_2) to the atmosphere. Despite their small areal extent, these emissions can be substantial compared to carbon fluxes in terrestrial ecosystems[3, 13, 15]. In small streams, high CO_2 emissions are often attributed to external sources such as groundwater inputs, which originate from soil organic matter decomposition or root respiration[17, 18, 159]. Internal production of CO_2 from in-stream metabolism, including gross primary production (GPP) and ecosystem respiration (ER), also contribute CO_2, with its influence generally increasing downstream and varying between ecosystem types[18, 30, 160]. GPP removes CO_2 from the stream, while ER adds it; when ER exceeds GPP, the streams act as a net CO_2 source. Metabolism is commonly estimated from diel changes in dissolved oxygen (DO) using inverse modeling of high-frequency sensor DO data[55].

Streams and ditches (hereafter referred to as streams) draining agriculture-influenced ecosystems may have higher rates of GPP and ER than other ecosystem types[161, 162]. Agricultural streams often drain open landscapes with low shading by trees resulting in higher light availability and thereby increased potential for GPP[161]. High nutrient inputs, due to excess fertilizer application, can stimulate high rates of both GPP and ER[162]. Elevated inputs of labile organic matter in agricultural streams can also support higher rates of ER[161-163]. High rates of ER have been linked to higher CO_2 concentrations, with agricultural streams exhibiting concentrations up to five times greater than forested stream networks [163, 164].

Despite agricultural land now representing 40% of the earth's surface[165], streams draining these areas are underrepresented in carbon emissions studies, creating uncertainty in carbon budget

assessments[140, 164, 166]. While agricultural streams typically have higher CO_2 concentrations than other ecosystems, there remains uncertainty whether these high CO_2 levels are also reflected in high emissions. CO_2 emissions are a function of both the supply of dissolved CO_2 and the physical conditions at the air-water interface, typically described by the gas transfer velocity (k_{600})[93, 167]. Because agricultural streams are often located in flat landscapes with channel networks characterized by low turbulence and slow flowing water (i.e. low k_{600}), gas exchange may be lower than from streams draining other ecosystem types, potentially leading to lower overall emissions. The interplay between high potential supply of CO_2 and low k_{600} and how this affects emission rates compared to other ecosystems is largely unknown.

Seasonal and temporal patterns of CO_2 emissions in agricultural catchments is another identified knowledge gap. Discharge often drives increased CO_2 emissions, especially during storm events through increased gas exchange and groundwater inflow[21, 22]. Stream discharge and gas exchange rates are generally positively correlated; although, this relationship can vary within a stream and between ecosystems[37], with lower-sloped streams often showing a weaker correlation[20, 122]. In-stream metabolism is also temporally variable, typically controlled by light, flow, and temperature, with respiration influenced by the timing and supply of organic matter[23]. High flow can increase ER through organic matter inputs[23, 168], while also suppressing GPP by reducing light and scouring autotrophs and reducing turnover time[169]. Nutrient supply may also regulate the magnitude of both ER and GPP, although a direct relationship between nutrient supply and algal biomass across different rivers has not been quantified[138, 170, 171]. Despite potential for high rates of metabolism in agricultural streams, it is currently unclear how hydrologic variation influences its contribution to CO_2 emissions.

For this study, we combine continuous measurements of DO and CO_2 sensor data to quantify in-stream metabolism and its role in CO_2 emissions from a low-land stream largely influenced by arable land. To our knowledge, this is the first study to pair high-frequency sensor-based rates of metabolism with independent estimates of CO_2 emissions in a highly arable watershed. We aim to (1) identify drivers of stream CO_2 emissions at a site highly influenced by arable land, (2) determine the contribution of in-stream metabolism on CO_2 dynamics and emissions, and (3) examine how in-stream metabolic processes change throughout a growing season under variable discharge and water quality conditions.

Methods

Study Site

The study was conducted at the Hågaån catchment located west of Uppsala, southern Sweden (Figure 4.1). The 122 km^2 catchment ranges in elevation from 3 to 77 masl with a mean slope of 0.016 (m m^{-1}), compared to 0.018 (m m^{-1}) for the study reach. Land cover consists of 59% forest, 21% arable land (mainly cereal production and pasture), 8% other open land, 7% wetland, 5% urban area, and 0.5% lakes and streams. While arable land covers only 21%, the downstream ca 2/3 of the main stream channel flows through a flat, open, landscape dominated by arable land, strongly influencing the biochemical conditions of the stream (Figure 4.1). Catchment area and characteristics were calculated based on a modified 10 m DEM resampled to 2x2m[172] and augmented with national hydrography. Land-cover distribution was based on a national land-cover data base[173].

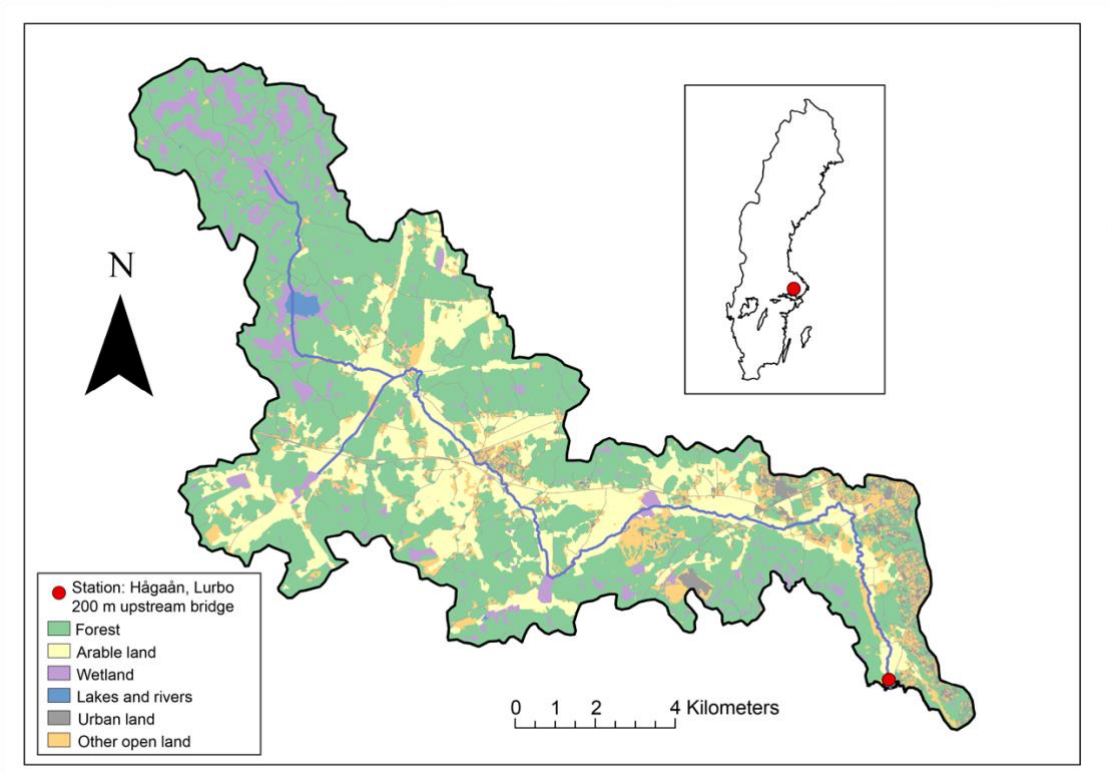

Figure 4.1 Site map of the Hågaån stream catchment. The catchment is composed of 21% arable land; most of the stream network drains directly through areas of arable land.

The long-term mean annual temperature is 6.5°C with 586 mm of precipitation, with precipitation occurring as both rain and snow (1991-2020, station: 97530, SMHI). The growing season length lasts an average of 195 days (mid-April to end of October), with peak streamflow during spring snowmelt.

Sampling Hågaån

Continuous oxygen concentration, specific conductivity and turbidity was measured all-year at the site during 2020-2023 using a multi sensor Aqua TROLL 600 at 15 second intervals (In-Situ, USA) fitted into a perforated plastic tube. The sensors were all fixed at ca 50 cm below the

average water surface. Regular maintenance and quality control of sensor data was performed according to Lannergård et al. (2019)[174]. During 2020, continuous CO_2 concentrations were measured using a eosGP sensor (Eosense, Canada) from February to October storing average values at 30 minute intervals. A description of the sensor calibration is provided in Text S4.1. Power loss resulted in missing CO_2 concentration data from September 3rd, 2020 to October 2nd, 2020.

Discharge was measured using an established stage height-discharge relationship based on manual velocity-cross section area measurements covering most of the observed discharge range. Stage height was continuously recorded at 30 min interval using a Tru-Track capacitance sensor (Tru-Track, New Zealand). Missing discharge data (2020-08-12 to 2020-08-24) was gap-filled using specific discharge from the nearby SMHI station Sävån (~10 km SW). As a proxy for photosynthetically active radiation (PAR), we used shortwave incoming radiation obtained from a nearby meteorological station (~5 km)[175]. Manual water samples were collected bimonthly since 2016 as part of Sweden's national monitoring program and analyzed using accredited methods at Swedish University of Agricultural Sciences, Uppsala[176].

Hågaån had slightly lower nutrient concentrations and slightly higher organic carbon than other Swedish streams (Table S4.1), but overall values were similar, supporting its representativeness as a typical Swedish agricultural stream.

Data Analyses

We estimated net ecosystem production (NEP) using *streamMetabolizer* in R, a state-space Bayesian stream metabolism model that gives the best fit of GPP, ER, and air-water gas

exchange of oxygen to match modeled and measured DO[61]. Stream metabolism was run using the Bayesian implementation in *streamMetabolizer* by accounting for both observation and processing errors with 6,000 saved steps (Text S4.4.). During some time periods, a diel signal was observed in the discharge data. *streamMetabolizer* assumes constant hydrodynamic conditions, specifically, a uniform discharge and reaeration rate over the diel cycle, which neglects the potential influence of diel flow fluctuations on DO dynamics[61]. We thus attempted to remove days that exhibited a strong diel signal in discharge before running *streamMetabolizer* described in Text S4.2). After quality-checking model estimates (Text S4.2), we were left with 773 days of metabolism estimates for the period 2020 – 2023. NEP was calculated as the difference of the modeled GPP and ER (g O_2 m^{-2} day^{-1}), where ER is reported as a negative flux to reflect oxygen consumed through respiration. To estimate the proportion of emissions that contributed to in-stream metabolism, we assumed a respiratory quotient of 1 mol C to 1 mol O to convert oxygen-based estimates to carbon equivalents, although we acknowledge that this quotient likely varies[177].

Stream CO_2 emissions were estimated daily based on the continuous CO_2 concentration data and estimates of the gas-transfer velocity, k_{CO_2}, (m day^{-1}). k_{CO_2} was derived using equation number 4 from Raymond et al. (2012)[51]. We selected the regression model that resulted in k_{600} values most similar to those predicted from *streamMetabolizer* estimates (Figure S4.5). Further method descriptions for the CO_2 emissions determination can be found in Text S4.3.

To examine the effect of discharge on metabolism and water chemistry, we used segmented process-discharge (P-Q) for ER and GPP and concentration-discharge (C-Q) relationships for water chemistry. P-Q relationships help clarify how discharge influences in-stream metabolism,

especially when processes differ between low and high flows[62]. Comparing P-Q relationships to concentration-discharge (C-Q) relationships can reveal how water chemistry variables including turbidity, conductivity, and nutrients, affect metabolism at various discharges. We used Davies tests from the *segmented* package in R[62, 178] to detect slope changes across 10 quantiles in log-transformed data. Slope differences were assessed using a two-tailed z-test[179], and chemostasis (the slope of the P-Q or C-Q relationship is zero) using ANOVA[62, 180].

Results

Continuous stream data

Median daily discharge ranged from 0.004 to 14.5 $m^3\ s^{-1}$ with a median of 0.44 $m^3\ s^{-1}$ during the period 2020-2023. Hågaån flow peaks during snow melt and comes to an annual low during the summer (Figure 4.2). 2020 was a drier year (median 0.35 $m^3\ s^{-1}$) than the 2020-2023 annual median discharge. From 2020 to 2023, DO ranged from 0.20 to 16.1 mg L^{-1} with a median of 10.8 mg L^{-1}. DO peaked each year at the end of the spring (typically April-May) and were at their lowest in July of each year. Oxygen was typically undersaturated (83%) with saturation levels ranging from 2.0 – 168% saturation. In 2020, the stream CO_2 concentrations ranged from 1330–22,300 µatm (median 3520 µatm). The CO_2 concentrations peaked in August, before a power outage in September. We examined departures from equilibrium of O_2 and CO_2 concentrations and found the stream concentrations were consistently offset above the 1:1 departure line (Figure S4.6).

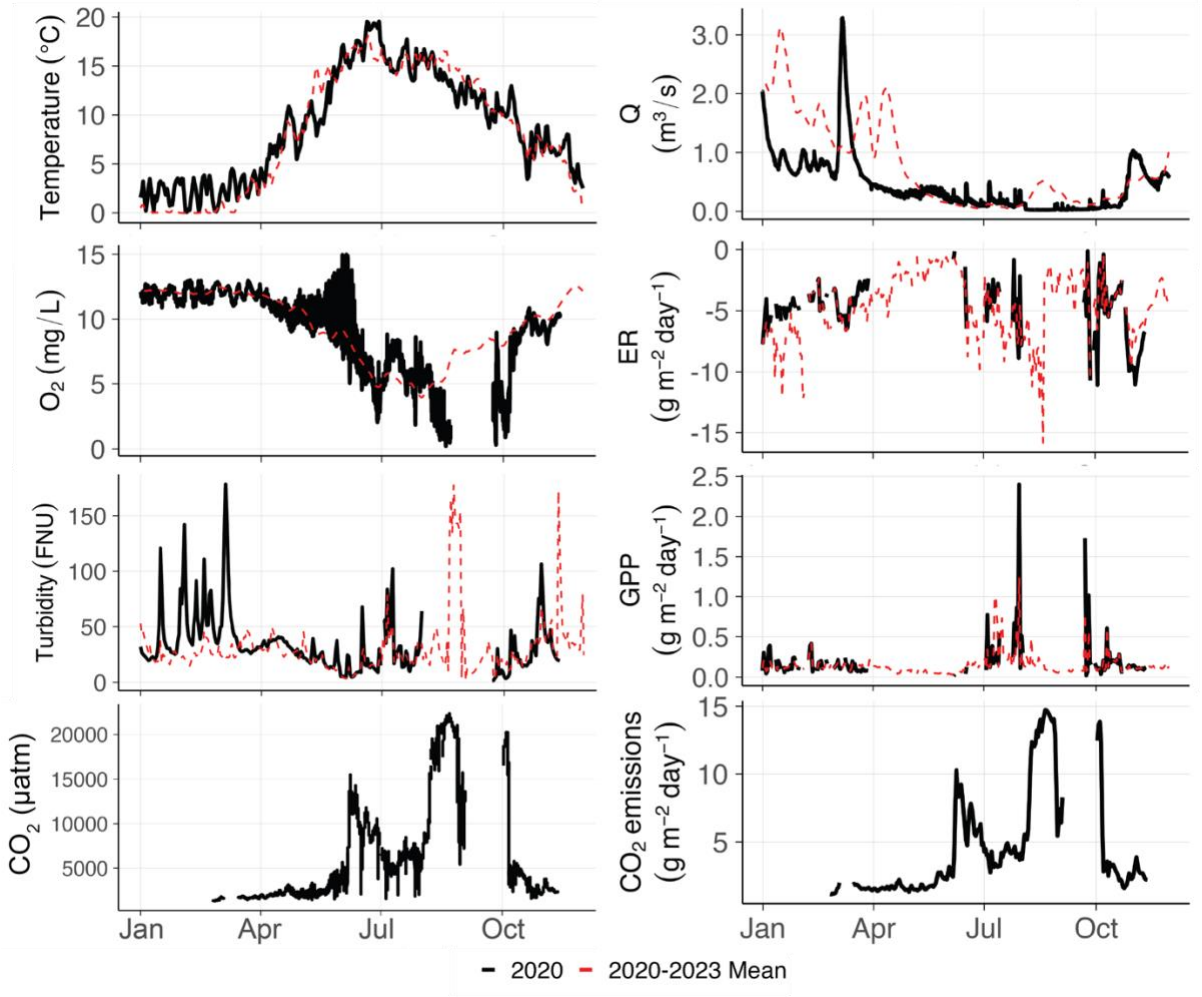

Figure 4.2 Mean daily data of measured water temperature, oxygen, turbidity, CO_2 concentration, and discharge at Hågaån, together with modeled metabolism (ER and GPP) and CO_2 emissions. The black line shows 2020 data when CO_2 measurements were included. The red dashed line shows the mean daily average from 2020-2023.

Stream metabolism

Rates of ER were consistently higher than GPP (Figure S4.7). ER, reported as the flux of O_2 consumption, ranged from -19.1 to -0.12 g O_2 m^{-2} day^{-1} (median -4.9 g O_2 m^{-2} day^{-1}). GPP ranged from 0.013 to 3.0 g O_2 m^{-2} day^{-1} (median 0.12 g O_2 m^{-2} day^{-1}). NEP was therefore almost always negative (contributing CO_2 to the stream) ranging from -19 to 0.26 g m^{-2} day^{-1} (median -4.7 g O_2 m^{-2} day^{-1}). The k_{600} estimated from *streamMetabolizer* ranged from 0.05 to 15.4 m day^{-1} (median

2.20 m day^{-1}). k_{600} did not have a strong relationship with discharge from the metabolism output (R^2 = 0.15, Figure S4.8). These values compared to the k_{600} estimated using regression equation with a range of 1.25 to 9.37 m day^{-1} (median 1.54 m day^{-1}).

CO_2 emissions estimates

Median daily CO_2 emissions estimates ranged from 1.7 to 22 g C m^{-2} day^{-1} (median 4.0 g C m^{-2} day^{-1}). CO_2 emissions estimates were highest when CO_2 concentrations were highest – in the summer into the fall (median of 9010 µatm in the summer). CO_2 emissions in the summer months had median 8.1 g C m^{-2} day^{-1} compared to 2.4 g C m^{-2} day^{-1} in the spring months. The k_{600} was slightly higher in the spring months (median 2.3 m day^{-1}) compared to the summer months (median 2.0 m day^{-1}).

Comparing rates of metabolism to CO_2 emissions, we determined that in 2020 metabolism contributed 46% (1%-118%) to total CO_2 emissions (Figure 4.3). Because CO_2 data were only collected in 2020, we could not estimate metabolic contributions to emissions across the full 2020–2023 period. However, metabolism rates were similar between 2020 and 2021–2023 (median -5.0 g O_2 m^{-2} day^{-1} vs. median -4.6 g O_2 m^{-2} day^{-1}). Contribution of metabolism to total emissions peaked during spring and fall, when CO_2 concentrations and emissions were low.

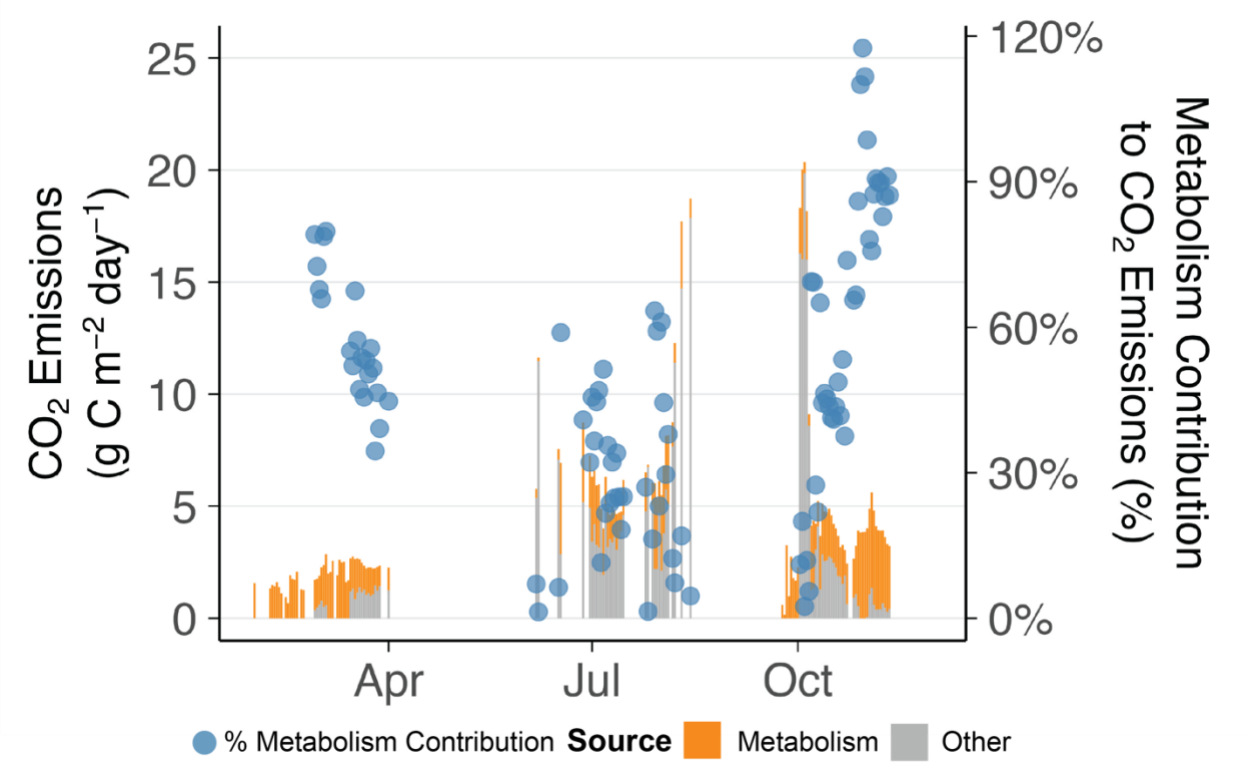

Figure 4.3 The metabolism contribution to total stream CO_2 emissions in 2020. The percent metabolism contribution is shown in blue. The total emissions colored by contributions (metabolism and other) are shown in grey and orange. The median contribution for available days of data in 2020 was 46%.

C-Q and P-Q Analysis

We found significant discharge-related breakpoints for ER and GPP near the median discharge (0.19 and 0.25 m s^{-1}, Table S2). Both ER and GPP decreased below the breakpoint and increased above the breakpoint (Figure 4.4), although GPP had smaller slopes (slope = -0.21 and 0.15). ER displayed steeper slopes below and above the breakpoints (slope = -0.56 and 0.48). Temperature decreased above its breakpoint, reflecting seasonal flow variations with low flow predominately occurring in the summer and high flow periods predominately occurring during snow melt and winter storms. Turbidity was chemostatic below the breakpoint (slope = 0.13) and increased above the breakpoint (slope = 0.39), with a similar breakpoint to ER and GPP (0.24 m s^{-1}). CO_2

had a higher breakpoint (0.54 m s^{-1}) decreasing below the breakpoint and increasing above the breakpoint (slope = -0.8, 0.37).

For some variables with non-continuous data collection, we observed discharge to have a significant effect above and below breakpoint values. We used the entire dataset for this analysis (2016-2023) because data were only measured biweekly. Nitrate-nitrogen (NO_3-N) had a positive relationship with discharge both above and below the breakpoint (0.06 m s^{-1}); the slope was higher below the breakpoint (slope = 2.4, 0.30). Total organic carbon (TOC) was positive below the breakpoint (0.83 m s^{-1}, slope = 0.25) and chemostatic above the breakpoint (slope = 0.017). We also observed significant breakpoints for pH, O_2, and specific conductivity (Figure S4.9) but found no significant breakpoints for PO_4-P, NH_4-N, Total P, Total N, and alkalinity (Table S4.2).

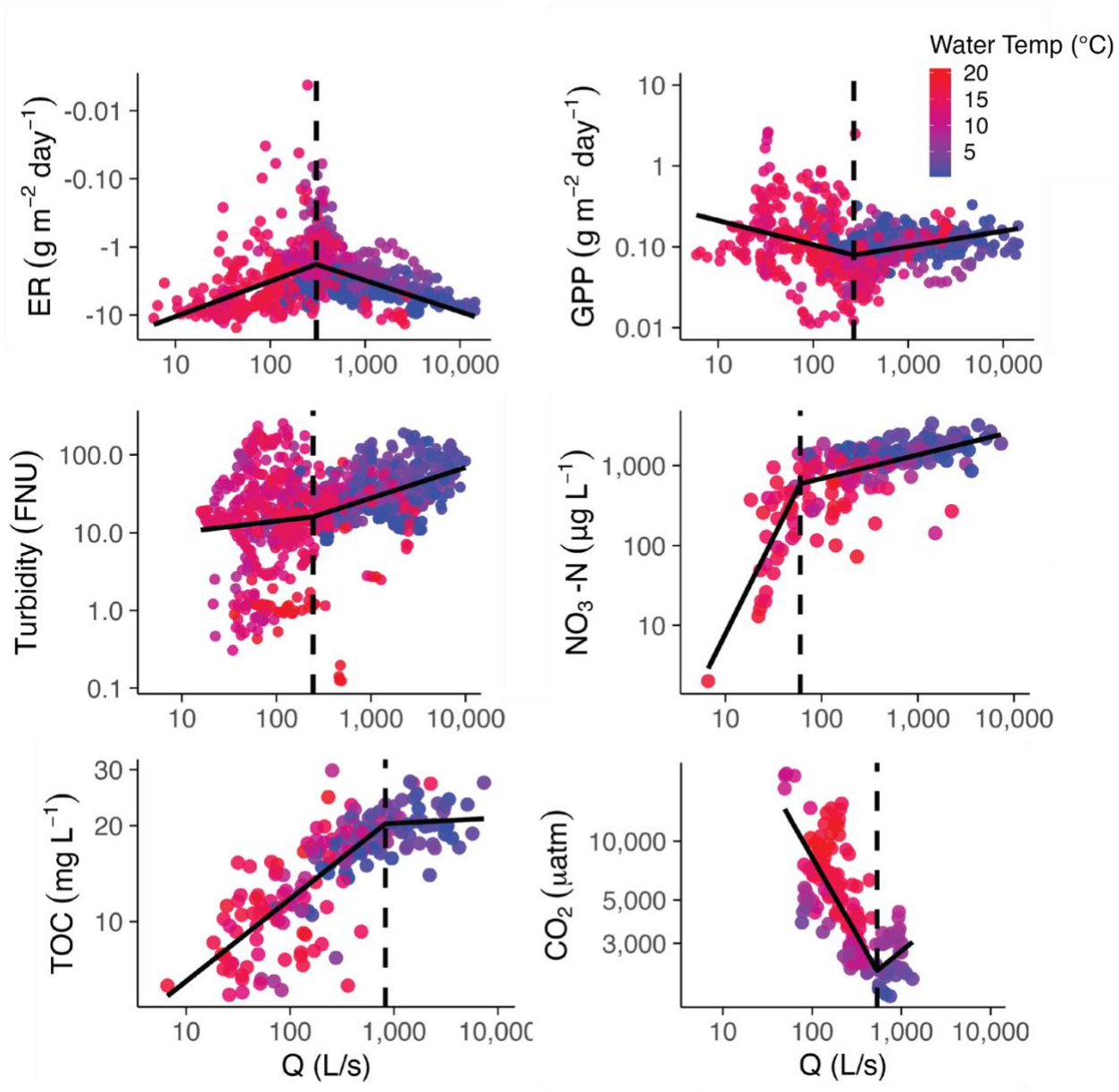

Figure 4.4 C-Q and P-Q plots for selected variables with significant breakpoints. Breakpoints were determined using Davies tests. All values are log-transformed and points are colored by water temperature.

Discussion

In-stream metabolism contribution to CO_2 emissions at an agricultural site

We found Hågaån, a site highly influenced by arable land, was consistently heterotrophic indicating in-stream respiration was a sustained source of CO_2 to the stream network. Net heterotrophy is common in agricultural streams[181-183]. Notably, the contribution of in-stream metabolism to emissions (median: 46%) was higher than expected for a stream of this size (23%[18]).

Although we had only 84 days with concurrent metabolism and emissions data, we found the highest metabolism contributions during days with low CO_2 concentrations, primarily during spring and late summer. On some days metabolism contributions appeared to exceed 100% of total emissions (Figure 4.3). This suggests CO_2 accumulation and downstream export, which has been observed in low- turbulence, organic-rich streams[30, 184]. We confirmed minimal impact of low-O2 groundwater inputs on ER estimates[185] (Supplementary Text 4.3). During summer, CO_2 concentrations peaked while metabolism's contribution declined, suggesting dominant external sources. A persistent offset between O_2 and CO_2 departures from equilibrium (Figure S4.6) supports a CO_2 source uncoupled from in-stream metabolism, such as via ground- or soil water inputs[186]. Higher temperature enhances soil and subsurface respiration in the summer, potentially leading to higher terrestrial CO_2 inputs[187, 188].

Overall, Hågaån CO_2 concentrations were high (median 3500 µatm), aligning with findings in other agricultural catchments[163, 164, 166]. High CO_2 concentrations in agricultural streams have been partially attributed to high rates of respiration due to high inputs of labile organic matter

and non-limiting nutrient concentrations[163, 183]. While our measurements of TOC during the CO_2 monitoring year were limited, concentrations were generally high (median 16.7 mg L^{-1}) and increased with discharge. Metabolism has a disproportionate impact on CO_2 emissions at this agricultural watershed, and understanding the drivers of metabolism can offer key insights into carbon emissions in agricultural streams.

Metabolism driven by seasonality and discharge at agricultural sites

Both ER and GPP showed significant responses to discharge. ER decreased below and increased above the ER-Q breakpoint, and storms have been shown to increase ER in agricultural catchments[189]. Our results indicate that while flow initially suppresses ER, it stimulates it at higher discharge due to increased delivery of organic matter and nutrients. Turbidity was chemostatic below the breakpoint and increased above the breakpoint, a pattern observed in other stream networks due to erosion and transport limitation[62, 190]. Increased turbidity is associated with increases in organic matter, microbial loads, and nutrients[191-193]. We found turbidity to have a similar breakpoint to ER, indicating at a certain discharge threshold, these inputs could support increased ER in the system.

While the breakpoint for organic matter and nutrients (NO_3-N and TOC) did not match the breakpoint for ER, an overall increase in organic matter and nutrients suggest higher ER at higher flow rates. Seasonality also influenced ER, with higher temperature likely stimulating ER to its highest rates during low summer flow. At other agricultural catchments sites, the coupling between solute supply and in-stream processing was most pronounced during low to intermediate flows especially during periods with high temperatures[183, 194, 195]. CO_2 concentrations did

decrease with increasing discharge, which may be attributed to dilution and slightly increased k_{600} during higher flow[27, 68].

Our results for GPP may also be attributed to seasonality – while we would expect GPP to decrease with increases in turbidity due to decreases in light[62, 169, 196], we found a slight increase in GPP after the breakpoint. Through visual observation, GPP was generally low in the spring and fall and peaked in the summer months when flow was low and temperature and light were highest. In some years, GPP increased slightly in the spring when flow was high which could be due to the growing season's favorable conditions for higher GPP even during periods of elevated flow due to increased nitrate uptake and increased daylight[189]. Overall, our estimated rates of GPP (median 0.12 g m^{-2} day^{-1}) were lower than found in other agricultural streams; for example, Frankforter et al. (2010)[197] reported a median of 0.6-1.7 g m^{-2} day^{-1} across 33 agricultural streams. In general, agricultural sites typically have higher GPP than forested streams due to elevated nutrient concentrations and increased light availability[194]. Hågaån is slightly lower in nutrient concentrations compared to other Swedish agricultural catchments potentially due to mixed land use (e.g. 1.9 mg L^{-1} vs. 6.3 mg L^{-1} Total-N and 0.06 mg L^{-1} vs. 0.19 mg L^{-1} PO_4-P[198], Table S4.1), and compared to other agricultural streams globally. For instance, streams in the United States had a median Total-N concentration of 4 mg L^{-1} and Total-P concentration of 0.25 mg L^{-1} compared to 1.9 mg L^{-1} and 0.06 mg L^{-1} at Hågaån, respectively[199]. Although our stream metabolism estimates passed applied quality checks and displayed low equifinality when comparing ER and GPP and k_{600} and ER (R^2 = 0.07 and 0.29), we acknowledge potential uncertainties in our metabolism estimates. While we also removed days with strong diel discharge signals, subtle or low-amplitude fluctuations may still have influenced depth and k_{600} estimates, potentially contributing to underestimation of GPP.

Implication for CO_2 emissions estimates from agricultural streams

CO_2 emissions from Hågaån were low (median 4.0 g C m^{-2} day^{-1}) below global (7.1 g C m^{-2} day^{1}) and north temperate streams (5.6 g C m^{-2} day^{-1})[12]. In contrast, CO_2 concentrations in Hågaån were high (median 3,500 µatm) exceeding both global (2,150 µatm) and north temperate stream averages (1,540 µatm)[12]. This discrepancy is explained by a lower k_{600} in Hågaån (median 1.5 m day^{-1}) versus global estimates (9.4 m day^{-1}) and estimates in north temperate streams (9.1 m day^{-1})[12]. Our derived k_{600} values for Hågaån were slightly lower than those modelled for agricultural streams in Sweden (3.5–5.1 m day^{-1}), and much lower than for forested streams (9.3 to 10.3 m day^{-1}) and alpine regions (19.6–44.5 m day^{-1})[200].

Surprisingly, emissions at Hågaån peaked in late summer when CO_2 concentrations were highest, rather than in spring when k_{600} and discharge were at their peak. This pattern contrasts with findings from Blackburn and Stanley (2021)[140], who reported an increase in CO_2 emissions with floods in ten agricultural reaches, although they did not report the slopes of the study streams. Typically, CO_2 emissions correlate strongly with discharge-driven increases in k_{600}[12, 21], though the relationship weakens in low-gradient reaches[20, 122]. Indeed, k_{600} values estimated from metabolism at Hågaån were weakly related to discharge ($R^2 = 0.15$). This weak coupling likely reflects the flat topography and slow, more laminar-like flow typical of many agricultural systems, where low gas exchange persists even during high-flow events. This decoupling of discharge and gas exchange allows CO_2 to accumulate in the water column over time, particularly during summer when elevated respiration in both stream and surrounding soils coincides with minimal flushing[188]. Thus, rather than being driven by episodic flood events,

seasonal emissions in Hågaån are shaped by sustained CO_2 buildup during low-flow periods with low k_{600}.

Although our observations are limited to one site, previous studies have shown that agricultural streams often behave differently from other ecosystems, with higher CO_2 concentrations, lower gas exchange, and potentially elevated primary production[140, 164, 166]. It has been suggested that these streams could be important CO_2 sources in regions with increasing precipitation and flooding[140], yet our results emphasize the importance of topography. In flatter catchments like Hågaån, emissions appear more strongly influenced by the supply of CO_2 under low-flow conditions than by transient flood events. At our site, CO_2 concentrations generally declined with increasing flow, except during the highest flow events, where concentrations increased. At other sites, the CO_2–discharge relationship has been observed to vary seasonally, with a positive correlation often occurring after periods of low flow when CO_2 accumulates in the stream or adjacent soils[166]. However, the pulse was typically short-lived, as the accumulated CO_2 is quickly flushed. We did not observe this pulse of CO_2 during periods of low flow with discharge, highlighting that the relationship between discharge and CO_2 is event-dependent and site-specific.

We propose a conceptual framework for CO_2 emissions from Hågaån (Figure 4.5). During higher flows, ER increases fueled by nutrient and organic matter loading[168]. Groundwater CO_2 contributions may rise or dilute depending on event characteristics[133, 166]. However, in low-slope systems, gas exchange remains subdued even at peak flow[122], potentially limiting emissions despite high CO_2 supply[93]. As a result, NEP can be a large percentage of total carbon emissions during high flow. Conversely, during low-flow periods, the combination of reduced gas

exchange, high metabolic activity, and potential sustained CO_2 inputs from soils and groundwater allows CO_2 to accumulate in the stream. This leads to modest but persistent emissions that are higher than during peak flow. These patterns likely vary with land use, ecosystem traits, and climate[182, 194, 201] reinforcing the need for site-specific, high-resolution data to constrain agricultural stream carbon budgets.

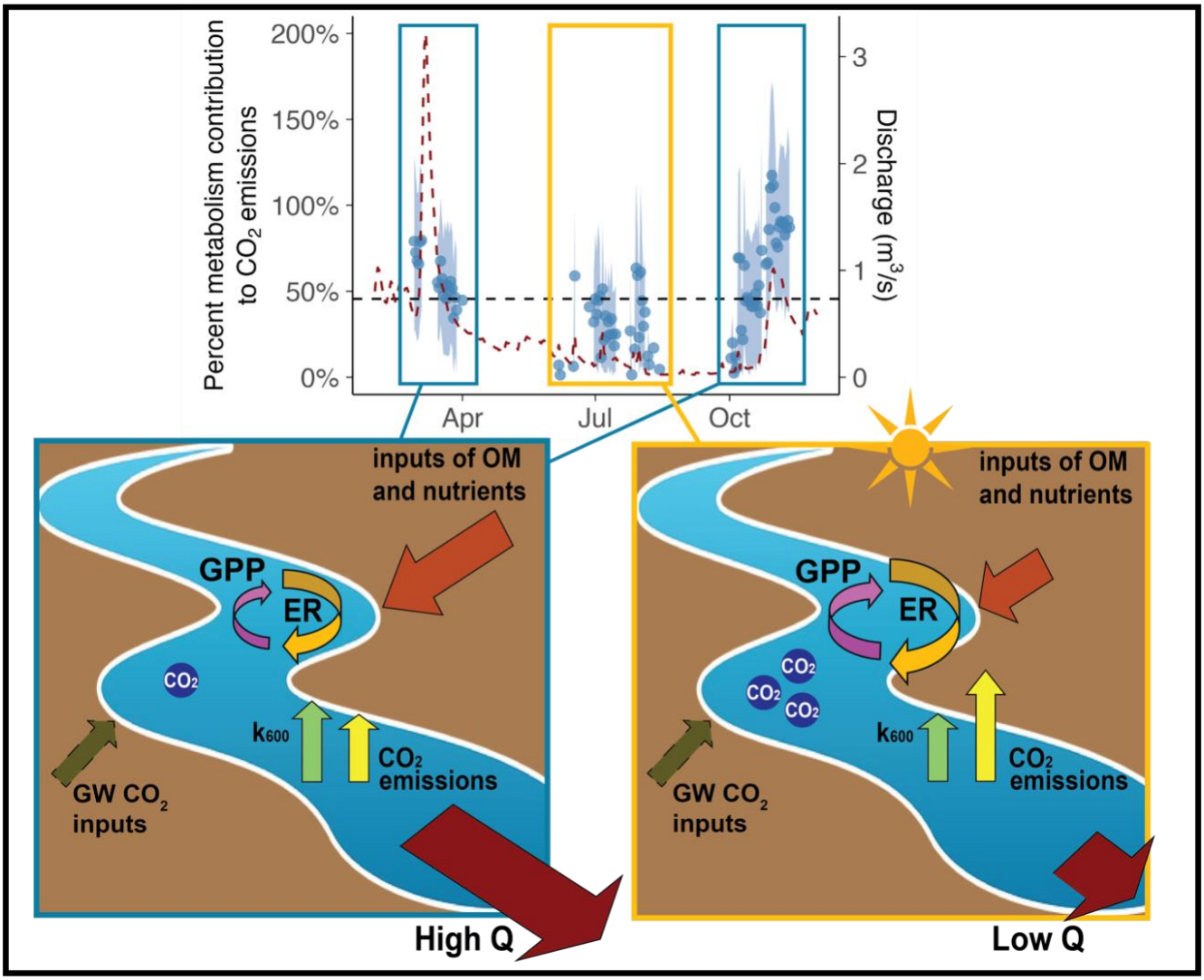

Figure 4.5 Conceptual framework for carbon cycling and CO_2 emissions low-gradient agricultural streams. During high flow, ER will increase with increased inputs of organic matter and nutrients while GPP will decrease with increased turbidity and less light. The gas transfer velocity (k_{600}) will only increase slightly in low sloped networks ultimately limiting CO_2 emissions. During low flow typically

occurring in the summer, the CO_2 source into the network can remain high with high ER driven by non-limiting nutrients and high temperatures. While the groundwater and soil inputs of CO_2 remain unresolved, increased respiration in both soil and the stream during the summer months could support high observed CO_2 concentrations (and therefore decrease the metabolism contribution to total emissions), which in turn cause slightly higher CO_2 emissions in the summer.

Conclusions

Our findings highlight the unique carbon dynamics in agricultural streams, where in-stream metabolism can play a disproportionate role in driving CO_2 emissions. At the Hågaån stream, metabolism contributed close to half of total CO_2 emissions, a higher proportion that typically observed in similar sized streams. Despite elevated in-stream CO_2 concentrations, overall CO_2 emissions from Hågaån were relatively low compared to other ecosystems due to consistently low k_{600}. Seasonal patterns further revealed that CO_2 emissions peaked not during high-flow spring periods, but in late summer when respiration was high and gas exchange remained low. Collectively, these results suggest that agricultural streams exhibit distinct CO_2 emissions patterns compared to streams draining other ecosystems, with emissions more tightly linked to biological activity than hydrologic variability. Recognizing that agricultural streams behave differently than other systems is crucial for refining carbon budgets and modeling efforts across human-impacted landscapes.

Supplementary Information

Text S4.1. Sensor measurements

The sensor was calibrated against known gas standards (400, 1000, 5000, and 20,000 µatm) before and after deployment, with no significant drift observed during the study period. The sensor was connected to a CR1000X data logger (Campbell Sci, UK) measuring a 1 minute interval and storing average values at 30 minute intervals. The sensor outputs were corrected for variations in temperature and pressure (atmospheric and water depth) using the methods described in Johnson et al. (2010)[202]. To validate sensor pCO_2 measurements, grab samples of pCO_2 were collected near the stream sensor over a 24-hour period. Manual and sensor based measurements were on average within 10%, and the same diel pattern was observed in both manual and sensor pCO_2 sensor data (Figure S4.1). We removed the 1st and 99th percentile thresholds for turbidity and specific conductivity, as well as outliers based on visual inspection. We removed outliers associated with sensor cleaning and power outages for continuous pCO_2 and O_2 data based on visual inspection (Figure S4.2).

Discharge was measured using an established stage height-discharge relationship based on manual velocity-cross section area measurements covering most of the observed discharge range. Stage height was continuously recorded at 30 min interval using a Tru-Track capacitance sensor (Tru-Track, New Zeeland). In the absence of data on photosynthetically active radiation (PAR), shortwave incoming radiation served as a proxy for available photosynthetic light. Shortwave radiation data were obtained from a nearby meteorological station ca 5 km from the stream sampling point. Manual water sampling as the site for a wide range of chemical variables has be conducted bimonthly since 2016 as part of a national monitoring program of surface waters

(Table S4.1). Water chemistry was analyzed using accredited methods at Swedish University of Agricultural Sciences, Uppsala.

Text S4.2. Stream metabolizer model description and quality checks

We estimated NEP based on the oxygen data using *streamMetabolizer* in R, a state-space Bayesian stream metabolism model that gives the best fit of GPP, ER, and air-water gas exchange of oxygen to match modeled and measured dissolved oxygen[61]. We estimated PAR using shortwave incoming radiation data with a ratio of PAR to shortwave radiation of 0.44 [203]. Average stream channel depth was calculated using a linear relationship from manual measurements of depth and stage height. We grouped discharge into six bins to associate with binned air–water gas exchange rate ($K_{600;}$ d^{-1}) estimates in the modeling framework to decrease the likelihood of equifinality of metabolism parameter estimates and constrain the air-water gas exchange as a function of discharge[62]. Before running *streamMetabolizer* we removed days that exhibited strong diel signals. First we removed event days as described in Lannergård et al. (2021)[204] to not mistake events for a diel signal. Next, we created a detrended time series where we determined the median streamflow and subtracted the time series from the original time series to create a time series with daily fluctuations isolated[205]. Strong diel days were then defined as those with more with a standard deviation more than 25% above the median daily variability (Figure S4.3).

We considered the impact of groundwater inputs of stream O_2 concentrations to ensure model assumptions were valid. We considered a uniform reach area of 400 m based on observations in the field indicating the reach was relatively uniform for 800 m above the outlet. We estimated a reach area of 1940 m^2 (based on a 4.8 m average width) and groundwater inputs of 0.01 m^3 s^{-1} (based on a median discharge of 0.36 m^3 s^{-1} and a 0.3% increase in drainage area along the reach). The ratio between the groundwater input and reach area was therefore 0.48 m day^{-1}, and

we concluded the groundwater inputs would had minimal impact (< 10%) on our estimation of respiration[29, 185].

To assess model convergence, we inspected the Gelman-Rubin convergence statistic (Rhat) and removed days when Rhat > 1.1 [62, 65]. We also removed days with biologically impossible parameter estimates of negative GPP or positive ER. To check for equifinality (multiple parameter combinations producing the same result), we plotted K_{600} versus ER and K_{600} versus GPP (Figure S4.3). We determined the relationship was weak between both variables for metabolism estimates ($R^2 = 0.29$, $R^2 = 0.07$). After removing days that did not pass our model quality checks, we were left with 773 days of metabolism estimates from 2020 – 2023.

Text S4.3. CO_2 emissions estimates

We used the continuous CO_2 data to estimate CO_2 emissions (F_{CO_2}, g m^{-2} day^{-1}) at the site where emissions are calculated by:

$$F_{CO_2} = h * (C_s - C_{atm}) * K_{CO_2}$$

Where C_S is the CO_2 concentration in the water measured by the sensor (g m^{-3}), C_{atm} is the CO_2 concentration that would have existed if in equilibrium with the atmosphere (assuming an atmospheric CO_2 of 410 ppm) (g m^{-3}), h is the average depth of the stream (m), and K_{CO_2} is the gas-transfer coefficient (day^{-1}). K_{CO_2} was converted to k_{CO_2}, the gas-transfer velocity (m day^{-1}) by multiplying times h. k_{CO_2} was calculated from k_{600} (m day^{-1}) using a temperature-corrected Schmidt number for CO_2 (sc_t) and a scaling factor of 0.5 [51, 67]:

$$k_{CO_2} = \frac{k_{600}}{(600/sc_t)^{-0.5}}$$

The Schmidt number for CO_2 was calculated from the stream temperature (T; K) as follows[123]:

$$sc_t = 1923.6 - 125.06T + 4.3772T^2 - 0.0857T^3 + 0.00070284T^4$$

We compared emissions estimates using the k_{600} predicted from *streamMetabolizer* to estimates predicting k_{600} from seven different physical model regression equations from the literature (Figure S4.4)[51]. We selected the regression model that resulted in k_{600} values most similar in magnitude to those predicted from *streamMetabolizer* estimates[51]:

$$k_{600} = 970 \times v^{0.90} s^{0.80}$$

where v is the velocity (m/day) of the stream and s is the slope of the stream, calculated from a DEM of the site.

Table S4.1. Hågaån water chemistry from 2016-2023

	Median	Mean	Min	Max	Median for other stream sites[1]
pH	7.55	7.55	7.14	8.04	NA
Water Temp (deg C)	7.50	8.20	0.00	20.7	NA
Conductivity (mS m^{-1})	46.1	46.6	18.6	72.3	NA
Turbidity (FNU)	15.0	21.0	3.40	120	NA
O_2 (mg/L)	10.6	9.95	4.01	19.0	NA
O_2 saturation (%)	83.5	82.1	150	42	NA
NH_4 – N (mg L^{-1})	0.034	0.069	0.004	0.58	0.09
NO_3 - N (mg L^{-1})	1.10	1.10	0.002	3.35	4.95
Total N	1.85	1.82	0.37	4.2	6.3
PO_4 – P (mg L^{-1})	0.026	0.035	0.006	0.20	0.05
Total P	0.06	0.069	0.029	0.34	0.19
TOC (mg L^{-1})	16.7	15.8	5.90	29.8	13.0

1. We compared Hågaån stream data compared to 18 agricultural catchments in Sweden from 2022 – 2023 for nutrients and TOC[198].

Table S4.2. Breakpoints for concentrations and process based discharge plots

Variable	Unit	p value from Davies	Estimated breakpoint (L s^{-1})	Slope below breakpoint	Slope above breakpoint	Slope difference (p value)
Ecosystem respiration	g O_2 m^{-2} day^{-1}	<0.001	189	-0.56	0.48	<0.001
Gross primary production	g O_2 m^{-2} day^{-1}	<0.001	252	-0.21	0.15	<0.001
Turbidity	FNU	0.04	240	0.13	0.39	0.006
Specific Conductivity	uS/cm	<0.001	163	-0.011	0.32	0.27
Temperature	deg C	0.011	123	-0.10	-0.80	0.003
Dissolved oxygen	mg L^{-1}	<0.001	58.3	0.93	0.14	<0.001
pCO_2	mg L^{-1}	<0.001	536	-0.80	0.37	<0.001
pH		<0.001	82.9	0.047	-0.11	<0.001
NO_3 -N	µg L^{-1}	<0.001	60	2.4	0.30	<0.001
TOC	mg L^{-1}	<0.001	827	0.25	0.017	<0.001
PO_4-P	µg L^{-1}	0.76	1360	0.15	0.34	0.232
NH_4-N	µg L^{-1}	0.16	624	0.29	-0.1	0.037
Total.N	µg L^{-1}	<0.001	158	0.48	0.20	<0.001
Total.P	µg L^{-1}	0.23	470	0.11	0.23	0.047
Alkalinity	meq_L^{-1}	0.45	83	0.05	-0.11	<0.001

Significant p values are $p < 0.05$. Slope difference is based on a two-sized Z-test[62].

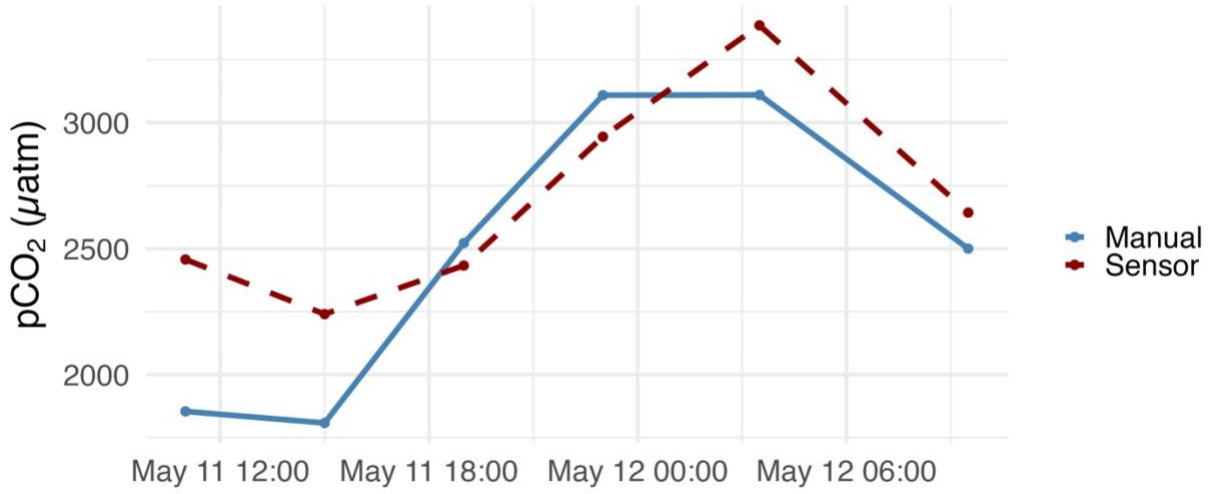

Figure S4.1. Manual pCO_2 measurements compared to continuous sensor measurements. The samples were collected using a headspace equilibrium method by equilibrating gas-tight syringes with ambient air in the field[206, 207]. Samples were analyzed within 24 hours with an Ultraportable Greenhouse Gas Analyzer (Los Gatos, USA). Manual and sensor based measurements were on average within 10% of each other, and we observed the same diel pattern with both the manual and sensor pCO_2 measurements.

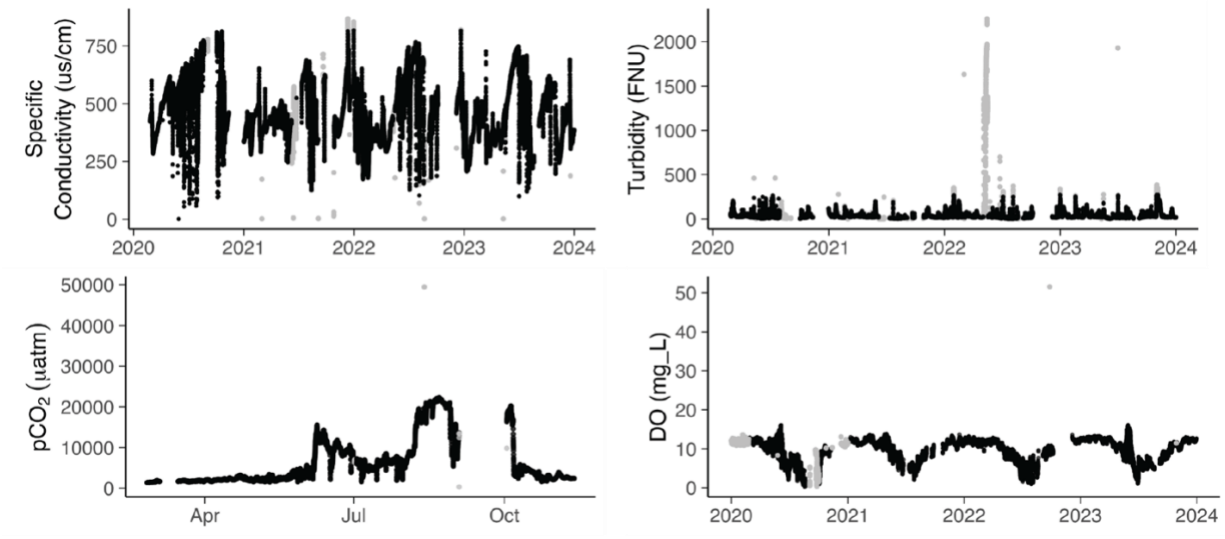

Figure S4.2. Data before and after quality checks. We removed the 1st and 99th percentile thresholds for turbidity and specific conductivity, as well as outliers based on visual inspection. We removed outliers associated with sensor cleaning and power outages for continuous pCO_2 and O_2 data based on visual inspection.

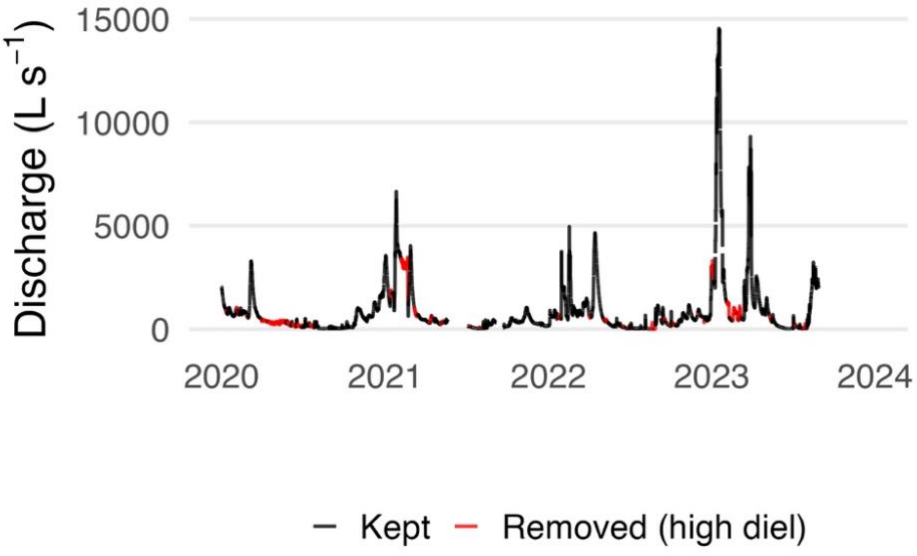

Figure S4.3. Diel discharge data identified and removed to run *streamMetabolizer*. Diel discharge days were identified as described in Text S4.2.

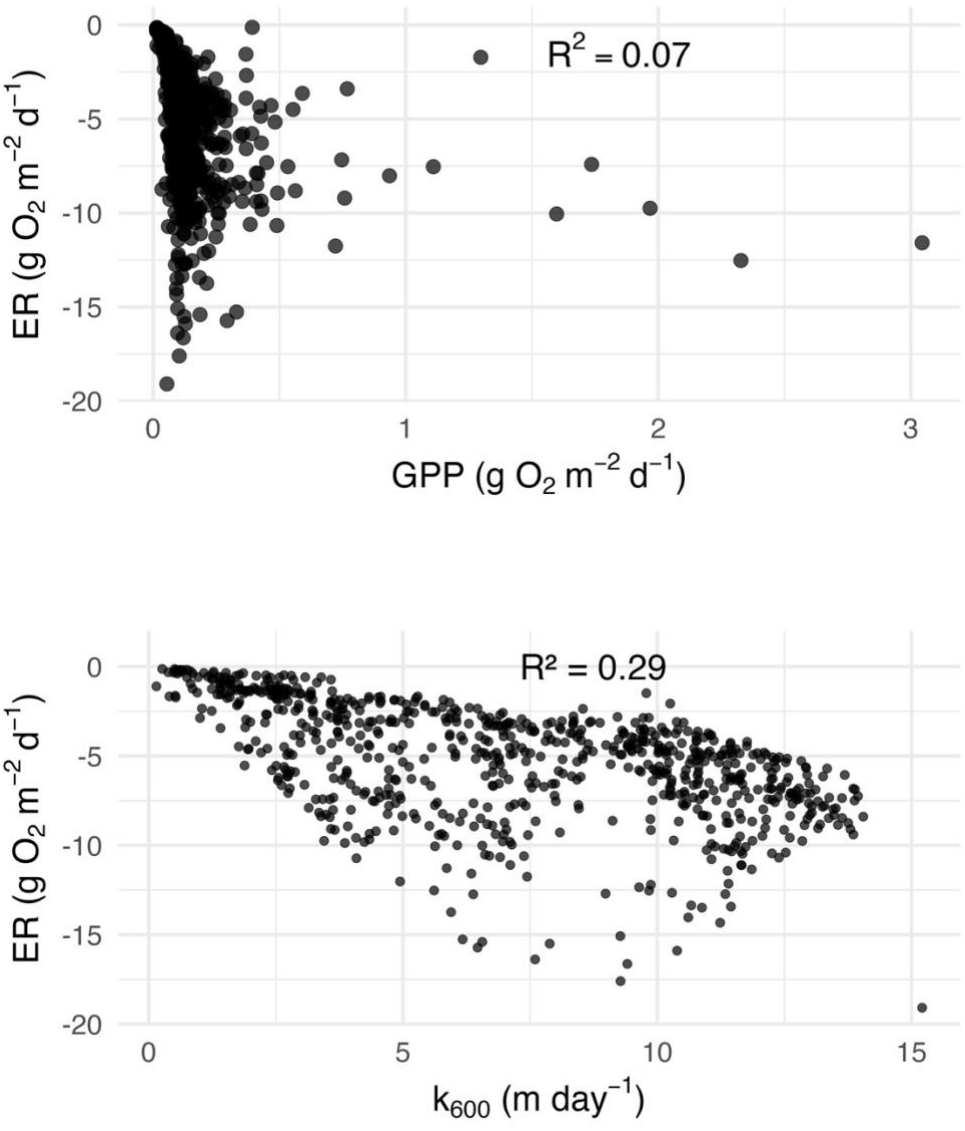

Figure S4.4. Metabolism checks for equifinality. We checked that ER and GPP and ER and k_{600} did not have a strong relationship to check for equifinality, multiple parameter combinations producing the same result. We found R^2 was small for both relationships.

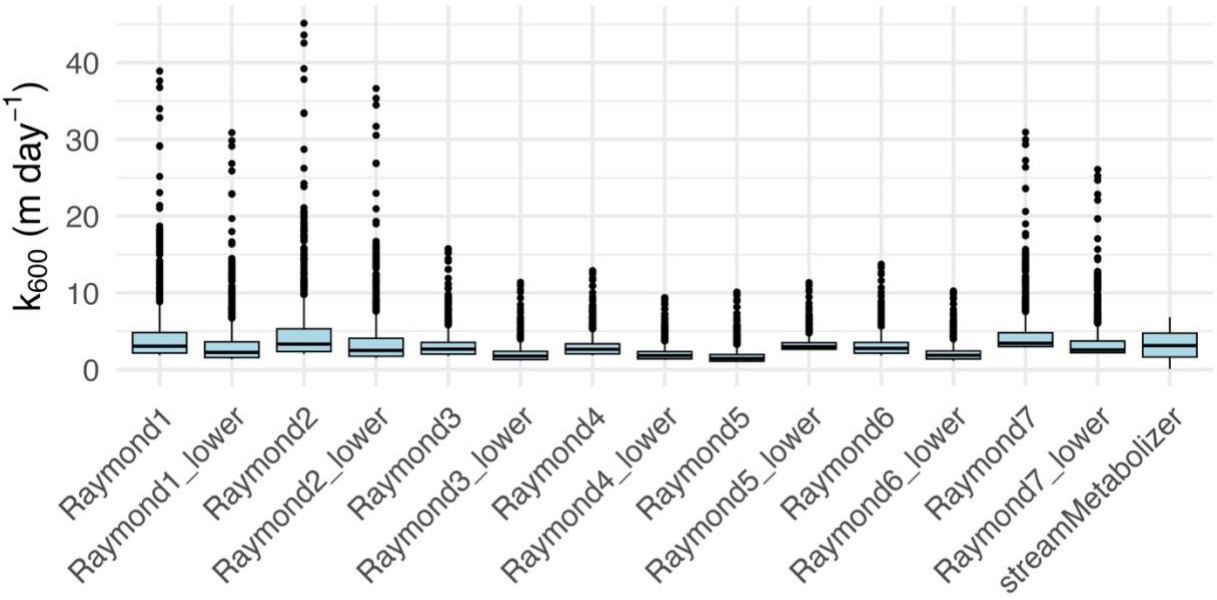

Figure S4.5. Comparison of streamMetabolizer k_{600} and Raymond equations. We selected equation Raymond 4 because of a similar mean to the streamMetabolizer estimated k_{600}.

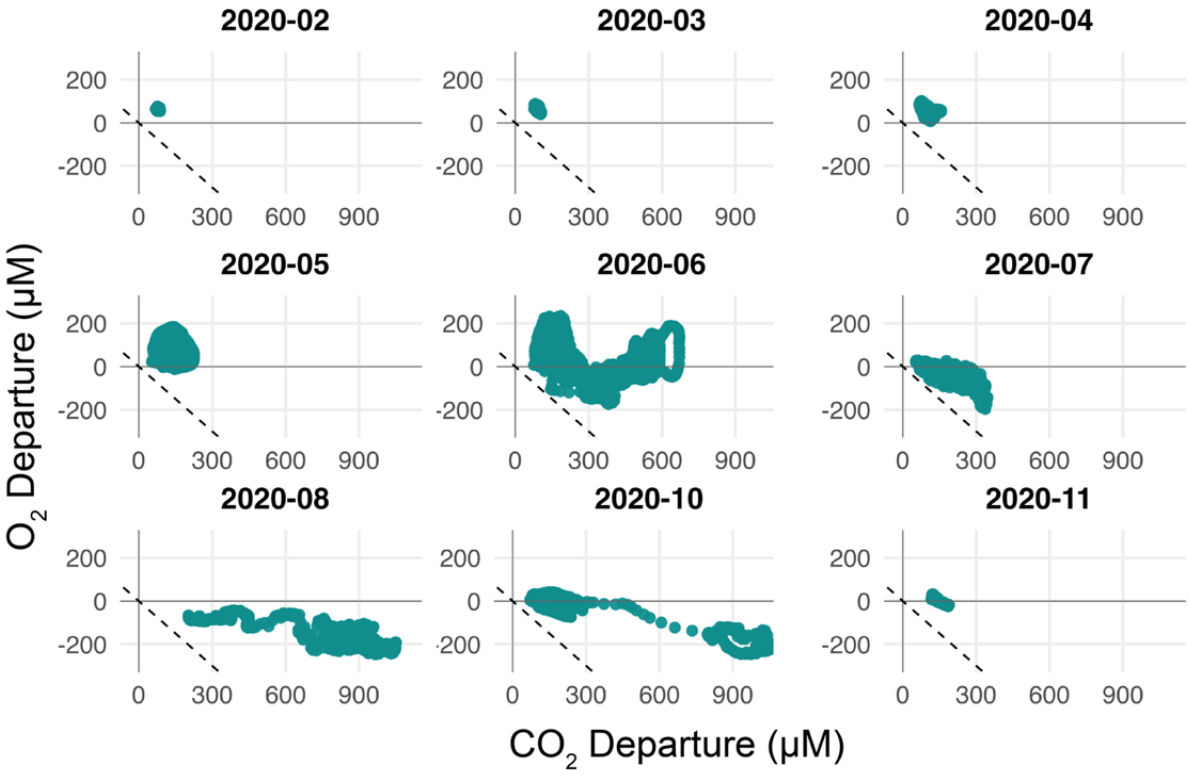

Figure S4.6. Departure from atmospheric equilibrium of CO_2 and O_2. Each point represents a 30 minute observation in 2020. The points are above the 1:1 line, suggesting that a portion of the CO_2 originated from inputs not coupled to in-stream oxygen dynamics, such as groundwater or soil contributions[186].

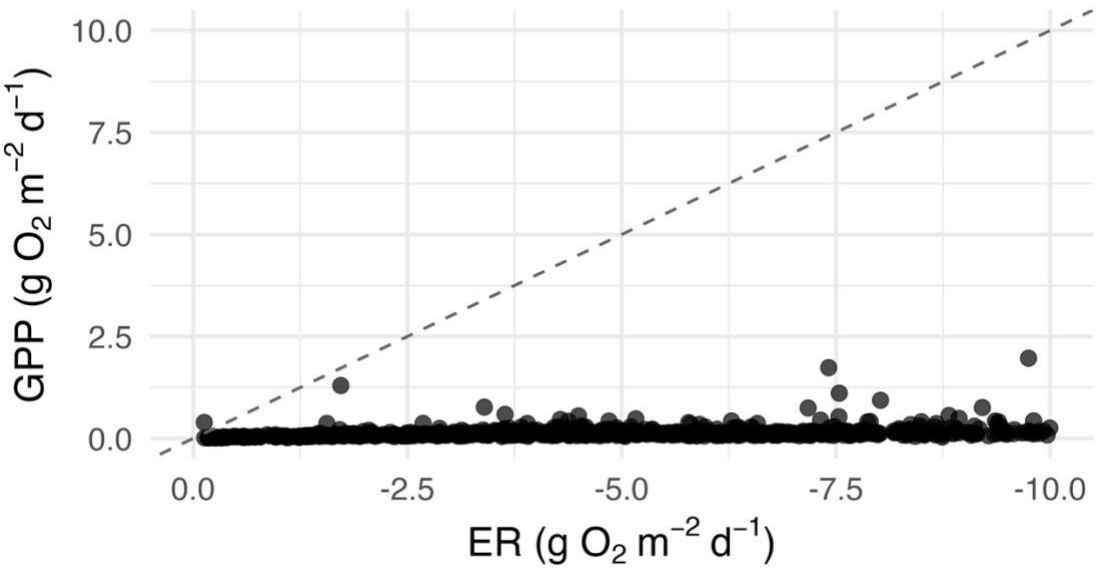

Figure S4.7. ER versus GPP. Rates of ER were consistently higher than GPP, indicating in-stream respiration was a sustained source of net source of CO_2 to the stream network.

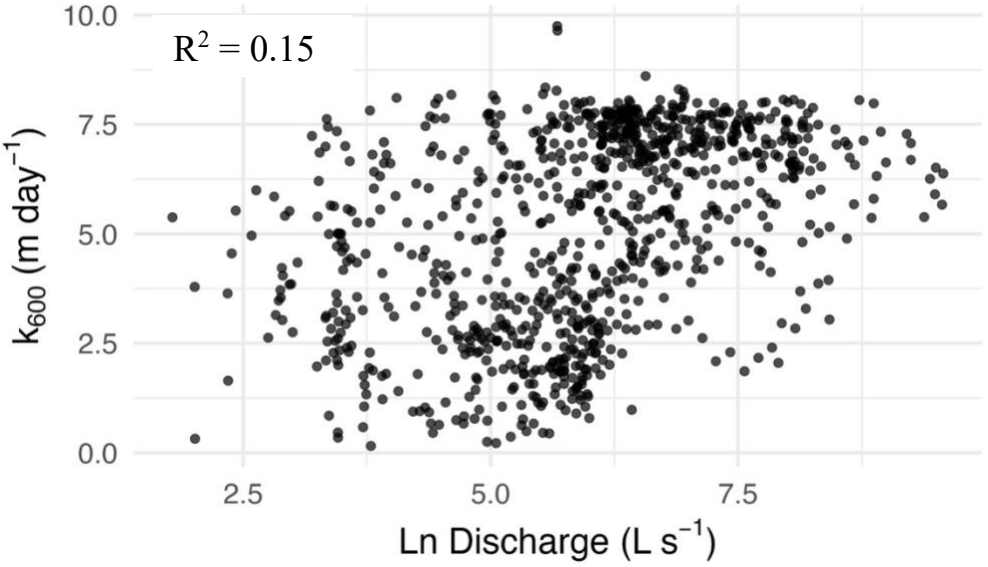

Figure S4.8. Discharge (plotted as natural log Q for clarity) versus k_{600} as predicted by *streamMetabolizer*. There is not a strong relationship between discharge and k_{600} at the site (R^2 = 0.15)

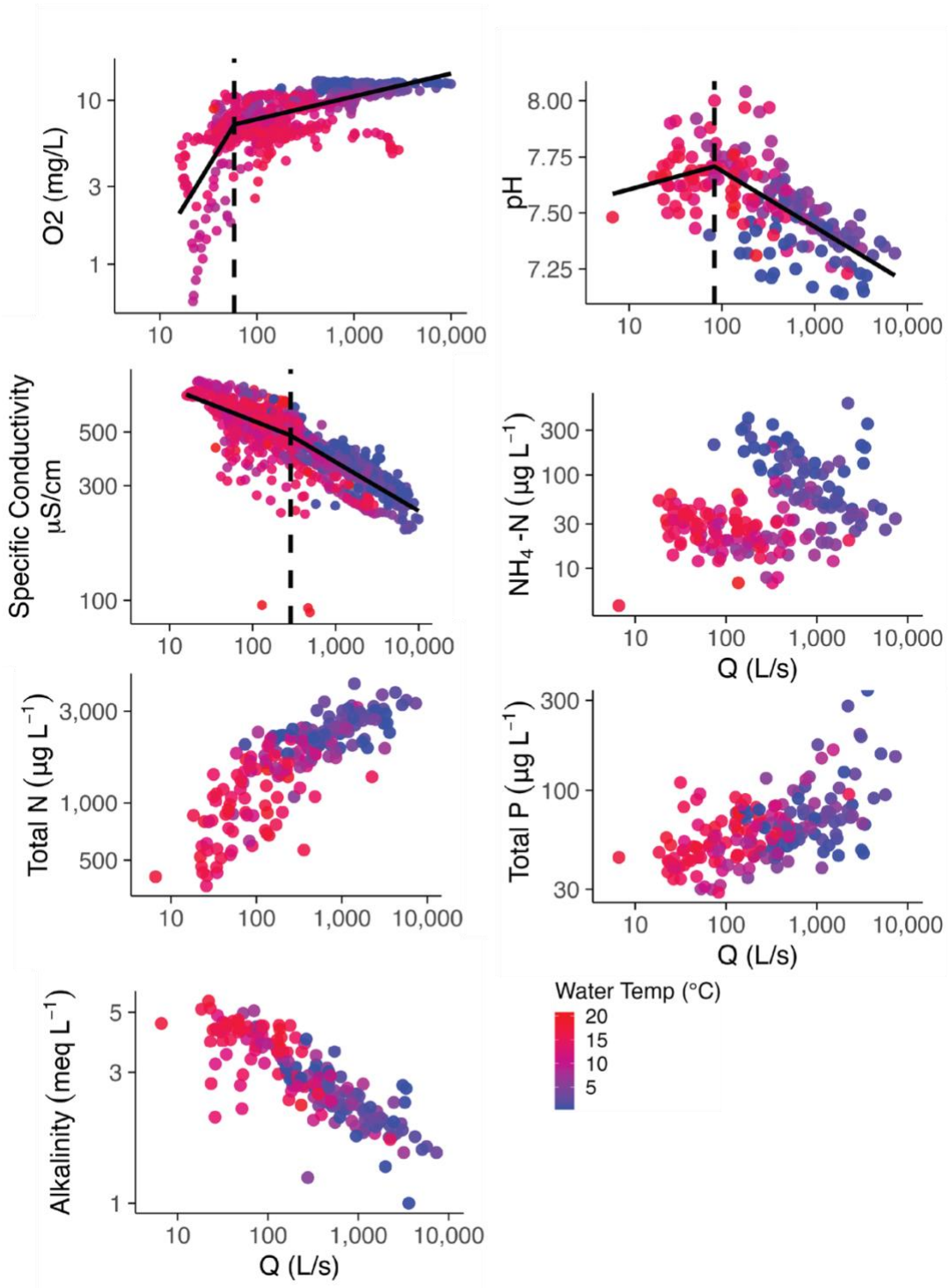

Figure S4.9. C-Q and P-Q plots for remaining variables. Breakpoints were determined using Davies tests. Points are colored by temperature. We show variables with significant breakpoints with breakpoints and slopes labeled here (O_2, pH, and specific conductivity). Variables without significant breakpoints were PO_4-P, NH_4-N, Total P, Total N, and alkalinity.

Chapter 5 Conclusions

To better quantify the global carbon cycle, it is imperative that we resolve current uncertainties. In this dissertation, I focused on the carbon emissions and export from headwater streams; an unresolved flux in the carbon cycle that could alter the calculation of terrestrial net ecosystem exchange (NEE). Our findings highlight carbon dynamics in headwater streams behave differently across stream networks with differences in biomes, topography, hydrologic regimes, land use and geology all underscoring the complexity of accurately quantifying carbon losses from headwater streams. Hydrologic regimes emerged as an especially important factor across stream networks in a diverse group of biomes.

In Chapter 2, we demonstrated how carbon emissions from a single stream network in Washington can vary substantially between high flow and base flow with increases in groundwater inputs, gas exchange velocity, and stream network area. In Chapter 3, we expanded this analysis to five stream networks in different biomes and found that at all five sites, a disproportionate amount of emissions and carbon losses (in the form of DIC and DOC) occurred during high discharge events. Within the networks in both chapters, we found the majority of emissions occurred in higher-sloped first order streams, emphasizing the importance of including first-order streams in emissions estimates and the role of topography in regulating emissions. This was further emphasized in Chapter 4, where we found at a low-sloped agricultural catchment, the expected coupling between discharge and CO_2 emissions was dampened because of a weaker relationship between slope and gas exchange velocity. Instead, we found the hydrologic regime regulated the magnitude of emissions by regulating the source, namely the higher in-stream metabolism contribution to emissions at a site with high nutrient and organic

matter inputs. In all chapters, I highlight how the source of CO_2 to the stream networks remains a large uncertainty, and better quantifying spatial and temporal inputs of groundwater and soil CO_2 is crucial for better emissions estimates.

Ultimately, we must understand how emissions estimates compare to the watershed terrestrial carbon flux. In Chapter 2, we compared CO_2 emissions estimates to the NEE of the Martha Creek watershed and found daily stream emissions in November (low terrestrial productivity and high flow) accounted for a much larger percentage of NEE than in August (high terrestrial productivity and low flow): 54% vs. 0.62%. While outside of the scope of Chapter 3, I can compare our estimates of carbon losses for each site to estimates of NEE at each site on an annual scale (Table 5.1).

Table 5.1 Total carbon losses per watershed area and proportion of total carbon losses[1]

Stream Network	Sum C losses, g m^{-2} y^{-1}	NEE[4] g m^{-2} y^{-1}	% total C loss of NEE
WALK	12.0 (11–13)	-500	2%
MART	16.5 (11–23)	-232	7%
CARI[2]	6.9 (6.5–7.3)	-13.7	50%
COMO[2,3]	3.9 (3.3–4.6)	136	3%
KING	5.1 (5.0–5.3)	-149	3%

1. All flux estimates are provided in g m^{-2} $year^{-1}$ and normalized by watershed area. Uncertainty is provided in parentheses.
2. Carbon losses are only estimated for non-frozen stream periods – May – September for Caribou Creek and May – October for Como Creek.
3. NEE estimates obtained from nearby Rocky Mountain National Park – positive NEE indicates a net release of CO_2 from the site, while negative NEE represents a net uptake of CO_2
4. Estimates derived from NEON, 2023[58, 208-210]

For the majority of the five stream networks, the export of carbon from the stream network was small compared to the terrestrial ecosystem (2 – 7%). Even the network with the highest total

carbon losses (largely due to high slopes and the highest annual discharge), Martha Creek, only emitted a fraction of the NEE of the surrounding watershed (7%). Only Caribou Creek, a boreal watershed with low overall terrestrial productivity, had a large portion of the terrestrial sink exported by the stream (50%). I highlight that the terrestrial ecosystem is the main driver for how important stream carbon export will be, and not the stream ecosystem itself. However, when examining trends in percent of NEE loss by streams across years, we find evidence that the stream will influence the magnitude of loss on a year to year basis. For sites with multiple years of NEE data (Martha Creek, and Como Creek, King's Creek), I found that streams appear to export a higher percentage of carbon from the total NEE during higher discharge years, mainly due to a tight relationship between discharge and carbon losses (Figure 5.1).

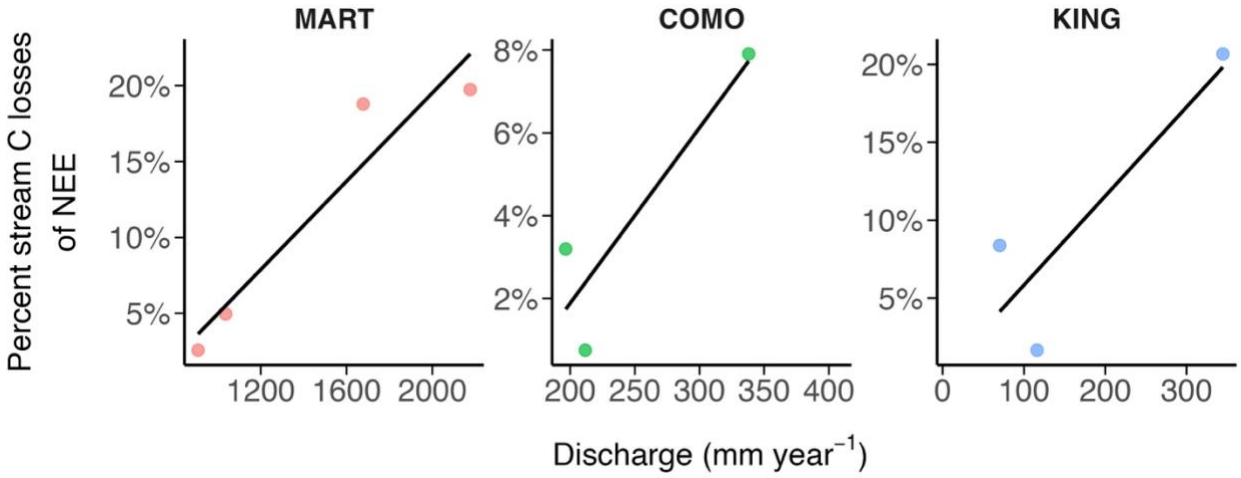

Figure 5.1 Discharge versus percent total carbon losses of NEE. The relationship is mainly driven by a tight relationship between discharge and carbon losses.

NEE has been previously observed to increase with precipitation, which is less apparent in our small dataset[211]. While we are limited by the number of years available to compare carbon losses and emissions, our findings suggest that, at some sites, the strong coupling between hydrology and stream carbon fluxes could outweigh the increase in NEE with precipitation. As climate

change is expected to cause some regions to become drier and others wetter[212], it will be essential to understand how these hydrologic shifts may alter the balance between terrestrial carbon uptake and aquatic carbon losses. In Chapter 3, I also explored how emissions estimates might change when accounting for variations in stream network size. As climate change is expected to alter the distribution of flow intermittency understanding these dynamics is increasingly important[213]. While our modeling approach indicated that incorporating stream permanence did not significantly affect annual emissions estimates, it did suggest potential shifts in the timing and spatial distribution of emissions across the network.

I also highlight the importance of considering differences in biomes. At Caribou Creek, a low-productivity boreal watershed, I show that carbon losses from the stream network are substantial, accounting for nearly 50% of net ecosystem exchange (NEE). Boreal climates are projected to undergo some of the most severe changes under climate change, where rising temperatures and widespread permafrost thaw are expected to mobilize large amounts of previously frozen organic carbon[214]. Warmer conditions will also shorten ice-covered periods and shift precipitation patterns toward more rainfall, which may increase stream discharge or result in more flashy streams[215]. Clearly defining how these systems behave with changes in discharge will therefore be crucial for accounting of aquatic carbon fluxes. Conversely, in Chapter 4, we found that an agricultural stream network exhibited relatively low carbon emissions, with fluxes that were less tightly coupled to changes in discharge. Nonetheless, significant uncertainty remains regarding the variability in emissions across agricultural systems, influenced by biome, topography, and the magnitude of carbon inputs. While agricultural landscapes are known to contribute substantial greenhouse gas emissions[216], the pathways and drivers of stream carbon fluxes

remain less well understood. Recognizing that stream networks in different biomes respond uniquely to climate and land-use pressures is essential for accurate aquatic carbon budgets.

References

1. Domke, G., et al., *Chapter 9: Forests. Second State of the Carbon Cycle Report*. 2018, U.S. Global Change Research Program.
2. Canadell, J.G. and E.D. Schulze, *Global potential of biospheric carbon management for climate mitigation.* Nature Communications, 2014. **5**(1): p. 5282.
3. Raymond, P.A., et al., *Global carbon dioxide emissions from inland waters.* Nature, 2013. **503**(7476): p. 355-359.
4. Cole, J.J., et al., *Plumbing the global carbon cycle: Integrating inland waters into the terrestrial carbon budget.* Ecosystems, 2007. **10**(1): p. 172-185.
5. Lauerwald, R., et al., *Spatial patterns in CO2 evasion from the global river network.* Global Biogeochemical Cycles, 2015. **29**(5): p. 534-554.
6. Butman, D. and P.A. Raymond, *Significant efflux of carbon dioxide from streams and rivers in the United States.* Nature Geoscience, 2011. **4**(12): p. 839-842.
7. Johnson, M.S., et al., *CO_2 efflux from Amazonian headwater streams represents a significant fate for deep soil respiration.* Geophysical Research Letters, 2008. **35**(17): p. L17401.
8. Liu, S. and P. Raymond, *Hydrologic controls on pCO2 and CO2 efflux in US streams and rivers.* Limnology and Oceanography Letters, 2018. **3**.
9. Horgby, Å., et al., *Unexpected large evasion fluxes of carbon dioxide from turbulent streams draining the world's mountains.* Nature Communications, 2019. **10**(1): p. 4888.
10. Butman, D.E., et al., *Inland waters.* Second State of the Carbon Cycle Report (SOCCR2): A Sustained Assessment Report, 2018: p. 568-595.
11. Hayes, D.J., et al., *Chapter 2: The North American carbon budget.*, in *Second State of the Carbon Cycle Report (SOCCR2): A Sustained Assessment Report*, N. Cavallaro, G. Shrestha, R. Birdsey, M. A. Mayes, R. G. Najjar, S. C. Reed, P. Romero-Lankao, Z. Zhu Editor. 2018, U.S. Global Change Research Program: Washington, DC, USA. p. 71-108.
12. Liu, S., et al., *The importance of hydrology in routing terrestrial carbon to the atmosphere via global streams and rivers.* Proceedings of the National Academy of Sciences, 2022. **119**(11): p. e2106322119.

13. Crawford, J.T., et al., *CO_2 and CH_4 emissions from streams in a lake-rich landscape: Patterns, controls, and regional significance.* Global Biogeochemical Cycles, 2014. **28**(3): p. 197-210.
14. Crawford, J.T., et al., *CO_2 time series patterns in contrasting headwater streams of North America.* Aquatic Sciences, 2017. **79**(3): p. 473-486.
15. Marx, A., et al., *A review of CO_2 and associated carbon dynamics in headwater streams: A global perspective: Carbon Dioxide in Headwater Streams.* Reviews of Geophysics, 2017. **55**(2): p. 560-585.
16. Downing, J.A., et al., *Global abundance and size distribution of streams and rivers.* Inland Waters, 2012. **2**(4): p. 229-236.
17. Duvert, C., et al., *CO_2 evasion along streams driven by groundwater inputs and geomorphic controls.* Nature Geoscience, 2018. **11**(11): p. 813-818.
18. Hotchkiss, E.R., et al., *Sources of and processes controlling CO_2 emissions change with the size of streams and rivers.* Nature Geoscience, 2015. **8**(9): p. 696-699.
19. Stets, E.G., et al., *Carbonate buffering and metabolic controls on carbon dioxide in rivers: Controls on CO_2 in Rivers.* Global Biogeochemical Cycles, 2017. **31**(4): p. 663-677.
20. Ulseth, A.J., et al., *Distinct air–water gas exchange regimes in low- and high-energy streams.* Nature Geoscience, 2019. **12**(4): p. 259-263.
21. Natchimuthu, S., et al., *Spatio-temporal patterns of stream methane and carbon dioxide emissions in a hemiboreal catchment in Southwest Sweden.* Scientific Reports, 2017. **7**(1): p. 39729.
22. Billett, M.F. and F.H. Harvey, *Measurements of CO_2 and CH_4 evasion from UK peatland headwater streams.* Biogeochemistry, 2013. **114**(1-3): p. 165-181.
23. Bernhardt, E.S., et al., *Light and flow regimes regulate the metabolism of rivers.* Proceedings of the National Academy of Sciences, 2022. **119**(8): p. e2121976119.
24. Barefoot, E., et al., *Temporally Variable Stream Width and Surface Area Distributions in a Headwater Catchment.* Water Resources Research, 2019. **55**(8): p. 7166-7181.
25. Kampf, S.K., et al., *Managing nonperennial headwater streams in temperate forests of the United States.* Forest Ecology and Management, 2021. **497**: p. 119523.

26. Botter, G. and N. Durighetto, *The Stream Length Duration Curve: A Tool for Characterizing the Time Variability of the Flowing Stream Length.* Water Resources Research, 2020. **56**(8).
27. Dinsmore, K.J., M.F. Billett, and K.E. Dyson, *Temperature and precipitation drive temporal variability in aquatic carbon and GHG concentrations and fluxes in a peatland catchment.* Global Change Biology, 2013. **19**(7): p. 2133-2148.
28. Rasilo, T., et al., *Transport and transformation of soil-derived CO_2, CH_4 and DOC sustain CO_2 supersaturation in small boreal streams.* Science of The Total Environment, 2017. **579**: p. 902-912.
29. Bernal, S., et al., *Stream metabolism sources a large fraction of carbon dioxide to the atmosphere in two hydrologically contrasting headwater streams.* Limnology and Oceanography, 2022. **67**(12): p. 2621-2634.
30. Rocher-Ros, G., et al., *Stream metabolism controls diel patterns and evasion of CO_2 in Arctic streams.* Global Change Biology, 2020. **26**(3): p. 1400-1413.
31. Martinsen, K.T., T. Kragh, and K. Sand-Jensen, *Carbon dioxide partial pressure and emission throughout the Scandinavian stream network.* Global Biogeochemical Cycles, 2020. **34**(12): p. e2020GB006703.
32. Uhlenbrook, S., *Catchment hydrology—a science in which all processes are preferential.* Hydrological Processes, 2006. **20**(16): p. 3581-3585.
33. McDonnell, J.J., *The influence of macropores on debris flow initiation.* Quarterly Journal of Engineering Geology and Hydrogeology, 1990. **23**(4): p. 325-331.
34. McDowell, M.J. and M.S. Johnson, *Gas Transfer Velocities Evaluated Using Carbon Dioxide as a Tracer Show High Streamflow to Be a Major Driver of Total CO_2 Evasion Flux for a Headwater Stream.* Journal of Geophysical Research: Biogeosciences, 2018. **123**(7): p. 2183-2197.
35. McClain, M.E., et al., *Biogeochemical hot spots and hot moments at the interface of terrestrial and aquatic ecosystems.* Ecosystems, 2003. **6**(4): p. 301-312.
36. Maurice, L., et al., *The Influence of Flow and Bed Slope on Gas Transfer in Steep Streams and Their Implications for Evasion of CO_2: Gas Transfer Tracer Paper.* Journal of Geophysical Research: Biogeosciences, 2017. **122**(11): p. 2862-2875.

37. Wallin, M.B., et al., *Spatiotemporal variability of the gas transfer coefficient (k_{CO2}) in boreal streams: Implications for large scale estimates of CO_2 evasion: Variability of K_{CO2} in Boreal Streams.* Global Biogeochemical Cycles, 2011. **25**(3): p. n/a-n/a.
38. Saccardi, B. and M. Winnick, *Improving Predictions of Stream CO_2 Concentrations and Fluxes Using a Stream Network Model: A Case Study in the East River Watershed, CO, USA.* Global Biogeochemical Cycles, 2021. **35**(12).
39. U. S. Geological Survey (USGS), *USGS National Hydrography Dataset Plus High Resolution (NHDPlus HR) for 4-digit Hydrologic Unit - 1707*. 2018, U.S. Geological Survey.
40. U.S. Geological Survey (USGS), *USGS 1/3 Arc Second n46w122 20211129*. 2021, U.S. Geological Survey.
41. Battelle. *Martha Creek NEON*. 2020 [cited 2024 December 16]; Available from: https://www.neonscience.org/field-sites/mart.
42. USDA Forest Service *Wind River Experimental Forest*. n.d.
43. USDA Forest Service, *Wind River Experimental Forest.* 2003: p. 6.
44. Western Regional Climate Center [WRCC]. *CARSON FISH HATCHERY, WASHINGTON (451160), Period of Record Monthly Climate Summary*. 2016 [cited 2022; Available from: https://wrcc.dri.edu/cgi-bin/cliMAIN.pl?wa1160.
45. National Ecological Observatory Network [NEON], *Single aspirated air temperature (DP1.00002.001)*. 2024, National Ecological Observatory Network (NEON).
46. National Ecological Observatory Network [NEON]. *Site Level Sampling Design*. 2022 [cited 2022 November]; Available from: https://www.neonscience.org/data-collection/site-level-sampling-design.
47. National Ecological Observatory Network [NEON], *Continuous discharge (DP4.00130.001)*. 2024, National Ecological Observatory Network (NEON).
48. Magen, C., et al., *A simple headspace equilibration method for measuring dissolved methane.* Limnology and Oceanography: Methods, 2014. **12**(9): p. 637-650.
49. Goodman, K. *AOS PROTOCOL AND PROCEDURE: SURFACE WATER DISSOLVED GAS SAMPLING*. 2021.
50. Wanninkhof, R., *Relationship between wind speed and gas exchange over the ocean.* Journal of Geophysical Research: Oceans, 1992. **97**(C5): p. 7373-7382.

51. Raymond, P.A., et al., *Scaling the gas transfer velocity and hydraulic geometry in streams and small rivers: Gas transfer velocity and hydraulic geometry.* Limnology and Oceanography: Fluids and Environments, 2012. **2**(1): p. 41-53.
52. USGS, *Alkalinity Calculator*. 2012.
53. Rounds, S., *Chapter A6. Section 6.6. Alkalinity and acid neutralizing capacity.* National Field Manual for the Collection of Water-Quality Data. U.S. Geological Survey Techniques of Water-Resources Investigations, Book 9, 2012.
54. National Ecological Observatory Network [NEON], *Temperature of groundwater (DP1.20217.001)*. 2024, National Ecological Observatory Network (NEON).
55. Hall, R. and E. Hotchkiss, *Stream Metabolism*, in *Methods in Stream Ecology: Third Edition*. 2017. p. 219-233.
56. Allen, G.H., et al., *Similarity of stream width distributions across headwater systems.* Nature Communications, 2018. **9**(1): p. 610.
57. Hack, J.T., *Studies of longitudinal stream profiles in Virginia and Maryland*, in *Geological Survey Professional Paper 294-B*. 1957. p. 45-95.
58. National Ecological Observatory Network [NEON], *NCAR-NEON gap-filled data*. 2023, National Ecological Observatory Network (NEON).
59. Wutzler, T., et al., *Basic and extensible post-processing of eddy covariance flux data with REddyProc.* Biogeosciences, 2018. **15**(16): p. 5015-5030.
60. National Ecological Observatory Network [NEON], *Vegetation indices - spectrometer - mosaic (DP3.30026.001)*. 2024, National Ecological Observatory Network (NEON).
61. Appling, A.P., et al., *Overcoming equifinality: leveraging long time series for stream metabolism estimation.* Journal of Geophysical Research: Biogeosciences, 2018. **123**(2): p. 624-645.
62. O'Donnell, B. and E.R. Hotchkiss, *Coupling Concentration- and Process-Discharge Relationships Integrates Water Chemistry and Metabolism in Streams.* Water Resources Research, 2019. **55**(12): p. 10179-10190.
63. National Ecological Observatory Network [NEON], *NEON Reaeration Repo*. 2023: Github.
64. Stan Developement, T., *Stan modeling language users guide and reference manual*. 2022.

65. Gelman, A. and D.B. Rubin, *Inference from Iterative Simulation Using Multiple Sequences.* Statistical Science, 1992. **7**(4): p. 457-472.
66. National Ecological Observatory Network [NEON], *Reaeration field and lab collection (DP1.20190.001)*. 2024, National Ecological Observatory Network (NEON).
67. Jähne, B., et al., *On the parameters influencing air-water gas exchange.* Journal of Geophysical Research: Oceans, 1987. **92**(C2): p. 1937-1949.
68. Crawford, J.T., et al., *Emissions of carbon dioxide and methane from a headwater stream network of interior Alaska: Carbon emissions from Alaska streams.* Journal of Geophysical Research: Biogeosciences, 2013. **118**(2): p. 482-494.
69. Jantze, E.J., et al., *Spatial variability of dissolved organic and inorganic carbon in subarctic headwater streams.* Arctic, Antarctic, and Alpine Research, 2015. **47**(3): p. 529-546.
70. Lyon, S.W., et al., *The relationship between subsurface hydrology and dissolved carbon fluxes for a sub-arctic catchment.* Hydrol. Earth Syst. Sci., 2010. **14**(6): p. 941-950.
71. Peter, H., et al., *Scales and drivers of temporal pCO_2 dynamics in an Alpine stream.* Journal of Geophysical Research: Biogeosciences, 2014. **119**(6): p. 1078-1091.
72. Duvert, C., et al., *Groundwater-Derived DIC and carbonate buffering enhance fluvial CO_2 evasion in two Australian tropical rivers.* Journal of Geophysical Research: Biogeosciences, 2019. **124**(2): p. 312-327.
73. Alin, S.R., et al., *Physical controls on carbon dioxide transfer velocity and flux in low-gradient river systems and implications for regional carbon budgets.* Journal of Geophysical Research, 2011. **116**(G1): p. G01009.
74. Botter, G., et al., *Steps dominate gas evasion from a mountain headwater stream.* Nature Communications, 2022. **13**(1): p. 7803.
75. Colson, T., et al., *Topographic and Soil Maps Do Not Accurately Depict Headwater Stream Networks.* National Wetlands Newsletter, 2008. **30**.
76. Fritz, K.M., et al., *Comparing the extent and permanence of headwater streams From two field surveys to values from hydrographic databases and maps.* JAWRA Journal of the American Water Resources Association, 2013. **49**(4): p. 867-882.

77. Nadeau, T.-L., et al., *Validation of rapid assessment methods to determine streamflow duration classes in the Pacific Northwest, USA.* Environmental Management, 2015. **56**(1): p. 34-53.
78. Gómez-Gener, L., et al., *Integrating Discharge-Concentration Dynamics Across Carbon Forms in a Boreal Landscape.* Water Resources Research, 2021. **57**(8): p. e2020WR028806.
79. Keller, P.S., et al., *Global CO_2 emissions from dry inland waters share common drivers across ecosystems.* Nature Communications, 2020. **11**(1): p. 2126.
80. Deirmendjian, L. and G. Abril, *Carbon dioxide degassing at the groundwater-stream-atmosphere interface: isotopic equilibration and hydrological mass balance in a sandy watershed.* Journal of Hydrology, 2018. **558**: p. 129-143.
81. Butman, D., et al., *Aquatic carbon cycling in the conterminous United States and implications for terrestrial carbon accounting.* Proceedings of the National Academy of Sciences, 2016. **113**(1): p. 58-63.
82. Hafen, K.C., et al., *The influence of climate variability on the accuracy of NHD perennial and nonperennial stream classifications.* JAWRA Journal of the American Water Resources Association, 2020. **56**(5): p. 903-916.
83. Conroy, H., *Martha-Creek-Stream-Network-: v2*. 2023: Zenodo.
84. Conroy, H., *Seasonality drives carbon emissions along a stream network ver 1*. 2023: Environmental Data Initiative.
85. Casas-Ruiz, J.P., et al., *Integrating terrestrial and aquatic ecosystems to constrain estimates of land-atmosphere carbon exchange.* Nature Communications, 2023. **14**(1): p. 1571.
86. Abril, G. and A.V. Borges, *Ideas and perspectives: Carbon leaks from flooded land: do we need to replumb the inland water active pipe?* Biogeosciences, 2019. **16**(3): p. 769-784.
87. Argerich, A., et al., *Comprehensive multiyear carbon budget of a temperate headwater stream.* Journal of Geophysical Research: Biogeosciences, 2016. **121**(5): p. 1306-1315.
88. Conroy, H.D., et al., *Seasonality Drives Carbon Emissions Along a Stream Network.* Journal of Geophysical Research: Biogeosciences, 2023. **128**(8).

89. Winter, T.C., *The role of ground water in generating streamflow in headwater areas and in maintaining base flow.* Journal of the American Water Resources Association, 2007. **43**(1): p. 15-25.
90. Öquist, M.G., et al., *Dissolved inorganic carbon export across the soil/stream interface and its fate in a boreal headwater stream.* Environmental Science & Technology, 2009. **43**(19): p. 7364-7369.
91. Mast, M.A., et al., *Winter fluxes of CO_2 and CH_4 from subalpine soils in Rocky Mountain National Park, Colorado.* Global Biogeochemical Cycles, 1998. **12**(4): p. 607-620.
92. Uehlinger, U., B. Kawecka, and C.T. Robinson, *Effects of experimental floods on periphyton and stream metabolism below a high dam in the Swiss Alps (River Spöl).* Aquatic Sciences, 2003. **65**(3): p. 199-209.
93. Rocher-Ros, G., et al., *Landscape process domains drive patterns of CO2 evasion from river networks.* Limnology and Oceanography Letters, 2019. **4**(4): p. 87-95.
94. Bretz, K.A., N.N. Murphy, and E.R. Hotchkiss, *Carbon Biogeochemistry and Export Governed by Flow in a Non-Perennial Stream.* Water Resources Research, 2023. **59**(9): p. e2022WR034004.
95. Looman, A., et al., *The carbon dioxide evasion cycle of an intermittent first-order stream: contrasting water–air and soil–air exchange.* Biogeochemistry, 2017. **132**(1): p. 87-102.
96. Bianchi, T.S., et al., *The experimental flow to the Colorado River delta: Effects on carbon mobilization in a dry watercourse.* Journal of Geophysical Research: Biogeosciences, 2017. **122**(3): p. 607-627.
97. Costigan, K.H., M.D. Daniels, and W.K. Dodds, *Fundamental spatial and temporal disconnections in the hydrology of an intermittent prairie headwater network.* Journal of Hydrology, 2015. **522**: p. 305-316.
98. National Ecological Observatory Network [NEON], *Temperature (PRT) in surface water (DP1.20053.001)*. 2024, National Ecological Observatory Network (NEON).
99. National Ecological Observatory Network [NEON], *Continuous discharge (DP4.00130.001)*. 2025, National Ecological Observatory Network (NEON).
100. National Ecological Observatory Network [NEON], *Elevation of groundwater (DP1.20100.001)*. 2025, National Ecological Observatory Network (NEON).

101. National Ecological Observatory Network [NEON], *Chemical properties of surface water (DP1.20093.001)*. 2024: National Ecological Observatory Network (NEON).
102. National Ecological Observatory Network [NEON], *Dissolved gases in surface water (DP1.20097.001)*. 2024, National Ecological Observatory Network (NEON).
103. Battelle. *Walker Branch NEON*. 2020 [cited 2024 December 16]; Available from: https://www.neonscience.org/field-sites/walk.
104. Battelle. *Kings Creek NEON*. 2020 [cited 2024 December 16]; Available from: https://www.neonscience.org/field-sites/king.
105. Battelle. *Como Creek NEON*. 2020 [cited 2024 December 16]; Available from: https://www.neonscience.org/field-sites/como.
106. Battelle. *Caribou Creek NEON*. 2020 [cited 2024 December 16]; Available from: https://www.neonscience.org/field-sites/cari.
107. Hafen, K.C., et al., *Estimating streamflow permanence with the watershed Erosion Prediction Project Model: Implications for surface water presence modeling and data collection.* Journal of Hydrology, 2023. **622**: p. 129747.
108. Lew, R., et al., *WEPPcloud: An online watershed-scale hydrologic modeling tool. Part I. Model description.* Journal of Hydrology, 2022. **608**: p. 127603.
109. Laflen, J.M., et al., *WEPP-Predicting water erosion using a process-based model.* Journal of Soil and Water Conservation, 1997. **52**(2): p. 96-102.
110. Nash, J.E. and J.V. Sutcliffe, *River flow forecasting through conceptual models part I — A discussion of principles.* Journal of Hydrology, 1970. **10**(3): p. 282-290.
111. Zambrano-Bigiarini, M., *hydroGOF: Goodness-of-fit functions for comparison of simulated and observed hydrological time series.* . 2024.
112. Brooks, E.S., et al., *Watershed-scale evaluation of the Water Erosion Prediction Project (WEPP) model in the Lake Tahoe basin.* Journal of Hydrology, 2016. **533**: p. 389-402.
113. Moriasi, D.N., et al., *Model evaluation guidelines for systematic quantification of accuracy in watershed simulations.* Transactions of the ASABE, 2007. **50**(3): p. 885-900.
114. U.S. Geological Survey (USGS), *Kings C NR Manhattan, KS - 06879650*. 2023.
115. National Ecological Observatory Network [NEON], *Atmospheric CO2 isotopes (DP1.00036.001)*. 2024, National Ecological Observatory Network (NEON).

116. Marzolf, N.S., et al., *Ecosystem metabolism estimates from the National Ecological Observatory Network (NEON) stream and river sites.* Scientific Data, 2025. **12**(1): p. 478.
117. Lupon, A., et al., *Groundwater-stream connections shape the spatial pattern and rates of aquatic metabolism.* Limnology and Oceanography Letters, 2023. **8**(2): p. 350-358.
118. Mejia, F.H., et al., *Stream metabolism increases with drainage area and peaks asynchronously across a stream network.* Aquatic Sciences, 2018. **81**(1): p. 9.
119. Roberts, B.J., P.J. Mulholland, and W.R. Hill, *Multiple Scales of Temporal Variability in Ecosystem Metabolism Rates: Results from 2 Years of Continuous Monitoring in a Forested Headwater Stream.* Ecosystems, 2007. **10**(4): p. 588-606.
120. Cawley, K.M., Hall, R. O., Hensley, R., Aho, K. S., *Gas exchange modeling code archived at github.com/NEONScience/NEON-reaeration/tree/main/gasExchangeBySite/MART.R release v0.0.1.* 2023.
121. Aho, K.S., et al., *Gas exchange velocities (k600), gas exchange rates (K600), and hydraulic geometries for streams and rivers derived from the NEON Reaeration field and lab collection data product (DP1.20190.001).* Earth Syst. Sci. Data, 2024. **16**(12): p. 5563-5578.
122. Aho, K.S., et al., *Gas transfer velocity () increases with discharge in steep streams but not in low-slope streams.* Limnology and Oceanography Letters, 2025. **n/a**(n/a).
123. Wanninkhof, R., *Relationship between wind speed and gas exchange over the ocean revisited.* Limnology and Oceanography: Methods, 2014. **12**(6): p. 351-362.
124. Zimmer, M.A., et al., *Zero or not? Causes and consequences of zero-flow stream gage readings.* WIREs Water, 2020. **7**(3): p. e1436.
125. Yu, S., M. Shanafield, and Mark J. Kennard, *Assessing the Influence of Zero-Flow Threshold Choice for Characterising Intermittent Stream Hydrology.* Hydrological Processes, 2024. **38**(10): p. e15300.
126. National Ecological Observatory Network [NEON], *Elevation - LiDAR (DP3.30024.001)*. 2025, National Ecological Observatory Network (NEON).
127. Torsney-Weir, T., *R Package optim.functions. Standard Benchmark Optimization Functions.* . 2017.

128. Rhea, S., M. Vlah, W. Slaughter, and N. Gubbins, *macrosheds: Tools for interfacing with the MacroSheds dataset.* . 2023.
129. Jawitz, J.W. and J. Mitchell, *Temporal inequality in catchment discharge and solute export.* Water Resources Research, 2011. **47**(10).
130. Hensley, R., et al., *Flow Extremes as Spatiotemporal Control Points on River Solute Fluxes and Metabolism.* Journal of Geophysical Research: Biogeosciences, 2019. **124**.
131. Mallard, J., B. McGlynn, and T. Covino, *Lateral inflows, stream-groundwater exchange, and network geometry influence stream water composition.* Water Resources Research, 2014. **50**(6): p. 4603-4623.
132. Lupon, A., et al., *Groundwater inflows control patterns and sources of greenhouse gas emissions from streams.* Limnology and Oceanography, 2019. **64**(4): p. 1545-1557.
133. Deirmendjian, L., et al., *Hydrological and ecological controls on dissolved carbon concentrations in groundwater and carbon export to surface waters in a temperate pine forest watershed.* Biogeosciences Discussions, 2017.
134. Marx, A., et al., *Groundwater data improve modelling of headwater stream CO2 outgassing with a stable DIC isotope approach.* Biogeosciences, 2018. **15**(10): p. 3093-3106.
135. Amundson, R.G. and E.A. Davidson, *Carbon dioxide and nitrogenous gases in the soil atmosphere.* Journal of Geochemical Exploration, 1990. **38**(1): p. 13-41.
136. Ledesma, J.L.J., et al., *The Riparian Zone Controls Headwater Hydrology and Biogeochemistry, Doesn't It? Reassessing Linkages Across European Ecoregions.* Global Biogeochemical Cycles, 2025. **39**(2): p. e2024GB008250.
137. Zimmer, M.A. and B.L. McGlynn, *Lateral, Vertical, and Longitudinal Source Area Connectivity Drive Runoff and Carbon Export Across Watershed Scales.* Water Resources Research, 2018. **54**(3): p. 1576-1598.
138. Bernhardt, E.S., et al., *The metabolic regimes of flowing waters.* Limnology and Oceanography, 2018. **63**(S1): p. S99-S118.
139. Iannucci, F.M., et al., *Temperature and Flow Control Organic Carbon Metabolism in Boreal Headwater Streams.* Journal of Geophysical Research: Biogeosciences, 2024. **129**(10): p. e2024JG008281.

140. Blackburn, S.R. and E.H. Stanley, *Floods increase carbon dioxide and methane fluxes in agricultural streams.* Freshwater Biology, 2021. **66**(1): p. 62-77.
141. Wallin, M.B., et al., *Evasion of CO_2 from streams - The dominant component of the carbon export through the aquatic conduit in a boreal landscape.* Global Change Biology, 2013. **19**(3): p. 785-797.
142. National Ecological Observatory, N., *Stable isotopes in surface water (DP1.20206.001)*. 2024, National Ecological Observatory Network (NEON).
143. Dhillon, G.S. and S. Inamdar, *Extreme storms and changes in particulate and dissolved organic carbon in runoff: Entering uncharted waters?* Geophysical Research Letters, 2013. **40**(7): p. 1322-1327.
144. Jeong, J.-J., et al., *Differential storm responses of dissolved and particulate organic carbon in a mountainous headwater stream, investigated by high-frequency, in situ optical measurements.* Journal of Geophysical Research: Biogeosciences, 2012. **117**(G3).
145. Schelker, J., et al., *CO2 evasion from a steep, high gradient stream network: importance of seasonal and diurnal variation in aquatic pCO2 and gas transfer.* Limnology and Oceanography, 2016. **61**(5): p. 1826-1838.
146. Wang, J., et al., *PFHydro: A new watershed-scale model for post-fire runoff simulation.* Environmental Modelling & Software, 2020. **123**: p. 104555.
147. Winnick, M.J. and B. Saccardi, *Impacts of Carbonate Buffering on Atmospheric Equilibration of CO2, δ13CDIC, and Δ14CDIC in Rivers and Streams.* Global Biogeochemical Cycles, 2024. **38**(2): p. e2023GB007860.
148. Ågren, A., et al., *Regulation of stream water dissolved organic carbon (DOC) concentrations during snowmelt; the role of discharge, winter climate and memory effects.* Biogeosciences, 2010. **7**(9): p. 2901-2913.
149. Clow, D.W., et al., *Aquatic Carbon Export and Dynamics in Mountain Headwater Streams of the Western U.S.* Journal of Geophysical Research: Biogeosciences, 2023. **128**(11): p. e2023JG007538.
150. Homer, C., et al., *Completion of the 2011 National Land Cover Database for the Conterminous United States – Representing a Decade of Land Cover Change Information.* Photogrammetric Engineering & Remote Sensing, 2015. **81**(5): p. 345-354.

151. Reybold, W.U. and G.W. TeSelle, *Soil geographic data bases.* Journal of Soil and Water Conservation, 1989. **44**(1): p. 28-29.

152. Zeleke, G., T. Winter, and D. Flanagan, *BPCDG: Breakpoint Climate Data Generator for WEPP Using Observed Standard Weather Data Sets.* 1999.

153. Srivastava, A., et al., *Modeling forest management effects on water and sediment yield from nested, paired watersheds in the interior Pacific Northwest, USA using WEPP.* Science of The Total Environment, 2020. **701**: p. 134877.

154. Macpherson, G.L., *Hydrogeology of thin limestones: the Konza Prairie Long-Term Ecological Research Site, Northeastern Kansas.* Journal of Hydrology, 1996. **186**(1): p. 191-228.

155. Belcher, W.R., D.S. Sweetkind, and P.E. Elliott, *Probability distributions of hydraulic conductivity for the hydrogeologic units of the Death Valley regional ground-water flow system, Nevada and California.* Water-Resources Investigations Report, 2002.

156. Dethier, D.P., N. Williams, and J.F. Fields, *Snowmelt-Driven Seasonal Infiltration and Flow in the Upper Critical Zone, Niwot Ridge (Colorado), USA.* Water, 2022. **14**(15): p. 2317.

157. Tucci, P., *Hydrology of Melton Valley at Oak Ridge National Laboratory, Tennessee*, in *Water-Resources Investigations Report*. 1992.

158. Knauer J, E.-M.T., Zaehle S, Migliavacca M *Bigleaf—An R package for the calculation of physical and physiological ecosystem properties from eddy covariance data.* . 2018; Available from: https://doi.org/10.1371/journal.pone.0201114.

159. Campeau, A., et al., *Current forest carbon fixation fuels stream CO2 emissions.* Nature Communications, 2019. **10**(1): p. 1876.

160. Gómez-Gener, L., et al., *Low contribution of internal metabolism to carbon dioxide emissions along lotic and lentic environments of a Mediterranean fluvial network.* Journal of Geophysical Research: Biogeosciences, 2016. **121**(12): p. 3030-3044.

161. J., B.M., et al., *Inter-regional comparison of land-use effects on stream metabolism.* Freshwater Biology, 2010. **55**(9): p. 1874-1890.

162. Ortega-Pieck, A., A.K. Fremier, and C.H. Orr, *Agricultural influences on the magnitude of stream metabolism in humid tropical headwater streams.* Hydrobiologia, 2017. **799**(1): p. 49-64.

163. Borges, A.V., et al., *Effects of agricultural land use on fluvial carbon dioxide, methane and nitrous oxide concentrations in a large European river, the Meuse (Belgium).* Sci Total Environ, 2018. **610-611**: p. 342-355.
164. Bodmer, P., et al., *Carbon dynamics and their link to dissolved organic matter quality across contrasting stream ecosystems.* Science of The Total Environment, 2016. **553**: p. 574-586.
165. FAO, *World Food and Agriculture – Statistical Yearbook 2023.* 2023(Rome.).
166. Wallin, M.B., et al., *Carbon dioxide dynamics in an agricultural headwater stream driven by hydrology and primary production.* Biogeosciences, 2020. **17**(9): p. 2487-2498.
167. Zappa, C.J., et al., *Environmental turbulent mixing controls on air-water gas exchange in marine and aquatic systems.* Geophysical Research Letters, 2007. **34**(10).
168. Demars, B.O.L., *Hydrological pulses and burning of dissolved organic carbon by stream respiration.* Limnology and Oceanography, 2019. **64**(1): p. 406-421.
169. Roberts, B.J. and P.J. Mulholland, *In-stream biotic control on nutrient biogeochemistry in a forested stream, West Fork of Walker Branch.* Journal of Geophysical Research: Biogeosciences, 2007. **112**(G4).
170. Hill, W.R., S.E. Fanta, and B.J. Roberts, *Quantifying phosphorus and light effects in stream algae.* Limnology and Oceanography, 2009. **54**(1): p. 368-380.
171. Dodds, W.K. and V.H. Smith, *Nitrogen, phosphorus, and eutrophication in streams.* Inland Waters, 2016. **6**(2): p. 155-164.
172. Lantmäteriet, *Produktbeskrivning: GSD-Höjddata, grid 2+ Lantmäteriet*. 2014, GSD Geografiska Sverige Data. p. Retrieved from National Land Survey of Sweden.
173. Swedish Environmental Protection Agency [SEPA], *Nationella marktäckedata, tilläggsskikt markanvändning*. 2022.
174. Lannergård, E.E., et al., *An evaluation of high frequency turbidity as a proxy for riverine total phosphorus concentrations.* Science of The Total Environment, 2019. **651**: p. 103-113.
175. *Uppsala väder*. 2025 [cited 2025; Available from: http://celsius.met.uu.se/.
176. Miljödata-MVM, *Swedish University of Agricultural Sciences (SLU). National data host lakes and watercourses, and national data host agricultural land.* . 2024.

177. Trentman, M.T., R.O. Hall Jr., and H.M. Valett, *Exploring the mismatch between the theory and application of photosynthetic quotients in aquatic ecosystems.* Limnology and Oceanography Letters, 2023. **n/a**(n/a).
178. Muggeo, V.M.R. and M. Vm. *segmented: An R package to Fit Regression Models with Broken-Line Relationships*. 2008.
179. Paternoster, R., et al., *Using the Correct Statistical Test for Equality of Regression Coefficients.* Criminology, 1998. **36**: p. 859-866.
180. Ott, L. and M. Longnecker, *An introduction to statistical methods and data analysis*. 5th ed. 2001, Australia: Duxbury.
181. Hoellein, T.J., D.A. Bruesewitz, and D.C. Richardson, *Revisiting Odum (1956): A synthesis of aquatic ecosystem metabolism.* Limnology and Oceanography, 2013. **58**(6): p. 2089-2100.
182. Griffiths, N.A., et al., *Agricultural land use alters the seasonality and magnitude of stream metabolism.* Limnology and Oceanography, 2013. **58**(4): p. 1513-1529.
183. Hallberg, L., Bernal, Susana, Bieroza, Magdalena, *Seasonal Variation in Flow and Metabolic Activity Drive Nitrate and Carbon Supply and Demand in a Temperate Agricultural Stream.* Journal of Geophysical Research: Biogeosciences, 2024. **129**(11): p. e2024JG008308.
184. Solano, V., et al., *Stream respiration exceeds CO evasion in a low-energy, oligotrophic tropical stream.* Limnology and Oceanography, 2023. **68**(5): p. 1132-1146.
185. Hall Jr., R.O. and J.L. Tank, *Correcting whole-stream estimates of metabolism for groundwater input.* Limnology and Oceanography: Methods, 2005. **3**(4): p. 222-229.
186. Vachon, D., et al., *Paired O2 – CO2 measurements provide emergent insights into aquatic ecosystem function.* Limnology and Oceanography Letters, 2020.
187. Bond-Lamberty, B. and A. Thomson, *Temperature-associated increases in the global soil respiration record.* Nature, 2010. **464**(7288): p. 579-82.
188. Jones, J.B. and P.J. Mulholland, *Influence of drainage basin topography and elevation on carbon dioxide and methane supersaturation of stream water.* Biogeochemistry, 1998. **40**(1): p. 57-72.

189. Roley, S.S., et al., *The influence of floodplain restoration on whole-stream metabolism in an agricultural stream: insights from a 5-year continuous data set.* Freshwater Science, 2014. **33**(4): p. 1043-1059.
190. Moatar, F., et al., *Elemental properties, hydrology, and biology interact to shape concentration-discharge curves for carbon, nutrients, sediment, and major ions.* Water Resources Research, 2017. **53**(2): p. 1270-1287.
191. Izagirre, O., et al., *Environmental controls of whole-stream metabolism identified from continuous monitoring of Basque streams.* Journal of the North American Benthological Society, 2008. **27**(2): p. 252-268.
192. Caillon, F. and J. Schelker, *Dynamic transfer of soil bacteria and dissolved organic carbon into small streams during hydrological events.* Aquatic Sciences, 2020. **82**(2): p. 41.
193. Honious, S.A.S., et al., *Turbidity Structures the Controls of Ecosystem Metabolism and Associated Metabolic Process Domains Along a 75-km Segment of a Semiarid Stream.* Ecosystems, 2022. **25**(2): p. 422-440.
194. Bernot, M.J.S., Daniel J., Hall Jr, Robert O., Mulholland, Patrick J., Dodds, Walter K., Webster, Jackson R., Tank, Jennifer L., Ashkenas, Linda R., Cooper, Lee W., Dahm, Clifford N., Gregory, Stanley V., Grimm, Nancy B., Hamilton, Stephen K., Johnson, Sherri L., McDowell, William H., Meyer, Judith L., Peterson, Bruce, Poole, Geoffrey C., Valett, H. Maurice, Arango, Clay, Beaulieu, Jake J., Burgin, Amy J., Crenshaw, Chelsea, Helton, Ashley M., Johnson, Laura, Merriam, Jeff, Niederlehner, B. R., O'Brien, Jonathan M., Potter, Jody D., Sheibley, Richard W., Thomas, Suzanne M., Wilson, Kym. , *Inter-regional comparison of land-use effects on stream metabolism.* Freshwater Biology, 2010. **55**(9): p. 1874-1890.
195. Burrell, T.K., et al., *Riparian shading mitigates stream eutrophication in agricultural catchments.* Freshwater Science, 2014. **33**(1): p. 73-84.
196. Hall Jr., R.O., et al., *Turbidity, light, temperature, and hydropeaking control primary productivity in the Colorado River, Grand Canyon.* Limnology and Oceanography, 2015. **60**(2): p. 512-526.

197. Frankforter, J.D., et al., *The relative influence of nutrients and habitat on stream metabolism in agricultural streams.* Environmental Monitoring and Assessment, 2010. **168**(1): p. 461-479.
198. Norberg, L.L., Helena; Blomberg, Maria; Valdén, Roger; Mårtensson, Kristina; Persson, Kristian; Kyllmar, Katarina, *Växtnäringsförluster från åkermark 2022/2023 : årsredovisning för miljöövervakningsprogrammet Observationsfält på åkermark.* Ekohydrologi, 2024. **184**(Institutionen för mark och miljö, Sveriges lantbruksuniversitet).
199. Dubrovsky, N.M., and Hamilton, P.A., *Nutrients in the Nation's streams and groundwater: National Findings and Implications.* U.S. Geological Survey Fact Sheet 2010. **2010-3078**.
200. Wallin, M.B., et al., *Carbon dioxide and methane emissions of Swedish low-order streams—a national estimate and lessons learnt from more than a decade of observations.* Limnology and Oceanography Letters, 2018. **3**(3): p. 156-167.
201. Trentman, M.T., et al., *Watershed-scale Land Use Change Increases Ecosystem Metabolism in an Agricultural Stream.* Ecosystems, 2022. **25**(2): p. 441-456.
202. Johnson, M.S., et al., *Direct and continuous measurement of dissolved carbon dioxide in freshwater aquatic systems—method and applications.* Ecohydrology, 2010. **3**(1): p. 68-78.
203. Akitsu, T.K., et al., *The variability and seasonality in the ratio of photosynthetically active radiation to solar radiation: A simple empirical model of the ratio.* International Journal of Applied Earth Observation and Geoinformation, 2022. **108**: p. 102724.
204. Lannergård, E.E., J. Fölster, and M.N. Futter, *Turbidity-discharge hysteresis in a meso-scale catchment: The importance of intermediate scale events.* Hydrological Processes, 2021. **35**(12): p. e14435.
205. Graham, C., et al., *Catchment scale controls the temporal connection of transpiration and diel fluctuations in streamflow.* Hydrological Processes, 2013. **27**.
206. Sobek, S., et al., *The catchment and climate regulation of pCO2 in boreal lakes.* Global Change Biology, 2003. **9**(4): p. 630-641.
207. Kokic, J., et al., *Carbon dioxide evasion from headwater systems strongly contributes to the total export of carbon from a small boreal lake catchment.* Journal of Geophysical Research: Biogeosciences, 2015. **120**(1): p. 13-28.

208. National Ecological Observatory Network [NEON], *AmeriFlux FLUXNET-1F US-xRM NEON Rocky Mountain National Park, CASTNET (RMNP)*. 2023: United States.
209. National Ecological Observatory Network [NEON], *AmeriFlux FLUXNET-1F US-xBN NEON Caribou Creek - Poker Flats Watershed (BONA)*. 2023: United States.
210. National Ecological Observatory Network [NEON], *AmeriFlux FLUXNET-1F US-xKZ NEON Konza Prairie Biological Station (KONZ)*. 2023: United States.
211. Garbulsky, M.F., et al., *Patterns and controls of the variability of radiation use efficiency and primary productivity across terrestrial ecosystems.* Global Ecology and Biogeography, 2010. **19**(2): p. 253-267.
212. Feng, H. and M. Zhang, *Global land moisture trends: drier in dry and wetter in wet over land.* Scientific Reports, 2015. **5**(1): p. 18018.
213. Messager, M.L., et al., *Global prevalence of non-perennial rivers and streams.* Nature, 2021. **594**(7863): p. 391-397.
214. Battin, T.J., et al., *River ecosystem metabolism and carbon biogeochemistry in a changing world.* Nature, 2023. **613**(7944): p. 449-459.
215. Yang, X., T.M. Pavelsky, and G.H. Allen, *The past and future of global river ice.* Nature, 2020. **577**(7788): p. 69-73.
216. Robertson, G.P., E.A. Paul, and R.R. Harwood, *Greenhouse Gases in Intensive Agriculture: Contributions of Individual Gases to the Radiative Forcing of the Atmosphere.* Science, 2000. **289**(5486): p. 1922-1925.